PUBLISHED BY IOP PUBLISHING AND SISSA
RECEIVED: *April 11, 2008*
ACCEPTED: *October 7, 2008*
PUBLISHED: *October 30, 2008*

The integration and engineering of the ATLAS SemiConductor Tracker Barrel

A. Abdesselam,[w] P.P. Allport,[n] C. Anastopoulos,[ac] B. Anderson,[ah] L. Andricek,[s] F. Anghinolfi,[g] R. Apsimon,[aa] T. Atkinson,[r] D.J. Attree,[ah] N. Austin,[n] A. Bangert,[s] G. Barbier,[k] P. Barclay,[aa] A.J. Barr,[w] L.E. Batchelor,[aa] R.L. Bates,[al] J.R. Batley,[f] G.A. Beck,[p] P.J. Bell,[q] W.H. Bell,[al] A. Belymam,[p] J. Benes,[z] P. Benes,[z] J. Bernabeu,[af] S. Bethke,[s] J.P. Bizzell,[aa] J. Blocki,[i] J. Bohm,[x] C.N. Booth,[ac] E.V. Bouhova-Thacker,[m] O. Brandt,[w] T.J. Brodbeck,[m] Z. Broklova,[y] J. Broz,[y] P.A. Bruckman de Renstrom,[w,1] S. Burdin,[n] C.M. Buttar,[al] J.M. Butterworth,[ah] E. Capocci,[aa] C. Carpentieri,[j] A.A. Carter,[p] J. R. Carter,[f] A. Catinaccio,[g] J.R. Catmore,[m] M. Chamizo llatas,[k] D.G. Charlton,[d] A. Cheplakov,[al] A. Chilingarov,[m] S. Chouridou,[ab] D. Chren,[z] M.L. Chu,[ad] V. Cindro,[o] A. Ciocio,[b] J.V. Civera,[af] A. Clark,[k] A.P. Colijn,[aj] M.J. Costa,[af] D. Costanzo,[ac] J. Cox,[w] C. Dabinett,[aa] W. Dabrowski,[h] J. Dalmau,[p] K.M. Danielsen,[v] S. D'Auria,[al] I. Dawson,[ac] P. de Jong,[aj] M.D. Dehchar,[w] B. Demirköz,[w] P. Dervan,[n] S. Diez Cornell,[af] S.D. Dixon,[ac] E. Dobson,[w] Z. Dolezal,[y] M. Donega,[k] M. D'Onofrio,[k] O. Dorholt,[v] M. Doubrava,[z] J.D. Dowell,[d] Z. Drasal,[y] I.P. Duerdoth,[q] R. Duxfield,[ac] M. Dwuznik,[h] S. Eckert,[j] L.M. Eklund,[g] R. Ely,[b] C. Escobar,[af] V. Fadeyev,[ab] D. Fasching,[ag] F. Fawzi,[r] L. Feld,[j] D. Ferguson,[ag] P. Ferrari,[g] D. Ferrere,[k] J. Fopma,[w] P. Ford,[aa] R. Fortin,[g] J.M. Foster,[q] H. Fox,[j] T.J. Fraser,[ah] J. Freestone,[q] R.S. French,[ac] J. Fuster,[af] S. Gadomski,[k] B.J. Gallop,[aa] M. Galuska,[z] F.C. Gannaway,[p] C. Garcia,[af] J.E. Garcia Navarro,[af] N. Ghodbane,[s] M.D. Gibson,[aa] S.M. Gibson,[w] T. Göttfert,[s] S. Gonzalez,[ag] S. Gonzalez-Sevilla,[af] M.J. Goodrick,[f] G. Gorfine,[ak] A. Gorišek,[o] E. Gornicki,[i] A. Greenall,[n] D. Greenfield,[aa] A.A. Grillo,[ab] J. Grosse-Knetter,[g] C. Haber,[b] R. Härtel,[s] K. Hanagaki,[u] T. Hansl-Kozanecka,[ab] K. Hara,[ae] M. Harris,[aa] F.G. Hartjes,[aj] D. Hauff,[s] B. M. Hawes,[w] T. Hayler,[aa] S.J. Haywood,[aa] F.E.W. Heinemann,[w] R.C.W. Henderson,[m] N.P. Hessey,[aj] A. Hicheur,[aa] J.C. Hill,[f] M.C. Hodgkinson,[ac] P. Hodgson,[ac] T.I. Hollins,[d] A. Holmes,[w] R. Holt,[aa] T. Holy,[z] T. Horazdovsky,[z] S. Hou,[ad] D.F. Howell,[w] G. Hughes,[m] T. Huse ,[v] M. Ibbotson,[q] Y. Ikegami,[l] C. Issever,[w] K. Jakobs,[j] J. Jakubek,[z] R.C. Jared,[ag] P. Jarron,[g] L.G. Johansen,[a] P. Johansson,[ac] A. Jones,[aa] M. Jones,[w] R.W.L. Jones,[m] T.J. Jones,[n] T.W. Jones,[ah] D. Joos,[j] J. Joseph,[ag] P. Jovanovic,[d] J. Jusko,[z] O. Jusko,[z] J. Kaplon,[g] M. Karagöz Ünel,[w] V. Kartvelishvili,[m] N. Kerschen,[ac] C. Ketterer,[j] A.G. Kholodenko,[ai] S.H. Kim,[ae] S. Kluth,[s] P. Kodys,[y] E. Koffeman,[aj] Z. Kohout,[z] T. Kohriki,[l] T. Kondo,[l] S. Koperny,[h] V. Koukol,[z] V. Kral,[z] G. Kramberger,[o] P. Kubik,[y]

2008 JINST 3 P10006

N. Kundu,[w] C. Lacasta,[af] V.R. Lacuesta,[af] W. Lau,[w] S.-C. Lee,[ad] R.P. Lefevre,[k] K.J.C. Leney,[n] C.G. Lester,[f] Z. Liang,[ad] M. Limper,[aj] S.W. Lindsay,[n] V. Linhart,[z] A.J. Lintern,[aa] G. Llosa Llacer,[af] C. Lockett,[aa] F.K. Loebinger,[q] M. Lozano Fantoba,[af] I. Ludwig,[j] J. Ludwig,[j] G. Lutz,[s] J. Lynn,[w] M. Maaßen,[j] D. Macina,[k] A. Macpherson,[g] C. Macwaters,[aa] C.A. Magrath,[aj] P. Malecki,[i] I. Mandić,[o] M. Mangin-Brinet,[k] S. Marti i Garcia,[af] G.F. Martinez-McKinney,[ab] T. Maruyama,[ae] J. Matheson,[aa] S.J. McMahon,[aa] T.J. McMahon,[d] J. Meinhardt,[j] B.R. Mellado Garcia,[ag] I. Messmer,[j] B. Mikulec,[k] M. Mikuž,[o] S. Mima,[t] M. Minano,[af] J. Mistry,[p] V.A. Mitsou,[af] P. Modesto,[af] S. Moed,[k] B. Mohn,[a] R.M. Moles Valls,[af] G. F. Moorhead,[r] J. Morin,[p] A.K. Morley,[r] M-C. Morone,[k] J. Morris,[p] M.C. Morrissey,[aa] H.G. Moser,[s] A. Moszczynski,[i] A.J.M. Muijs,[aj] W.J. Murray,[aa] K. Nagai,[z] Y. Nagai,[ae] D. Naito,[t] K. Nakamura,[ae] I. Nakano,[t] C. Nelson,[aa] A. Nichols,[aa] R. Nicholson,[ac] R. B. Nickerson,[w] R. Nisius,[s] M. Olcese,[c] M. Olivo Gomez,[s] V. O'Shea,[al] B. Ottewell,[w] O. Oye,[a] E. Paganis,[ac] M.J. Palmer,[f] M.A. Parker,[f] U. Parzefall,[j] S. Pataraia,[s] J.R. Pater,[q] G. Pellegrini,[af] H. Pernegger,[g*] E. Perrin,[k] A.W. Phillips,[f] P.W. Phillips,[aa] K. Poltorak,[h] S. Pospisil,[z] T. Pritchard,[g] K. Prokofiev,[ac] P.N. Ratoff,[m] P. Reznicek,[y] V.N. Riadovikov,[ai] R.H. Richter,[s] A. Robichaud-Veronneau,[k] D. Robinson,[f] S. Roe,[g] K. Runge,[j] H.F. Sadrozinski,[ab] J. Sanchez,[af] H. Sandaker ,[a] J. Santander,[af] D. Scheirich,[y] J. Schieck,[s] K. Sedlak,[w] A. Seiden,[ab] A. Sfyrla,[k] T. Slavicek,[z] T.J. Sloan,[m] B. Smith,[aa] M. Smizanska,[m] S.W. Snow,[q] M. Solar,[z] A.O. Solberg,[a] B. Sopko,[z] V. Sopko,[z] L. Sospedra Suay,[af] E. Spencer,[ab] H. Spieler,[b] E. Stanecka,[i] S. Stapnes,[v] J. Stastny,[x] I. Stekl,[z] M. Stodulski,[i] A. Stradling,[ag] B. Stugu,[a] P. Sutcliffe,[n] R.R. Szczygiel,[i] R. Takashima,[e] R. Tanaka,[t] G.J. Tappern,[aa] J. Tarrant,[aa] G. N. Taylor,[r] P.K. Teng,[ad] S. Terada,[l] R.J. Thompson,[q] M. Titov,[j] D.R. Tovey,[ac] S.N. Tovey,[r] A. Tricoli,[aa] M. Turala,[i] M. Tyndel,[aa] F. Ukegawa,[ae] M. Ullan Comes,[af] Y. Unno,[l] V. Vacek,[z] S. Valkar,[y] E. Van der Kraaij,[aj] T. Vickey,[ag] G.H.A. Viehhauser,[w] E.G. Villani,[aa] A.P. Vorobiev,[ai] J. H. Vossebeld,[n] V. Vrba,[x] T. Vu Anh,[k] R.S. Wallny,[g] C.P. Ward,[f] R. Wastie,[w] P. Webb,[aa] M. Webel,[j] M. Weber,[aa] A. R. Weidberg,[w] P.M. Weilhammer,[g] C. Weiser,[j] P.S. Wells,[g] P. Werneke,[aj] M.J. White,[f] M. Wiesmann,[s] I. Wilhelm,[y] I. Wilmut,[aa] J.A. Wilson,[d] M.W. Wolter,[i] S. L. Wu,[ag] H.Z. Zhu[ac] and A. Zsenei[k]

[a] *University of Bergen, Department for Physics and Technology, Allegaten 55, NO - 5007 Bergen, Norway*
[b] *Lawrence Berkeley National Laboratory and University of California, Physics Division, MS50B-6227, 1 Cyclotron Road, Berkeley, CA 94720, United States of America*
[c] *INFN Genova and Università di Genova, Dipartimento di Fisica, via Dodecaneso 33, IT - 16146 Genova, Italy*
[d] *School of Physics and Astronomy, University of Birmingham, Edgbaston, Birmingham B15 2TT, United Kingdom*
[e] *Kyoto University of Education, 1 Fukakusa, Fujimori, fushimi-ku, Kyoto-shi, JP - Kyoto 612-8522, Japan*
[f] *Cavendish Laboratory, University of Cambridge, J J Thomson Avenue, Cambridge CB3 0HE, United Kingdom*
[g] *CERN, CH - 1211 Geneva 23, Switzerland*

2008 JINST 3 P10006

[h]*Faculty of Physics and Applied Computer Science of the AGH-University of Science and Technology, (FPACS, AGH-UST), al. Mickiewicza 30, PL-30059 Kraków, Poland*
[i]*The Henryk Niewodniczanski Institute of Nuclear Physics, Polish Academy of Sciences, ul. Radzikowskiego 152, PL - 31342 Kraków, Poland*
[j]*Physikalisches Institut, Universitaet Freiburg, Hermann-Herder Str. 3, D - 79104 Freiburg i.Br., Germany*
[k]*Université de Genève, Section de Physique, 24 rue Ernest Ansermet, CH - 1211 Genève 4, Switzerland*
[l]*KEK, High Energy Accelerator Research Organization, 1-1 Oho, Tsukuba-shi, Ibaraki-ken 305-0801, Japan*
[m]*Physics Department, Lancaster University, Lancaster LA1 4YB, United Kingdom*
[n]*Oliver Lodge Laboratory, University of Liverpool, P.O. Box 147, Oxford Street, Liverpool L69 3BX, United Kingdom*
[o]*Jožef Stefan Institute and Department of Physics, University of Ljubljana, SI-1001 Ljubljana, Slovenia*
[p]*Department of Physics, Queen Mary, University of London, Mile End Road, London E1 4NS, United Kingdom*
[q]*School of Physics and Astronomy, University of Manchester, Manchester M13 9PL, United Kingdom*
[r]*School of Physics, University of Melbourne, Parkville, Victoria 3010, Australia*
[s]*Max-Planck-Institut für Physik, (Werner-Heisenberg-Institut), Föhringer Ring 6, 80805 München, Germany*
[t]*Okayama University, Faculty of Science, Tsushimanaka 3-1-1, Okayama 700-8530, Japan*
[u]*Graduate School of Science, Osaka University, Machikaneyama-machi 1-1, Toyonaka, Osaka 560-0043, Japan*
[v]*Department of Physics, University of Oslo, Blindern, NO - 0316 Oslo 3, Norway*
[w]*Department of Physics, Oxford University, Denys Wilkinson Building, Keble Road, Oxford OX1 3RH, United Kingdom*
[x]*Institute of Physics, Academy of Sciences of the Czech Republic, Na Slovance 2, CZ - 18221 Praha 8, Czech Republic*
[y]*Charles University in Prague, Faculty of Mathematics and Physics, Institute of Particle and Nuclear Physics, V Holesovickach 2, CZ - 18000 Praha 8, Czech Republic*
[z]*Czech Technical University in Prague, Zikova 4, CZ - 166 35 Praha 6, Czech Republic*
[aa]*Rutherford Appleton Laboratory, Science and Technology Facilities Council, Harwell Science and Innovation Campus, Didcot OX11 0QX, United Kingdom*
[ab]*University of California Santa Cruz, Santa Cruz Institute for Particle Physics (SCIPP), Santa Cruz, CA 95064, U.S.A.*
[ac]*University of Sheffield, Department of Physics & Astronomy, Hounsfield Road, Sheffield S3 7RH, United Kingdom*
[ad]*Insitute of Physics, Academia Sinica, Taipei 11529, Taiwan*
[ae]*University of Tsukuba, Institute of Pure and Applied Sciences, 1-1-1 Tennoudai, Tsukuba-shi, Ibaraki 305-8571, Japan*
[af]*Instituto de Fisica Corpuscular (IFIC), Centro Mixt Univ. de Valencia - CSIC, Apdo. 22085, ES - 46071 Valencia; and Instituto de Microelectronica de Barcelona (IMB-CNM), Dept. de Fisica Atomica, Molecular y Nuclear, Univ. de Valencia, Spain*

2008 JINST 3 P10006

[ag]*University of Wisconsin, Department of Physics, Madison, WI 53706, United States of America*
[ah]*Department of Physics and Astronomy, University College London, United Kingdom*
[ai]*Institute for High Energy Physics, Protvino, Russia*
[aj]*NIKHEF, Amsterdam, The Netherlands*
[ak]*Bergische Universität Wuppertal, Wuppertal, Germany*
[al]*University of Glasgow, Department of Physics and Astronomy, Glasgow G12 8QQ, United Kingdom*
[1]*On leave of absence from Cracow*
E-mail: heinz.pernegger@cern.ch

ABSTRACT: The ATLAS SemiConductor Tracker (SCT) was built in three sections: a barrel and two end-caps. This paper describes the design, construction and final integration of the barrel section. The barrel is constructed around four nested cylinders that provide a stable and accurate support structure for the 2112 silicon modules and their associated services. The emphasis of this paper is directed at the aspects of engineering design that turned a concept into a fully-functioning detector, as well as the integration and testing of large sub-sections of the final SCT barrel detector. The paper follows the chronology of the construction. The main steps of the assembly are described with the results of intermediate tests. The barrel service components were developed and fabricated in parallel so that a flow of detector modules, cooling loops, opto-harnesses and Frequency-Scanning-Interferometry (FSI) alignment structures could be assembled onto the four cylinders. Once finished, each cylinder was conveyed to the next site for the mounting of modules to form a complete single barrel. Extensive electrical and thermal function tests were carried out on the completed single barrels. In the next stage, the four single barrels and thermal enclosures were combined into the complete SCT barrel detector so that it could be integrated with the Transition Radiation Tracker (TRT) barrel to form the central part of the ATLAS inner detector. Finally, the completed SCT barrel was tested together with the TRT barrel in noise tests and using cosmic rays.

KEYWORDS: Particle tracking detectors; Solid state detectors; Detector design and construction technologies and materials; Large detector systems for particle and astroparticle physics.

2008 JINST 3 P10006

*Corresponding author.

Contents

1. Introduction **2**

2. Material budget and barrel radiation length contributions **5**

3. Assembly of single barrels **8**

3.1 Barrel cylinders and module support 9

3.1.1 Design of the barrel cylinder 9

3.1.2 Manufacturing of the cylinders 9

3.1.3 Preparation of cylinders and measurements 10

3.1.4 Design and integration of module supports on cylinder 11

3.2 Barrel cooling 14

3.2.1 Description of the SCT cooling system 14

3.2.2 Design of the cooling-loops 17

3.2.3 Production of cooling-loops, capillaries and interconnects 17

3.3 Power supply and readout services 19

3.3.1 Electrical and optical services 19

3.3.2 Mechanical and thermal interfaces 19

3.4 Integration of harnesses and cooling-loops 20

3.4.1 Harness to barrel integration 20

3.4.2 Cooling-loop to barrel integration 21

3.4.3 Design of the cooling-loop to bulkhead connection 21

3.4.4 Design and production of the heat exchangers 22

3.5 integration of the FSI system 22

3.6 Module to barrel assembly 24

3.7 Transport of the barrels 26

3.7.1 Requirements 26

3.7.2 Designs of the transportation containers 26

3.7.3 Transport 26

3.8 Barrel thermal enclosure and grounding 27

3.8.1 Overview and requirements 27

3.8.2 Outer thermal enclosure 28

3.8.3 Side panels 30

3.8.4 Inner thermal enclosure cylinder 30

3.8.5 Bulkhead 31

3.8.6 End panels and heaters 31

3.8.7 Grounding and shielding 32

3.8.8 Production techniques and experience 33

4. Assembly of the four barrels and integration to TRT **33**
4.1 Four-barrel assembly 33
4.1.1 Description of barrel assembly 33
4.1.2 ESD precautions 34
4.1.3 Integration with the thermal enclosure and sealing 34
4.1.4 Description of the procedure 34
4.1.5 Barrel interlinks 37
4.1.6 The Intermediate Service Support Structure (ISSS) 39
4.1.7 Tests done during four-barrel assembly 40
4.1.8 Photogrammetry survey 41
4.2 Integration into the TRT 41
4.2.1 Support requirements of the SCT inside the TRT 41
4.2.2 Integration procedure 41
4.2.3 Relative alignment between SCT and TRT 43

5. Tests of single barrels **44**
5.1 Test setup for single barrels 44
5.1.1 Detector control system 45
5.1.2 Detector readout system 46
5.1.3 Test procedure 46
5.2 Results of electrical tests on single barrels 47
5.3 Results of thermal tests on single barrels 49

6. Final combined tests before installation **52**
6.1 Operation of the SCT inside the TRT 53
6.2 Results of barrel calibration tests inside the TRT 54
6.3 Noise and cosmic-ray tests with the TRT 57
6.3.1 Noise tests 58
6.3.2 Cosmic-ray tests 58

7. Summary **60**

A. Acronyms **61**

2008 JINST 3 P10006

1. Introduction

The ATLAS [1] SemiConductor Tracker (SCT) is part of the ATLAS inner detector system [2, 3], which provides charged-particle tracking in the centre of the ATLAS experiment. The inner detector system (ID) consists of a hybrid-pixel detector in its centre, followed by the SCT silicon strip detector and the gas straw-tube transition radiation tracker (TRT) surrounding the SCT. A typical track will generate three measurements in the pixel detector, traverse eight silicon strip

Table 1. Layout parameters of the SCT barrel detector.

silicon area [m^2]	34.4
number of layers	4 barrels
number of channel [10^6]	3.2
number of modules	2112
intrinsic design resolution in sensor plane [μm]	23
effective space-point $R\phi$ resolution [μm]	17
effective space-point z resolution [μm]	580
pseudorapidity coverage	$\lvert\eta\rvert \lesssim 1.3$
radial coverage [mm]	$299 < R < 514$

detectors (to give four space-points) and 36 straw tubes. The ID sub-detectors act together to provide tracking of charged particles for momentum measurement as well as primary and secondary vertex reconstruction in a pseudorapidity range of $|\eta| < 2.5$.[1]

The entire tracker is surrounded by a solenoid, which provides a magnetic field of 2 T. The SCT consists of four concentric barrels for tracking at mid-rapidity and two end-caps which extend tracking to the forward region. Each end-cap is comprised of nine disks surrounding the beam axis. The overall layout parameters for the barrel are summarised in table 1, with a schematic drawing of the ATLAS inner detector showing the SCT barrels and end-caps in figure 1. The basic building blocks of the SCT are the silicon strip modules for barrel and end-caps [4, 5]. Each barrel module consists of four silicon sensors [6]: two sensors on each side are daisy-chained to give 768 strips of approximately 12 cm length and with a strip pitch of 80 μm. A second pair of identical sensors is glued back-to-back to the first pair at a stereo angle of 40 mrad around a thermo-mechanical base board [7] to provide space-points. The module strips are read out by 12 radiation-hard ABCD3TA front-end readout chips [8]. The readout ASIC's are integrated on a multi-layer Cu-polyimide flex circuit [9] and are connected to the silicon strips by wire bonding. The flex circuit is mounted above the silicon sensors of the barrel modules and at the end of the silicon sensors of the end-cap modules. The hit information is "binary": only the channel address of a hit strip is read out optically from each module side to the counting room; no analogue information of the signal is provided during normal running. The intrinsic spatial resolution in the sensor plane orthogonal to the strip direction is 23 μm.[2] Using the hit information from each module side, a space-point is constructed. The effective design measurement precision of the space-point measured per SCT layer is 17 μm in the $R\phi$-direction and 580 μm along the z-direction. The silicon sensors are maintained at a temperature around -7°C to minimise the effect of radiation damage. Mechanical and thermal performance parameters of barrel modules are summarised in [4].

The support structure of the SCT barrel consists of four concentric carbon-fibre reinforced plastic (CFRP) light-weight sandwich cylinders with integrated flanges at both ends. The four cylinders have 32, 40, 48 and 56 rows of 12 modules for barrels 3, 4, 5 and 6 respectively, with barrel 3 being the innermost barrel and barrel 6 the outermost. The modules are fastened directly

[1] The pseudorapidity is defined as $\eta = -\ln[\tan(\theta/2)]$, where θ denote the relative angle to the beam axis.

[2] The intrinsic resolution with binary readout is given through the strip pitch divided by $\sqrt{12}$. A slight improvement over this intrinsic resolution can be expected for hits with charge sharing.

2008 JINST 3 P10006

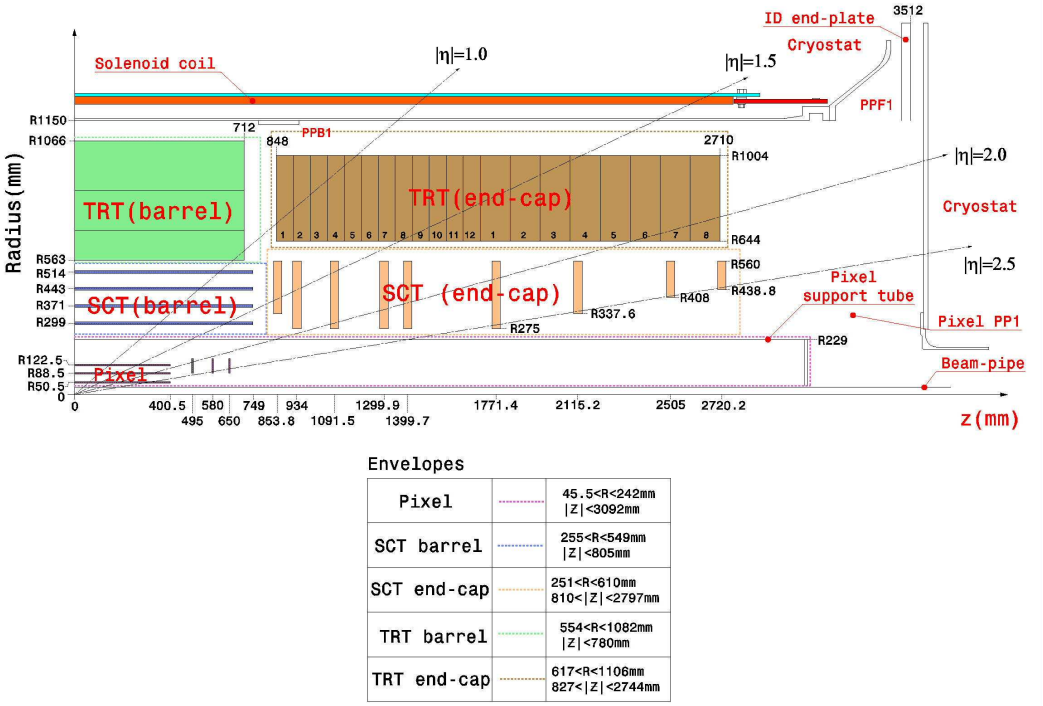

Figure 1. Schematic drawing of one of the quadrants of the ATLAS inner detector and SCT barrel and end-cap detectors.

via special brackets to machined pads bonded to the outside surface of the cylinder. The cylinders also offer support for the cooling circuits (see section 3.2), the harnesses servicing each module (see section 3.3) and the frequency scanning interferometry (FSI) position-monitoring system (see section 3.5). The full SCT barrel is enclosed in a thermal enclosure (TE) (see section 3.8), which separates the cold, ambient environment of the SCT from the room-temperature environment of the TRT. The TE also acts as a Faraday cage for the SCT barrel.

Every component of the SCT has to comply with stringent radiation hardness requirements. For the expected 10 years' lifetime for silicon components, this is estimated to be 2×10^{14} 1-MeV equivalent neutrons/cm^2 for non-ionising energy loss (NIEL) and 100 kGy(Si) of ionising energy loss. As the non-ionising energy loss is dominated by charged hadrons (pions and protons) at the radii of the SCT, many radiation-hardness tests were carried out at the CERN PS accelerator up to a fluence of 3×10^{14} 24-GeV protons/cm^2. Furthermore, all components are required to be non-magnetic as the SCT is located in a 2 T magnetic field.

The integration of the SCT barrel detector from single modules to the completed detector ready for installation within the ATLAS experiment has the following major steps:

1. Preparation of the four barrel support cylinders.

2. Assembly of services for cooling, FSI, powering and readout to the barrel support cylinder.

3. Mounting of modules to each barrel.

2008 JINST 3 P10006

4. Test of each complete single barrel.
5. Assembly of the four single barrels into each other and the thermal enclosure (TE).
6. Insertion of the completed SCT barrel into the TRT barrel.
7. Final test of the SCT barrel inside the TRT barrel and a combined test SCT + TRT with cosmic rays.

Details of assembly steps (1), (2) and (3) are summarised in section 3; steps (5) and (6) in section 4. The testing carried out in steps (4) and (7) is described in sections 5 and 6 respectively. Figure 2 shows a schematic flow chart of the assembly and integration process for the SCT barrel detector. An explanation of commonly used acronyms is given in appendix A.

The barrel support structures were prepared at the University of Geneva. The individual CFRP cylinders complete with module supports were sent to RAL[3] for service assembly to each barrel. From there, the cylinder was transported to Oxford University where modules were mounted to each cylinder to complete the single barrels. The single barrels where then transported to the CERN inner detector integration facility located in the ATLAS surface building, CERN-SR1. Detailed acceptance tests on single barrels were carried out in Oxford before transport and at CERN-SR1 after transport. After the completion of the tests, the four SCT barrels were assembled into each other and the thermal enclosure in CERN-SR1. The last integration step in CERN-SR1 was the insertion of the completed SCT barrel into the completed TRT barrel, and a combined test and cosmic-ray run with the SCT and TRT barrels. Following the final test of the combined SCT and TRT barrel in the inner detector integration facility, the two sub-detector sections were transported together to the experimental cavern. Once in the cavern, they were installed in the cryostat of the ATLAS liquid-argon calorimeter [2] as one physical object ready for cabling.

2. Material budget and barrel radiation length contributions

The performance requirements of the ATLAS inner detector are more stringent than any tracking detector built so far for operation at a hadron collider. The conflicting requirements of good mechanical stability, low mass and, at the same time, high detector granularity with its associated on-detector electronics, readout services and cooling within a small detector volume, make the overall weight and material budget (in terms of radiation length X_0 and interaction length λ_I) much larger than for previous tracking detectors.

A detailed simulation of the ID has been made. Figure 3 shows a map of generated photon conversion vertices in the ID volume for electrons with $p_T \geq 0.5\,\text{GeV}$ from photons originating at the primary vertex in minimum bias events. The figure shows the location of conversions, integrated over azimuth, with their radial (R) and axial (z) coordinate. The integration over the top half of the detector is displayed as "positive" radius, the integration over the bottom half is displayed as "negative" radius. The figure corresponds to a sample of 500,000 simulated events. The SCT barrel and disk layers are clearly recognisable. It should be noted that many structural elements, for example the end-plates of both the barrel and end-cap, are azimuthally discrete and have been modelled accurately.

[3]Rutherford Appleton Laboratory, Science and Technology Facilities Council, Didcot, OX11 0QX, UK.

2008 JINST 3 P10006

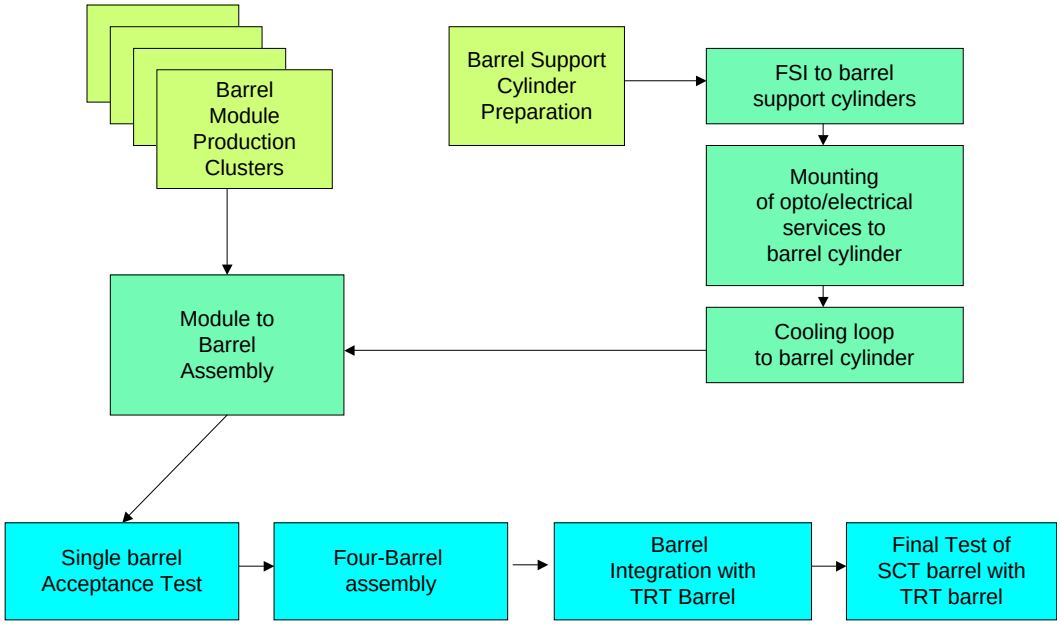

Figure 2. Flow chart of the assembly and integration process for the SCT barrel detector.

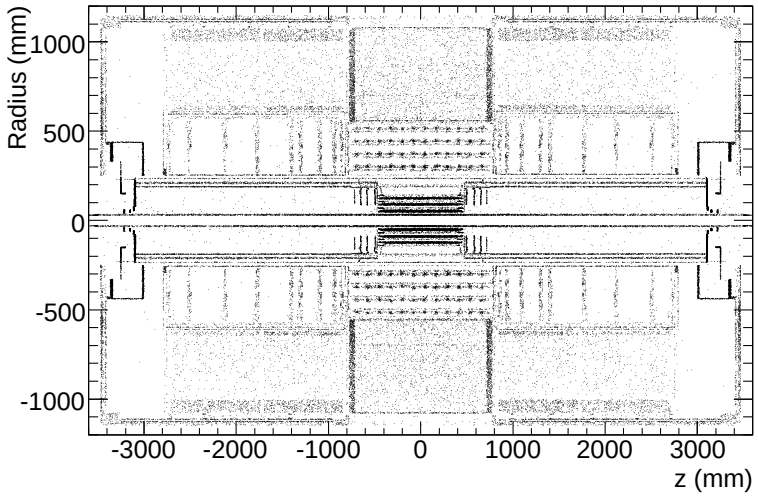

Figure 3. Mapping of photon conversions as a function of z and radius, integrated over ϕ, for the ID. The mapping has been made from 500,000 simulated minimum bias events using ~90,000 conversion electrons of $p_T \geq 0.5$ GeV originating from primary photons.

Figures 4 and 5 show the integrated X_0 and λ_I traversed by a straight track as a function of $|\eta|$ at the exit of the ID envelope. The SCT contribution is shown in this figure. A striking feature is the onset of material from non-active services and structures at the interface of the SCT barrel and

2008 JINST 3 P10006

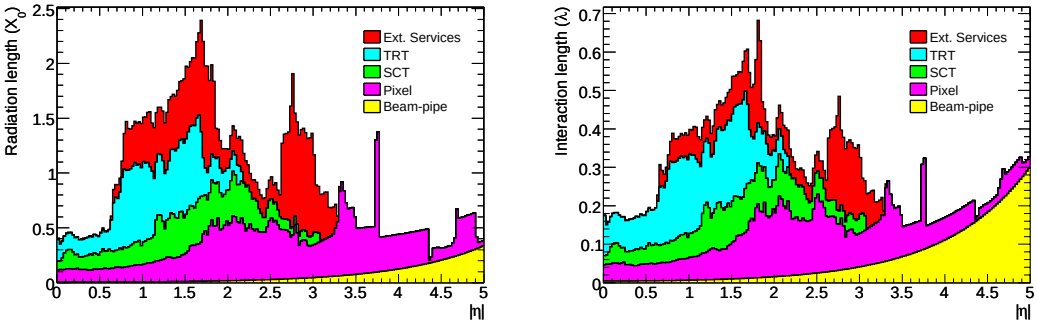

Figure 4. Material distribution (X_0, λ_I) at the exit of the ID envelope, including the services and thermal enclosure. The distribution is shown as a function of $|\eta|$, averaged over ϕ. The breakdown indicates the contribution of external services, individual sub-detectors including the SCT, and services in their active volume.

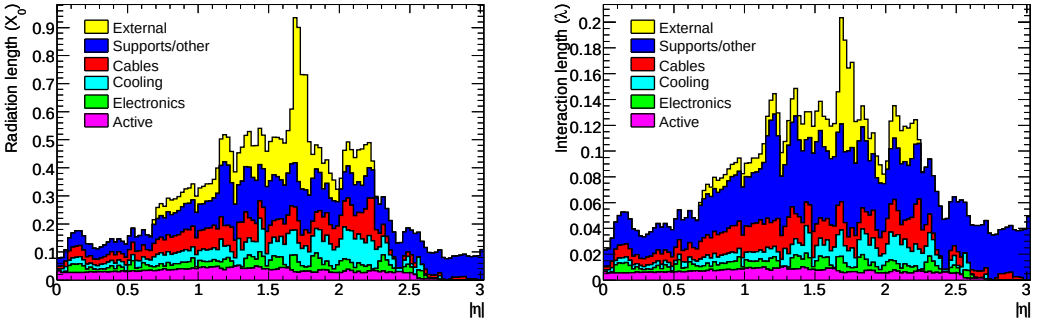

Figure 5. Material contribution (X_0, λ_I) of the SCT barrel and end-caps. The distribution is shown as a function of $|\eta|$, averaged over ϕ. The breakdown shows the contribution of different SCT components.

end-cap regions. This includes cooling connections at the end of the SCT barrel, and SCT barrel services extending radially to the PP1 patch-panel connection box on the cryostat and then along the cryostat wall. A large fraction of the service and structural material is external to the active ID envelope, therefore preserving the tracking performance.

The consequences of the material's overall radiation length and interaction length in the Inner Detector are quite serious:

a) Many electrons lose most of their energy through Bremsstrahlung before reaching the electromagnetic calorimeter.

b) Approximately 40% of photons convert into an electron-positron pair before reaching the liquid-argon cryostat and the electromagnetic calorimeter.

c) Even in the case of low-energy charged pions, a significant fraction will undergo an inelastic hadronic interaction inside the inner detector volume.

For incident tracks at $|\eta|$=0, the total X_0 of the SCT barrel is 8.6%. When averaged over the active area, the total X_0 of the barrel layers becomes 11.8% (2.96% per layer including 1.33% for

2008 JINST 3 P10006

Table 2. Bottom-up measurement of individual components of the SCT barrels, before and after detector installation. The pre-integration weight includes modules, the barrel structure and services excluding the cooling fluid, and off-detector services including the cooling capillaries, the thermal enclosure and the barrel interlinks. The on-barrel laser alignment, estimated as 2 kg, is not included. The post-integration weight includes services up to the PP1 patch panels. In principle, the simulations should agree with the post-integration weight.

Component	**Weight (kg) from component measurements**				
	Barrel 3	Barrel 4	Barrel 5	Barrel 6	Total
Modules	9.578	11.875	14.250	16.625	52.26
Cylinder Flanges Brackets	5.710	8.175	9.102	10.738	33.73
Cooling Services	3.068	3.864	4.692	5.510	17.14
Remove coolant					-2.708
Electrical Services	5.186	5.575	7.786	9.085	27.81
Total					128.23
	Off-barrel services and structure				58.44
	Estimated pre-integration weight (kg)				186.7±5
	Estimated post-integration weight (kg)				222±6
	Measured weight (kg)				201±20
	Simulation post-integration weight (kg)				222

modules, 1.15% for services and 0.48% for the support structure). The module budget includes sensors (0.61%), hybrids (0.22%), module extension flexible circuit and baseboards. Services include the electrical services, cooling blocks and pipes. Off-barrel or off-disk services, especially at the interface between the barrels and end-caps, and items such as the thermal enclosures, are not included.

A check has been made on the assumed SCT material by comparing its measured weight with a bottom-up inventory of the SCT components. Table 2 shows the status of that comparison. There is good agreement between the measured and estimated weights of the barrel sub-detectors and their services.

3. Assembly of single barrels

This section summarises the assembly of single barrels, starting with the preparation of barrel support cylinders, the integration of services on the cylinder and finally the mounting of SCT barrel modules on the cylinder to complete the single SCT barrels.

2008 JINST 3 P10006

3.1 Barrel cylinders and module support

3.1.1 Design of the barrel cylinder

Highly demanding specifications in term of precision, dimensional stability and material budget [3] led to the choice of carbon fibre reinforced plastic (CFRP) sandwich structures. Simulations and tests were performed to optimise the structural design and to evaluate different concepts to support the detector modules. In parallel, candidate materials were investigated and tested. Finally the decision was made to mount the modules directly onto four concentric cylindrical structures without intermediate local support. For the cylinders themselves, the choice was to use a sandwich-type construction with very thin skins over a CFRP honeycomb core. Each cylinder was reinforced with a CFRP flange at each end; this also allowed the implementation of the fixation points for connecting the four cylinders with radial CFRP interlinks. The fibre-resin system chosen is based on a cyanate ester resin (RS-3) and high-modulus carbon fibres (YSH50A). This product was delivered in 3K unidirectional prepreg form from YLA.[4] The CFRP honeycomb chosen is Ultracor UCF-83-1/4-3.0 from Ultracor.[5] To achieve high mounting precision, PEEK pads were bonded to the outside surface of the CFRP cylinders and machined, thus offering precise mounting points for the brackets supporting the modules (see section 3.1.4) and opto components. The inner surface of the cylinder is equipped with frequency scanning interferometry (FSI) components.

3.1.2 Manufacturing of the cylinders

After completion of the design, a prototype cylinder was produced. This work was subcontracted to CASA.[6] The prototype was completed in 1998 and submitted to thermal expansion measurements in the manufacturer's plant. Further tests were made at the University of Geneva to develop the techniques to bond and machine the PEEK module bracket attachment (MBA) pads designed to receive the module-mounting brackets. In parallel, for the fabrication of the four barrel cylinders, specifications and production drawings were issued, reviewed, and possible manufacturers were qualified with criteria described in the CERN market survey MS2434/PPE. After a production readiness review, a call for tender was made and finally the contract was awarded to Astrium.[7] This company used the proposed carbon fibre resin system and subcontracted the machining to a specialised company, WEKON.[8] Machining was done in a temperature-controlled workshop. The preparatory steps were as follows:

- The lay-up of the three layers of unidirectional (UD) prepreg forming the inner-cylinder facing on a mandrel.
- The addition of preformed honeycomb panels to it, spliced at the junction of honeycomb panels and at both ends of the cylinder.
- The addition of three layers of UD prepreg forming the outer facing.

[4] YLA Inc, 94510 Benicia, CA, USA.
[5] Ultracor Inc, 94551 Livermore CA, USA; previously YLA Cellular Products, USA.
[6] CASA Alvarez Division Espacio 28022, Madrid, Spain.
[7] EADS Astrium GmbH - Friedrichshafen, D-88090 Immenstaad, Germany.
[8] WEKON Heinz Schnedler GmbH, D-61185 Rosbach, Germany.

2008 JINST 3 P10006

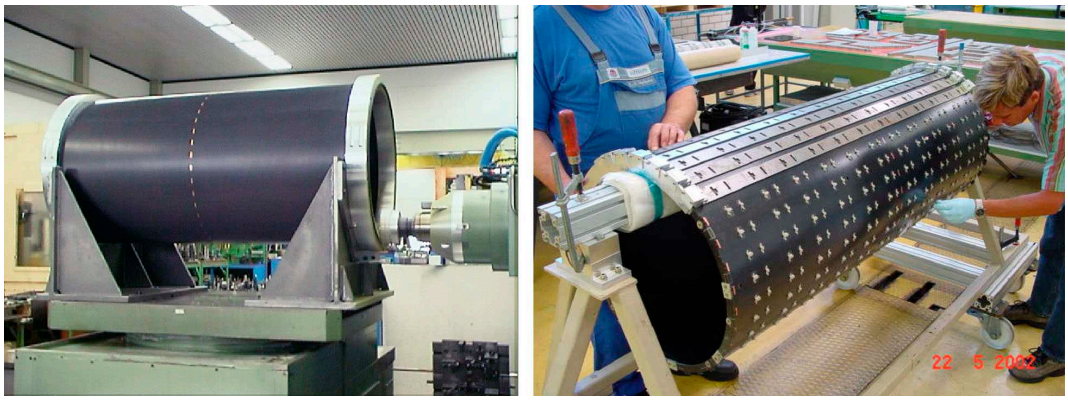

Figure 6. Machining of the delivered cylinder (left) and bonding on module bracket pads to barrel 3 (right).

- The addition of thin metal sheets and vacuum bags.

The cylinder was then cured in an autoclave at 180°C. After removal from the mandrel, the cylinder length was machined and the geometry of each cylinder measured. In parallel, the flanges were laminated on a special mandrel and cured in an autoclave. Bending and ultrasonic tests were performed to verify the integrity of the sandwich, and the flanges were bonded to the cylinders. This was followed by another bending test and the machining of the end faces of the flanges. The module-bracket attachment pads were positioned with guides and bonded to the outer skin of the cylinder. After curing, the final machining of the pads was performed and the cylinders were ready for the final metrology before acceptance. This was done by Messtronik.[9] Finally, the first cylinder (barrel 3) was delivered to CERN in October 2002 and the last one (barrel 4) in March 2003. Figure 6 shows the CFRP cylinder during milling (left) and during the bonding of module bracket pads (right).

During manufacture and machining, the following problems were encountered: The flanges turned out to be far more labour intensive to manufacture than expected and during machining, it was difficult to fasten the cylinders onto the machine without inducing distortions. Finally, a few pads were broken during machining and had to be re-bonded in situ on the milling machine.

3.1.3 Preparation of cylinders and measurements

Following delivery of each cylinder, the excess of adhesive was removed and cleaned. The functionality of the service clips integrated into the bonded pads, which later hold the opto and electrical services in place, was verified. A dry assembly of three of the four cylinders together with temporary interlinks was performed to cross-check their assembly (figure 7). For schedule reasons, the four cylinders were never available together at the same place before their final assembly at CERN.

With barrels 3 and 6 already at RAL for service assembly, it was discovered that a few module-bracket pads had become de-bonded. It was decided to reinforce all pads with miniature M1 stainless-steel screws, bolting the pads through the CFRP sandwich into a special light PEEK mushroom plug. After pad reinforcement, the cylinders were equipped with the module-support

[9]Messtronik Weisser GmbH Prüflabor, D-78112 St. Georgen, Germany.

2008 JINST 3 P10006

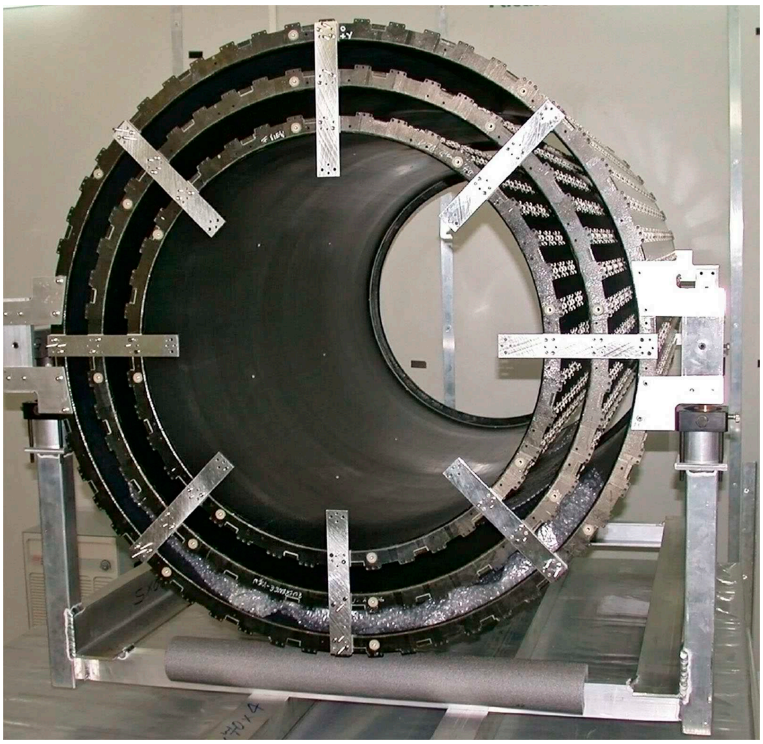

Figure 7. Test assembly of three completed cylinders.

bracketry and some FSI components on their inside surface before being packed in containers and shipped to RAL for the continuation of the work.

3.1.4 Design and integration of module supports on cylinder

Hermetic coverage of the barrel surfaces with sensors is achieved by mounting modules with overlapping detector edges. To achieve overlaps in ϕ and reduce the effects of the Lorentz angle, the modules are inclined by 11° in barrels 3 and 4 and 11.5° in barrels 5 and 6 with respect to the tangential plane. Figure 8 shows the module inclination and overlap between adjacent rows of modules. The module in figure 8 is shown while being inserted into its final position: it has been inserted into the third mounting point (PEEK spring clamp) at the left edge but has not yet made contact with the cooling block.

Overlap of modules along the *z*-axis (the axial direction of the cylinder) was achieved by staggering the modules in the radial direction by 2.8 mm, by using high or low brackets for alternate rings of modules. The module overlap in the *z*-direction was calculated to have full overlap for tracks with $p_T > 1\,\mathrm{GeV}$ originating from within 2σ of the nominal interaction point. Figure 9 shows a mechanical-grade module used for test assembly and mounted onto a module-support bracket on a cylinder. The module is positioned by two mounting bushes in one bracket (top of figure 9) and a third (sliding) mounting point on the bracket in the adjacent row (bottom of figure 9).

The choice was made to support each module via a CFRP bracket precisely located and bolted onto PEEK pads bonded to the cylinders. A further third point was added to offer a stiffer and more

2008 JINST 3 P10006

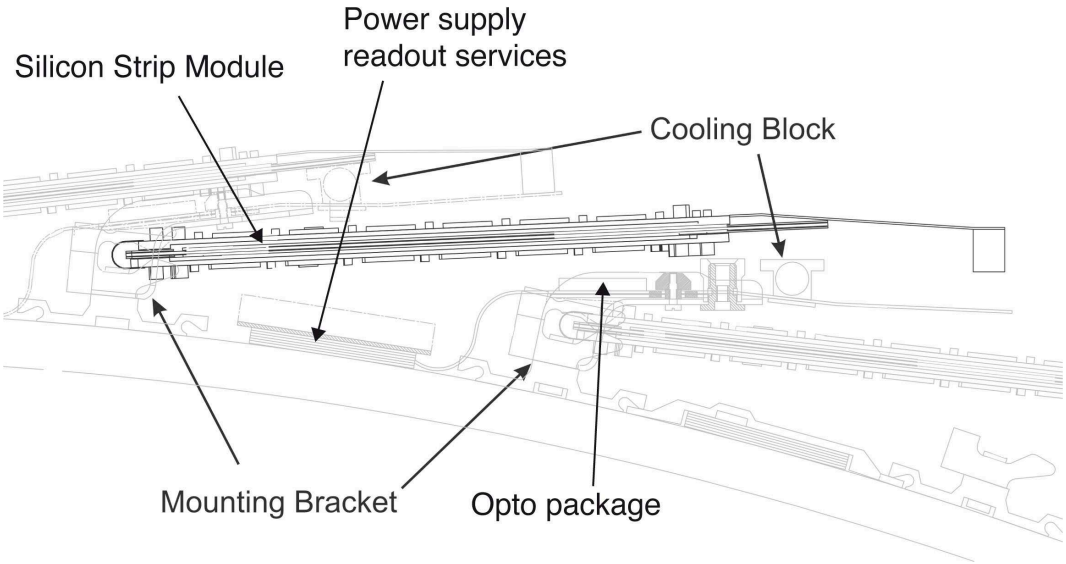

Figure 8. Cross-section of the insertion of a module (dark) into a barrel. Existing parts of the barrel (brackets, services and mounted modules) are in a lighter grey.

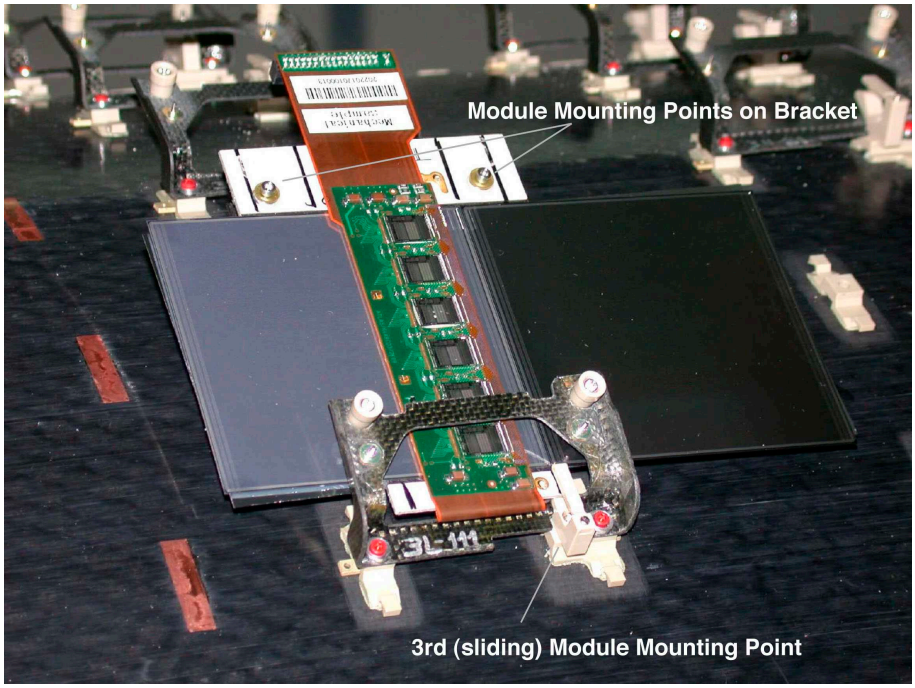

Figure 9. Mechanical-grade module mounted on a support bracket.

precise fixation of the other side of the module. Several options were considered for the bracket production. The limited volume available, the small clearances and specific requirement of each barrel required eight different bracket types (two per barrel) with a total of 2112 brackets. Finally, a plastic molded version was abandoned in favour of a CFRP-laminated, parylene-coated bracket, shown in figure 10.

2008 JINST 3 P10006

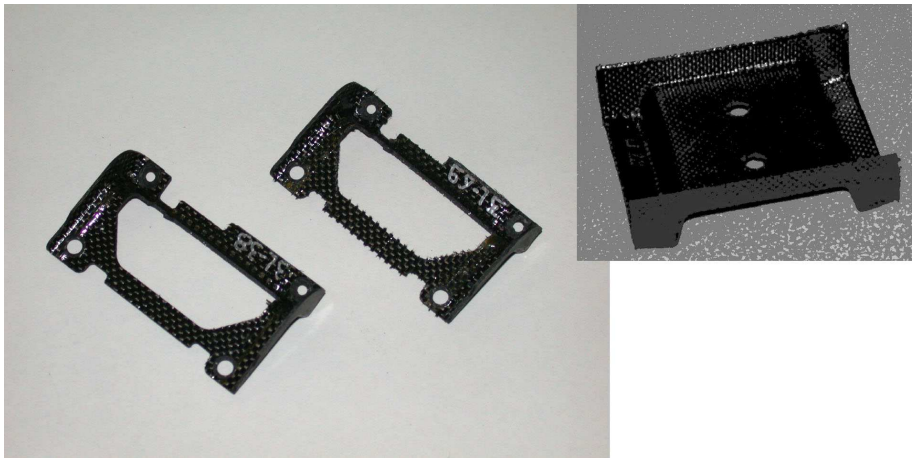

Figure 10. Module-support brackets during manufacture.

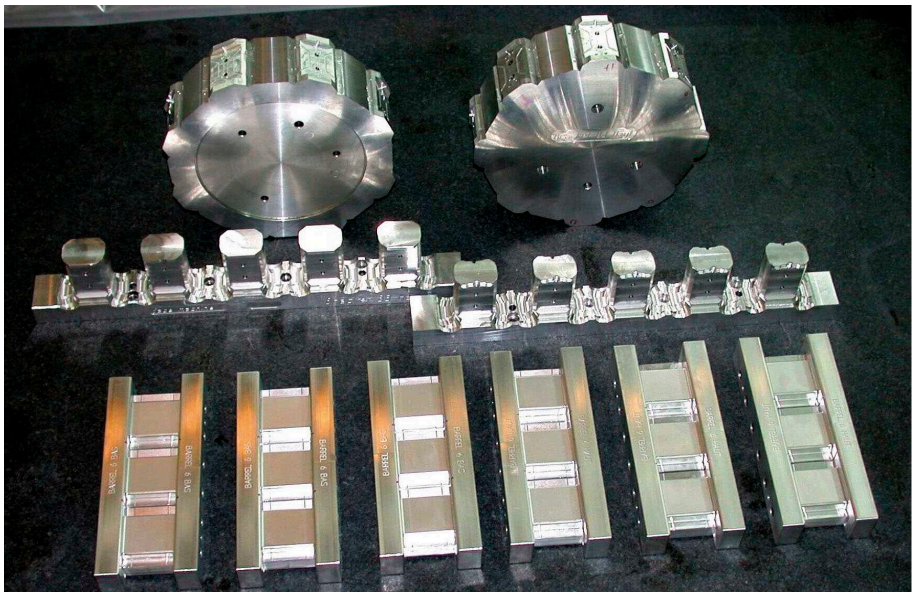

Figure 11. Tools and jigs for bracket production: the six molds, each allowing the lamination of three shells, and the contouring and finishing jigs to support the bracket during machining.

These CFRP brackets offered the benefit of better performance at lower mass but were complicated to produce. After a few trials, a 5-ply molded laminate of T300/RS-3C 1K PW fabric prepreg (from YLA) in a 0°/45°/0°/45°/0° lay-up was chosen.

After the bracket design and production drawings were completed the production method was developed in collaboration with Composite Design.[10] Prepregs were cut to shape with templates and laid up in the molds. Silicon pressure parts were added and the mold was then vacuum-bagged and the laminate cured in autoclave at 180°C. All the tools and jigs for the different operations of the bracket machining (figure 11) were developed and produced using 3D CAD transfer between the design office and the workshop. The shells were later machined to become brackets and sent to

[10]Composite Design, CH-1026 Echandens, Switzerland.

2008 JINST 3 P10006

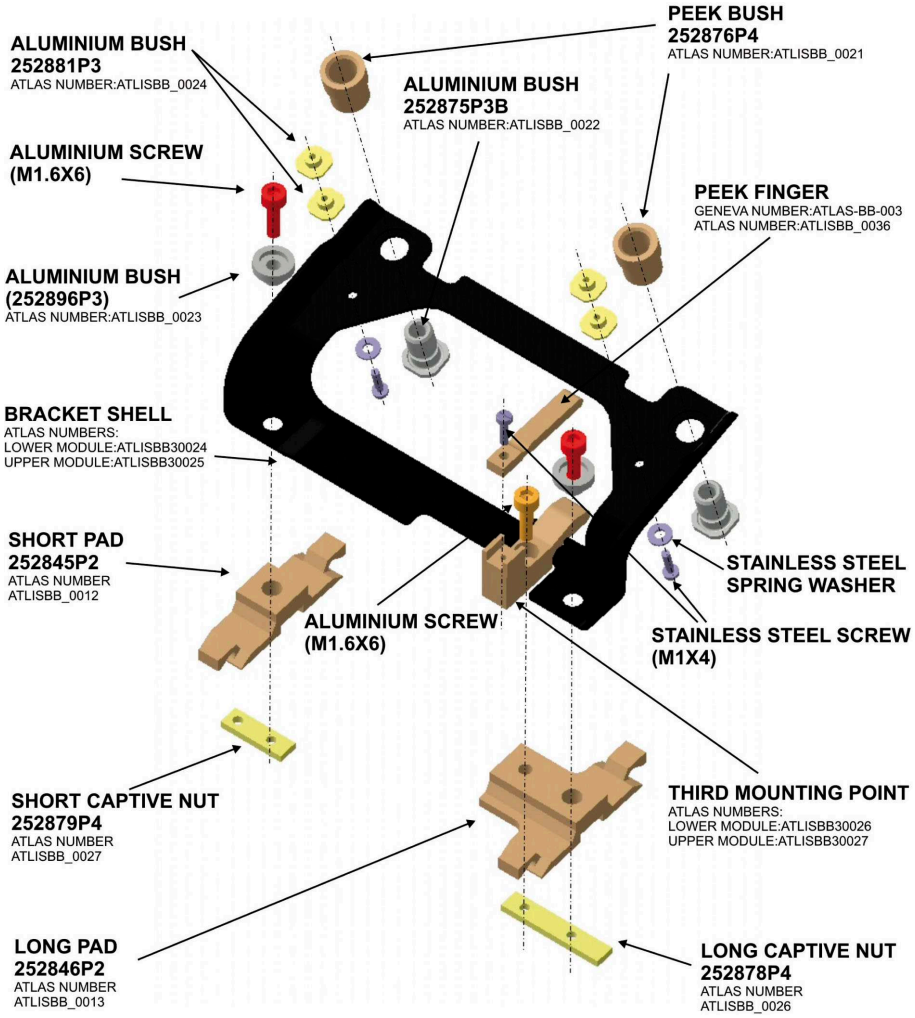

Figure 12. Bracket and small components for fastening modules and services onto the SCT cylinder.

COMELEC[11] to be parylene coated. Then the brackets were equipped with small components, as shown in figure 12, and they were mounted in position by means of screws and centring bushes on the barrels. Figure 13 shows a completed cylinder with module supports ready to be shipped for services mounting.

3.2 Barrel cooling

3.2.1 Description of the SCT cooling system

The ATLAS pixel and SCT detectors are cooled with an evaporative fluorocarbon system, designed to minimise the material in the detector volume, maintain a low temperature on the detector and keep the inlet and outlet tubes at room temperature. The selected refrigerant, C_3F_8, is non-flammable, non-conductive and radiation resistant [12, 13]. It has a good heat-transfer coefficient

[11] COMELEC, CH-2300 La Chaux de Fonds, Switzerland.

2008 JINST 3 P10006

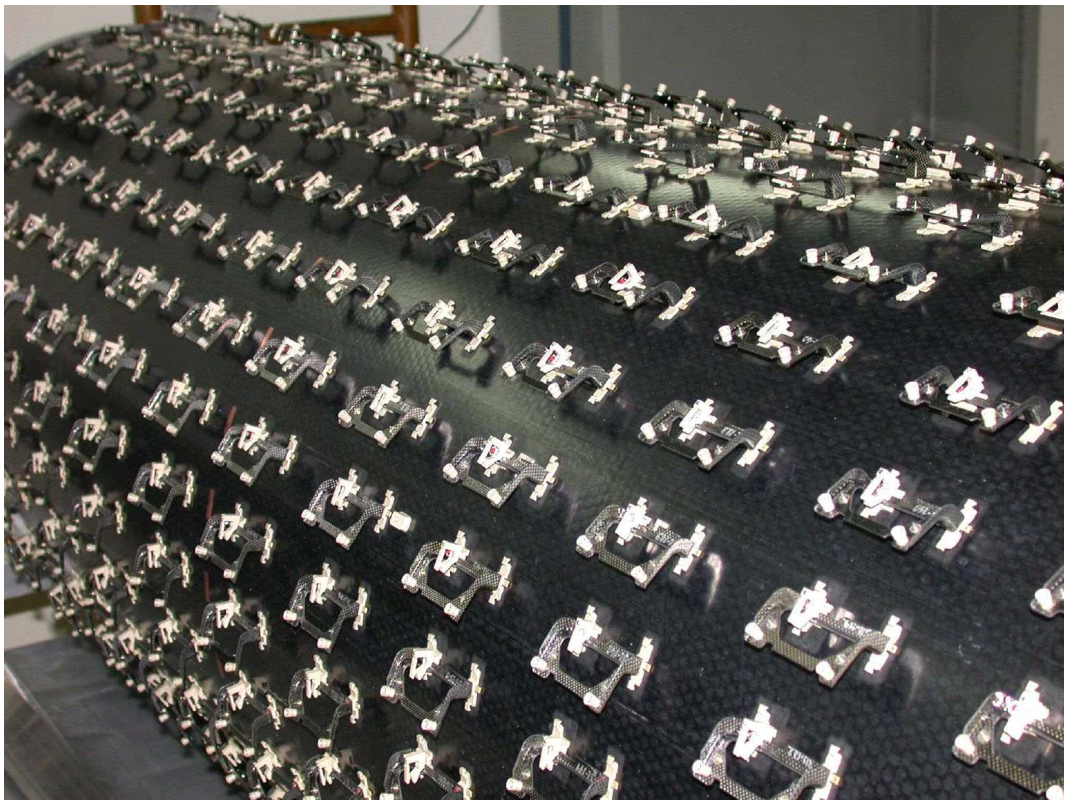

Figure 13. Barrel support cylinder complete with module support brackets.

and a small vapour specific volume allowing minimal tube sizes. The total cooling power required is 62.4 kW for the pixel and SCT detectors. The scope of the evaporative cooling system is to cool the detectors, maintaining the maximum temperature of the silicon sensors at -7°C by operating the cooling system at a minimum evaporation temperature of -25°C. This requirement applies to the fully irradiated sensors and electronics and allows the effect of the radiation damage to be minimised and the detector to survive at least ten years of operation. During the initial operation, when the detectors are only mildly irradiated, this requirement is less stringent and the acceptable temperature may be significantly higher than -7°C. Testing in CERN-SR1 was carried out with cooling-pipe temperatures around $+13^{\circ}$C and these same conditions will be used for the initial operation in ATLAS. Details of the cooling plant and its control systems can be found in [14] and a schematic view of the system is given in figure 14. The technical specifications for the inner detector cooling are available in [15].

The barrel is divided into 44 almost identical cooling-loops. Each loop cools 48 modules, so for example, barrel 6 supports 14 loops cooling 672 modules. Figure 15 shows a barrel cooling-loop with its two inlets on the left (at the top and the bottom) and the exhaust connector in between the inlet connectors. The incoming coolant arrives at the detector under high pressure at room temperature. The coolant to each loop is pre-cooled by the passage through a heat exchanger (HEX). This facilitates the flow of heat from the incoming warm liquid to the colder, returning vapour/liquid mixture. Pre-cooling allows for increased cooling capacity at a given coolant mass

2008 JINST 3 P10006

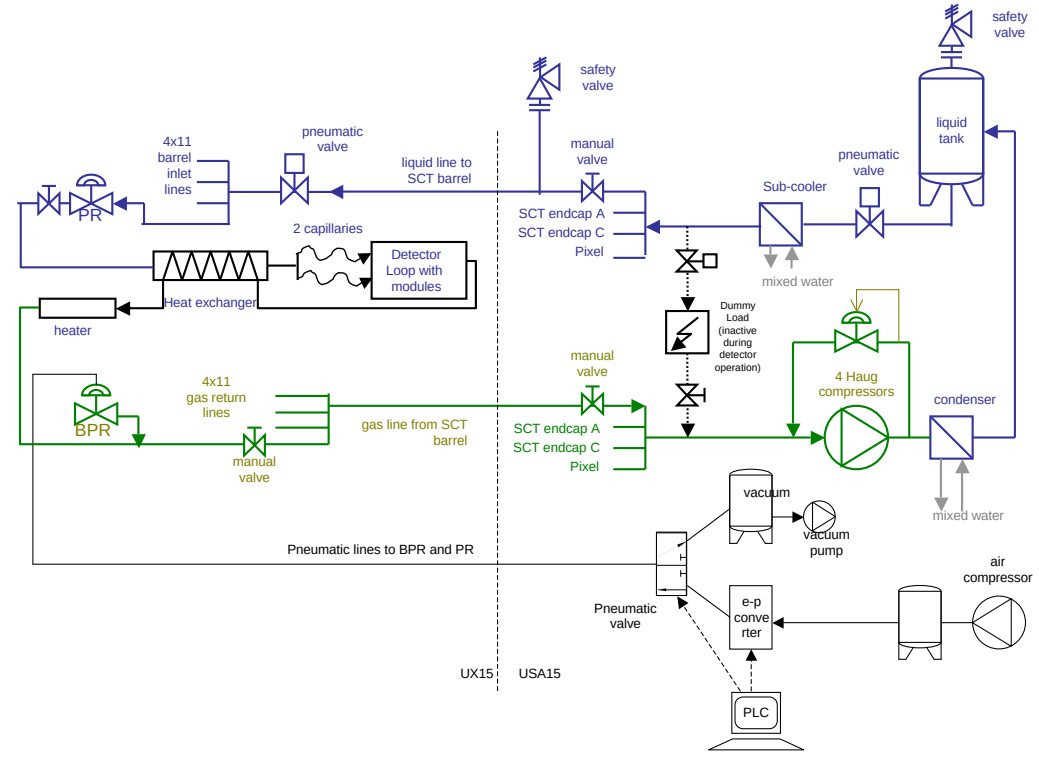

Figure 14. Internal and external parts of the inner detector evaporative cooling system in a simplified schematic.

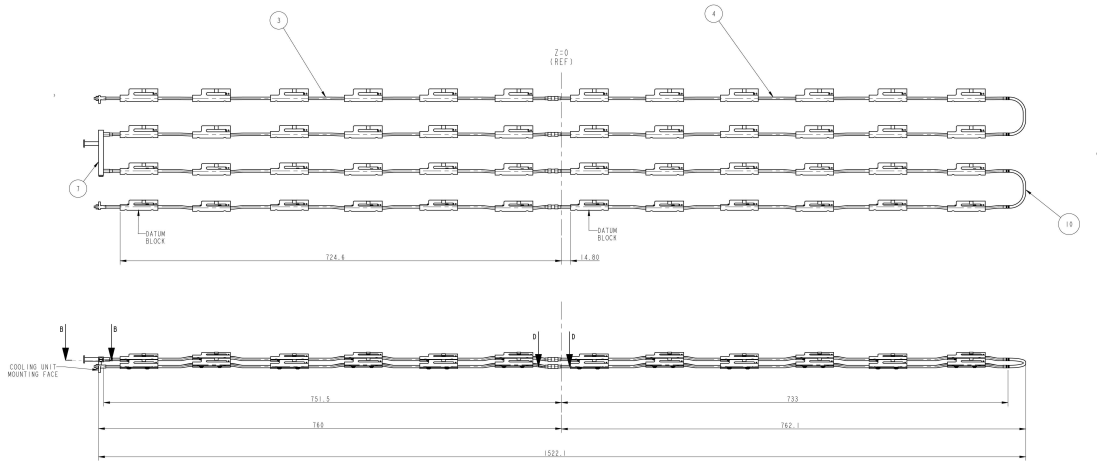

Figure 15. Drawing of a barrel cooling-loop.

flow. The inlet splits into two 0.76 mm inner-diameter annealed cupro-nickel (Cu-Ni) capillaries. Each capillary has been trimmed to give an identical mass flow at a standard pressure (∼5.5 g/sec at absolute pressure of 13.0 bar(a)).[12] The final trimmed length ranges from 650 to 750 mm, with

[12] In the following pressure values are given as absolute pressures denoted as “bar(a)”.

2008 JINST 3 P10006

a mean value of just below 720 mm. The two capillaries on each loop are connected through custom-made Cu-Ni connectors using a 0.6 mm indium-wire compression-seal. The returning liquid/vapour mixture is removed via a single exhaust manifold, again sealed with an indium-wire gasket of 0.8 mm diameter wire. The back-pressure on the exhaust can be set remotely with a pressure regulator to allow the adjustment of the cooling temperature.

3.2.2 Design of the cooling-loops

The cooling-loops on the barrel transport the coolant along the module row underneath the module mounting surface. At each module location, a cooling block is attached to the cooling-loop with an optimised cooling contact surface between the pipe and module. The coolant enters the loop on one barrel end, follows the module row to the other barrel end, where the pipe turns around to the adjacent module row and flows in the adjacent module row back to the barrel end where it entered.

The candidate tube materials were aluminium alloy, austenitic stainless steel and cupro-nickel (Cu/Ni 70:30). The final decision was based on a desire to reduce the total material budget, to avoid risks of corrosion in the cooling components and to provide a relatively simple and flexible assembly technique. To withstand 25 bar without permanent deformation, aluminium would require a wall thickness of around 250 μm. A Cu-Ni pipe offering the same radiation length would have a wall thickness of only about 40 μm. For stainless steel, the number would rise to 50 μm. Cu-Ni was selected because it offered excellent corrosion resistance and ease of fabrication. A wall thickness of 70 μm was chosen for the final production, despite the penalty of an increased radiation-length budget. This was because leaks were discovered in early, thinner samples of this material when they were tested after the annealing process. The origin of these leaks was traced to the grain growth that is observed in copper-based alloys undergoing annealing. The recommendations from the relevant ASTM code[13] led to the conclusion that at least three grain thicknesses were needed in any tube wall. In the worst case, this implied a wall thickness of 70 μm.

The cooling-loops were manufactured from non-magnetic material with a high degree of resistance to both corrosion and radiation damage. The circuits were designed for an evaporation temperature of -25°C, corresponding to an evaporation pressure of 1.67 bar(a). The minimum pressure in the liquid part of the circuit is driven by the need to operate above the saturation point. At 40°C the saturation pressure is 12.8 bar(a); 13 bar(a) is then set as the minimum pressure in the inlet circuit at the inlet of the capillary. The additional pressure drop between the plant and the capillaries is around 3 bar. Therefore, the maximum pressure at the outlet of the liquid pump of the cooling plant is 16 bar. This defines the proof-pressure test required for the downstream components. It is generally accepted that a proof-pressure test >1.5 times the maximum applicable pressure should be applied for at least 30 seconds. The figure used was rounded up to 25 bar(a).

3.2.3 Production of cooling-loops, capillaries and interconnects

The cooling-loops were assembled from identical "6-block sections". These were fabricated by first annealing the pipe and then leak testing. The pipe was then bent in a series of machined jigs to provide three module cooling-block locations aligned to one (upper) module plane and a further three positions set to the lower module plane. The aluminium alloy[14] cooling blocks were made

[13] ASTM E1382-97.

[14] BS 1470 / 5083.

2008 JINST 3 P10006

as split halves and were plated with Ni/Cu/Au (3 μm, 12 μm, 0.5 μm respectively). They were soft-soldered using a tin-lead solder[15] and a suitable flux.[16]

The control of the height difference between the upper and lower module cooling blocks is critical to maintaining good thermal contact between the module and the block. This was achieved by machining the step height to the correct value after the upper and lower parts of the block were fixed to the pipe. The step height was checked in a jig with glass microscope slides set with the appropriate step height acting as modules. A small amount of dilute ink was smeared onto the slides and the 6-block cooling-loop section was offered from below. In the case of good step heights the loop is held by surface tension. Any gaps or twists in the loop are easily seen as a void in the otherwise uniform layer of ink.

Each module block served the dual purpose of cooling both the module and the associated opto-flex, as described in section 3.3. The dimensions of the surface of the cooling block used for the thermal contact to the module are 8 mm by 62 mm. As mentioned earlier, the thermal interface between both the module and opto-flex and the cooling block is a sliding one, by nature of its design. To allow for a sliding contact between the cooling block and the module, thermal grease was applied to the cooling block.[17] It was essential to test that this displacement did not have a detrimental effect on the module-position stability. This was answered by mounting mechanically and thermally accurate, non-functional modules on a prototype sector of an ATLAS SCT support cylinder complete with brackets, opto harnesses and a cooling-loop. The entire structure was mounted inside a large freezer so that the cooling-loop could be operated in an ambient temperature of around -7°C. Then the mechanical modules were mounted with precision cubes whose displacements could be measured by capacitive probes. The largest displacements (10-70 μm) observed were in the R-direction (radial) and were caused, principally, by the capacitive probe support. In the z- and ϕ-directions, the displacements were always $<$10 μm.

After each 6-block section was completed, the cooling-block faces were re-machined to eliminate any distortions caused by soldering. The assembly of a complete loop involved mounting eight 6-block sections into a jig and connecting them with short Cu-Ni pipes whose ends were swaged to allow insertion of the 6-block sections. Two "U-bends" were added in a similar way and each joint was soldered to complete the loop. The assembly jig ensured that the cooling-block faces maintained their planarity and positional accuracy. The exhaust manifolds were fabricated using the same alloy and plating as the cooling blocks. Figure 15 shows the drawing of a completed cooling-loop. In many cases, the manifolds had to be designed to access a space among the other barrel services. The final step was to solder the exhaust manifolds and inlet connectors into place and to attach Litz wire ground connections to each exhaust and U-bend. These Litz wires would be soldered to the cooling reference disks (CRD). The CRD serves as a common grounding plane at the barrel ends and is made from 25 μm copper-plated polyimide. During the four-barrel integration, the cooling-loop Litz wires were soldered to the CRD to reference electrically the cooling-loops to ground.

[15] BS 219 Sn/Pb 60:40.

[16] Castolin Eutectic 197c.

[17] Dow Corning DC340

2008 JINST 3 P10006

3.3 Power supply and readout services

3.3.1 Electrical and optical services

The electrical power distribution has to provide all the low and high voltages and DC control lines to operate the SCT modules and the associated opto-electronics. Also there are two temperature sensing signals for each module, carried on the electrical distribution system back to the temperature-sensing circuitry in the power supply units. The SCT power supply and distribution systems are described in [10]. The optical links read out the data from each module and provide the timing, trigger and control (TTC) data to each module. The SCT optical links are described in [11].

In order to design a hermetic detector with a minimal area of silicon, there is very limited space available for the optical and electrical services and their contribution to the total detector radiation length needs to be minimised. Due to these severe space and material constraints, the electrical power distribution from the local patch panels (PPB1) to each barrel detector module is incorporated within harnesses together with the opto transmission. In order to reduce the radiation-length budget, the electrical power is distributed using low-mass tapes (LMT's) made of 50 μm thick aluminium conductors on polyimide. The LMT's are connected to the modules with copper-polyimide opto-flex circuits [11]. Furthermore, the heat dissipated by the on-detector opto-electronics has to be transported efficiently to the cooling system so as to avoid excess heating of the silicon detectors.

3.3.2 Mechanical and thermal interfaces

The vertical clearance from the opto-package to the neighbouring module is only 1.39 mm. This clearance is critical to avoid damage to exposed wire bonds on the modules. Therefore the thicknesses were measured at several stages during the assembly of the opto-package and opto-flex circuit.

In order to minimise the pick-up by the module of any electrical noise on the cooling block, a shunt-shield flexible circuit was used over the cooling block. To optimise the capacitive shielding, a small overhang of 1 mm was added to the shunt shield. This also had the benefit of providing extra protection against HV breakdown between the module and the cooling block. The shunt shield was made from 18 μm copper on 25 μm polyimide and was connected to the analogue ground of the module by a 4-pin electrical connector. The option of changing the grounding scheme to connect the cooling block to the module analogue ground was made available by a tab which could be connected to the cooling block by an M1.6 aluminium screw; however, this connection was never required. The thermal impedance of the shunt shield has to be minimised in order not to increase significantly the temperature difference between the cooling block and the module. To this end, the shunt shields were attached to the cooling blocks with 20 μm of boron-nitride loaded epoxy.

The power consumption of the opto-electronics for one module is 360 mW. In order to avoid heating the silicon detectors, the opto-flex has to be in thermal contact with the cooling block. However, when the detector is cooled down, the cooling blocks move by distances of up to 1 mm. Therefore, the thermal connection was made using thermally-conductive grease[18] to allow for a sliding grease joint. A specially designed PEEK clip was used to ensure that the opto-flex kept good thermal contact with the cooling block. In order to optimise the thermal impedance from the

[18] Dow Corning DC340

2008 JINST 3 P10006

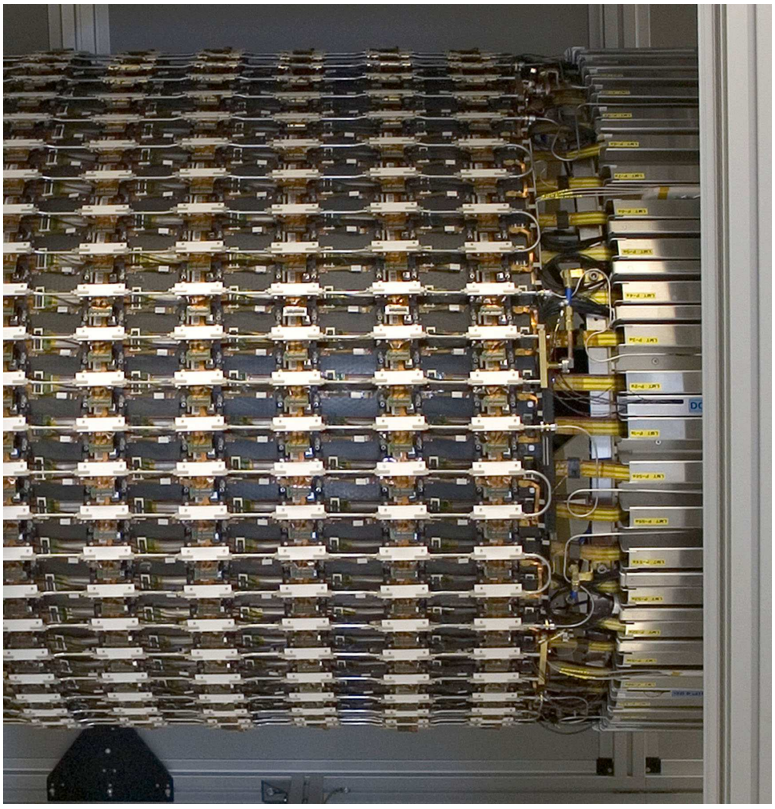

Figure 16. Part of the assembled barrel 6 before module mounting.

opto-electronics to the cooling block, an aluminium-nitride (AlN) ceramic stiffener was glued on the opto-flex underneath the opto-electronics. In addition, thermal vias were used to enhance the thermal conduction from the opto-electronics to the AlN stiffener.

Figure 16 shows part of the assembled barrel 6 with harnesses and cooling-loops mounted to the support cylinder. On the right edge of the photograph the service cage can be seen, which supports the patch panels during the assembly.

3.4 Integration of harnesses and cooling-loops

3.4.1 Harness to barrel integration

To minimise the number of connection cycles made with final patch-panel connectors and to protect the patch panel itself, a temporary patch panel (TPP) was connected to the final patch panel and together they were positioned in an aluminium support. Therefore, any test involving the connection to the harness, e.g. subsequent module tests, only used the temporary patch panels for outside connection.

Prior to installation, the electrical continuity and proper function of a complete harness, servicing six modules in a row, was tested as described in [11]. The harness was positioned on the barrel and secured with PEEK service clamps which lock into the module bracket pads. Fibres were carefully routed to the barrel ends, respecting their minimal bending-radius, and secured with PEEK fibre clips. After installation, the harness was retested. As a final check mechanical “enve-

2008 JINST 3 P10006

lope" modules were mounted on each location to verify the clearances. The clearance at the end of the barrel, allowing for all the tolerances, was calculated to be 1.8 mm. Therefore, the thickness of the LMT's and the total height of the stacks of six LMT's were checked during the assembly.

The weight of the patch panels at the end of the harness was supported by a temporary service support-cage. Excess lengths of fibres and LMT's were stored in dedicated slots of the service support-cage. Patch panels were positioned such that all connectors on patch panels and fibres were accessible for future tests of the single barrels.

3.4.2 Cooling-loop to barrel integration

The first cooling-loop assembly step was to fit the barrel-end cooling loop. Mounting brackets were fitted to the barrel flange using countersunk screws. For barrel 6, a combined bearing and bracket was used. Visual inspection was carried out to check that the mounting holes were clear and that the brackets were square to the barrel surface. This inspection also ensured that all harnesses were correctly located under their clamps. Next, the cooling-loop installation frame guides were mounted on the barrel ends and a check made to ensure that the cooling-loop installation frame could be correctly located into them. A cooling-loop installation frame was required during loop manipulation because the cooling-loops are not self-supporting.

All loops had been helium leak-tested and cleaned during the final stages of the quality control procedures. The next step was to transfer the cooling-loop from the assembly jig into a final assembly fixture. The frame was lowered over the loop and transverse members were fitted to complete the frame and provide additional torsional rigidity. The cooling-loop tubes were located in the recesses in the tooling. Screws securing the loop at the manifold end were removed and a check made to ensure all Litz wires and shunt-shield tails were clear.

The loop was then lifted out of the assembly frame and transported to the barrel on the installation frame. The frame was located on guides and lowered to an adjustable stop. After checking for potential conflicts, the frame was lowered using a fine adjustment. When in place, the mechanical-grade modules were screwed to the module brackets. The inlet and exhaust manifolds were secured to brackets at the end of the barrel and PEEK clips were inserted to secure the opto-flex to the underside of the cooling block. PEEK module clips were also added to apply pressure to the cooling blocks and the mechanical-grade modules, thus trapping the cooling-loop in its final position. The ground connector on the shunt shields was also connected to the opto-flex. The Litz wires were attached to the loop U-bends. The transverse members were unclipped and the support frame was removed. A final step was the removal of the barrel-end guides. Figure 16 shows a cooling-loop after installation on the barrel.

3.4.3 Design of the cooling-loop to bulkhead connection

Each cooling-loop terminates near the barrel end. To connect the cooling-loop exhaust to the connector in the thermal enclosure (TE) bulkhead (described in section 3.8.5), intermediate pipes, called "spiders", were designed. Each spider connects one cooling-loop exhaust to the TE bulkhead.

Calculations were carried out to estimate the maximum force that could be transmitted to the exhaust-manifold flange by exhaust spiders during a temperature change of 50°C (e.g. from -25°C to $+25$°C). The exhaust spiders are "L-shape" copper pipes of 8 mm outer diameter and 200 μm

2008 JINST 3 P10006

wall thickness. At each end is a custom connector to mate with the exhaust manifold and the HEX. Different geometrical layouts were considered:

- The spider clamped at both ends: resulted in a maximum force of $\sim$18 kgf.
- The spider hinged at both ends: resulted in a maximum force of $\sim$1.05 kgf.
- The spider hinged at the bulkhead and clamped at the flange: resulted in a maximum force of $\sim$1.4 kgf. It was this arrangement that was followed in the final assembly.

In the case of two rigidly clamped ends, "force filtering" would be induced by stressing the spider above its yield point. Furthermore, it was ensured that the spiders were fully annealed after fabrication. In this case, the maximum yield strength falls to 6 kgf/mm^2, which limits the maximum force to $\sim$3.7 kgf. The change of length of spiders is small (100-200 μm) and the force drops rapidly if one end moves slightly, which led to the choice of a mount with one hinged and one fixed end.

To check these calculations, the yield point on two of the final barrel 6 manifolds was measured. Although the yield point is difficult to assess for copper due to the inevitable work-hardening caused by the measurement, the results for these two samples showed a yield point of $\sim$4.5 kgf/mm^2. Further "filtering" of the force was obtained by clamping the spiders at the bulkhead in a way that allowed them lateral movement of up to 80 μm.

3.4.4 Design and production of the heat exchangers

As described in section 3.2.1, the C_3F_8 fluid is pre-cooled. This is done by delivering the fluid in a pipe through the outgoing exhaust vapour in a recuperative heat exchanger (HEX). After passage through the HEX, the exhaust vapour temperature remains significantly below the prevailing dew point (about 11°C). Therefore, a heater is connected in series with each heat exchanger to raise the temperature of the returning coolant and evaporate any remaining liquid coolant. The demountable joint used between the HEX and the heater has to be both leak-tight and electrically isolating. Both the inlet and exhaust pipes are connected with breakable but non-isolating couplings at the thermal enclosure (TE) bulkhead. The inlet pipe enters the HEX volume, passes through the colder exhaust vapour and emerges close to the TE bulkhead, where the incoming flow is split into the two capillaries for each loop. The entire HEX is made from Cu-Ni tube and is of a soft-soldered construction. The heater is made of stainless steel and is fitted with polyimide-insulated cables for both power and temperature sensors. The HEX's are encased in pre-formed thermal insulation within their cable trays on the wall of the liquid-argon calorimeter cryostat [2]. A filter is inserted between the end of the inlet pipe and beginning of the capillaries to remove particles that could block a capillary. The 44 (22 per side) HEX/heater assemblies are arranged in bunches of either six or five against the liquid-argon cryostat wall.

3.5 integration of the FSI system

The relative positions of the silicon modules must be determined to $<$12 μm in $R\phi$ so as not to degrade the tracking performance by $>$20% [3]. As it is impossible to guarantee the short-term mechanical stability of the detector, the SCT has been equipped with an optical alignment system

2008 JINST 3 P10006

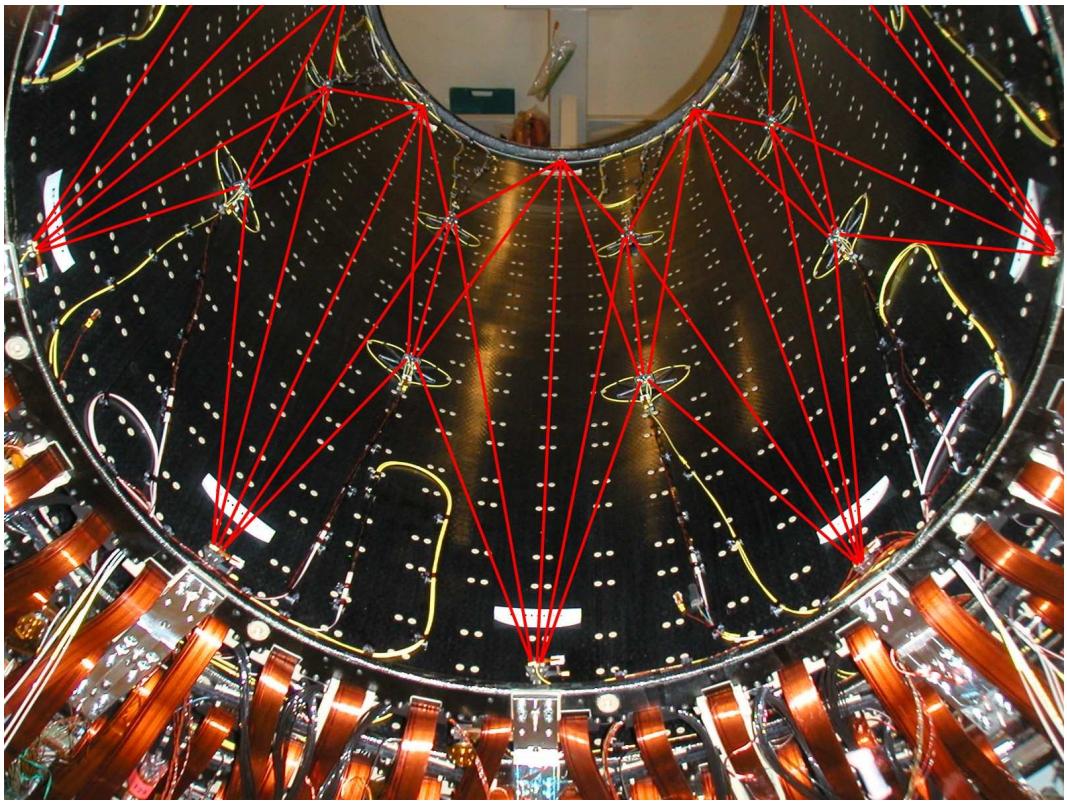

Figure 17. Part of the FSI geodetic grid inside an SCT barrel support cylinder. The grid-line lengths are simultaneously measured to a precision of <1 μm. Further radial lines (not shown) directly monitor silicon modules on the adjacent barrel.

that can monitor micron-scale motion of the detector in real-time. The alignment system consists of 842 interferometers built into the SCT and arranged as a geodetic grid of distance measurements between nodes. The technique of frequency scanning interferometry [16] has been developed to measure simultaneously the interferometer lengths to a precision of <1 μm. The positions of the 3D grid nodes can be reconstructed to <5 μm in the critical directions [17, 18]. Repeated measurements of the FSI grid follow time-dependent, correlated displacements of silicon modules. The FSI system offers access to the short-timescale, low spatial-frequency detector deformations.

In the SCT barrel, the FSI components are attached to the inner surfaces of the four concentric CFRP cylinders that support the silicon modules. The precise shape of each cylinder is monitored by an inner barrel grid, which consists of 32 grid nodes connected by 80 grid-line interferometers (GLI's), as shown in figure 17. 48 GLI's employ a mirror to measure radially inwards to certain modules of the adjacent smaller barrel, to help constrain radial deformations. Two barrel-flange grids, each of 72 GLI's, also link the four single barrels in the transverse plane at either end of the SCT barrel. The combined total of 512 grid lines permits complex, subtle deformations of the SCT barrel to be determined.

Each grid line is a fibre-coupled interferometer, which is formed between two components (described in more detail in [18]). The main component is called a "quill". It is manufactured from two parallel delivery and return fibres in a PEEK support, and is attached to a fused silica

2008 JINST 3 P10006

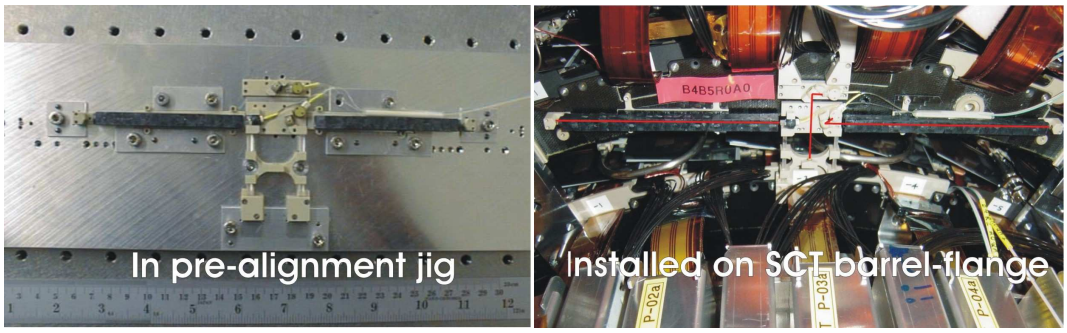

Figure 18. One of the 48 assemblies of the barrel-flange FSI grid that monitor rotations and translations between support cylinders of the SCT barrel.

beam-splitter. The quill illuminates a distant retro-reflector. The distance between a quill in one jewel and a retro-reflector in another jewel is measured by FSI. The jewels were placed in a jig that replicated the grid geometry in ATLAS, so that the GLI's could be pre-aligned and verified. The quill pointing was adjusted to maximise the interference fringe visibility, and then Araldite 2011 was applied to fix the alignment. The jewels were installed into precisely machined slots in PEEK inserts on the SCT support cylinders. This method ensured pointing alignment was maintained to well within the 2.5° divergence of the laser beam.

The barrel-flange FSI components were glued directly to the SCT barrel flange during the four-barrel assembly (see figure 18) using temporary jigs. The installation proceeded in three stages, as each pair of adjacent barrels was brought together during four-barrel assembly. A PEEK cover was added to protect the FSI components before unfolding the services from the barrels. Also the services were prevented from obscuring the lines of sight by protective tubes. Thermistors were attached to each inner-barrel grid node to monitor the ambient gas temperature near the light path so that refractive index corrections can be applied.

3.6 Module to barrel assembly

To achieve reliable assembly and cope with the tight clearances between modules, a robotic assembly procedure [19] was chosen. To be able to work on two barrel assemblies in parallel, two assembly stations with one robot each were used simultaneously in the assembly cleanroom.

The robot had to 1) pick up the module from a protective box, 2) insert the module and position it precisely on its support bracket, and 3) insert and tighten the M1.6 mounting screws. It also had to be capable of reversing this sequence if a module had to be removed. Prior to mounting modules, the robot surveyed the mounting points on the barrel optically to achieve the location precision. With the layout of modules on the barrel, it was natural to assemble the modules by rows. First, the six lower modules in a row were mounted and tested, and then the rows were completed by mounting the six upper modules. Travel along the length of a row, and the actual insertion, was achieved by mechanical stages driven by stepper motors. Different rows on the barrel were selected by rotating the barrel by hand and locating it with an indexing wheel. Module insertion was always done from the side of the barrel. A picture of the robot in front of an SCT barrel is shown in figure 19. Once the assembly procedures were well established, modules in several adjacent rows were mounted in a group to make the switch between mounting and testing more efficient.

2008 JINST 3 P10006

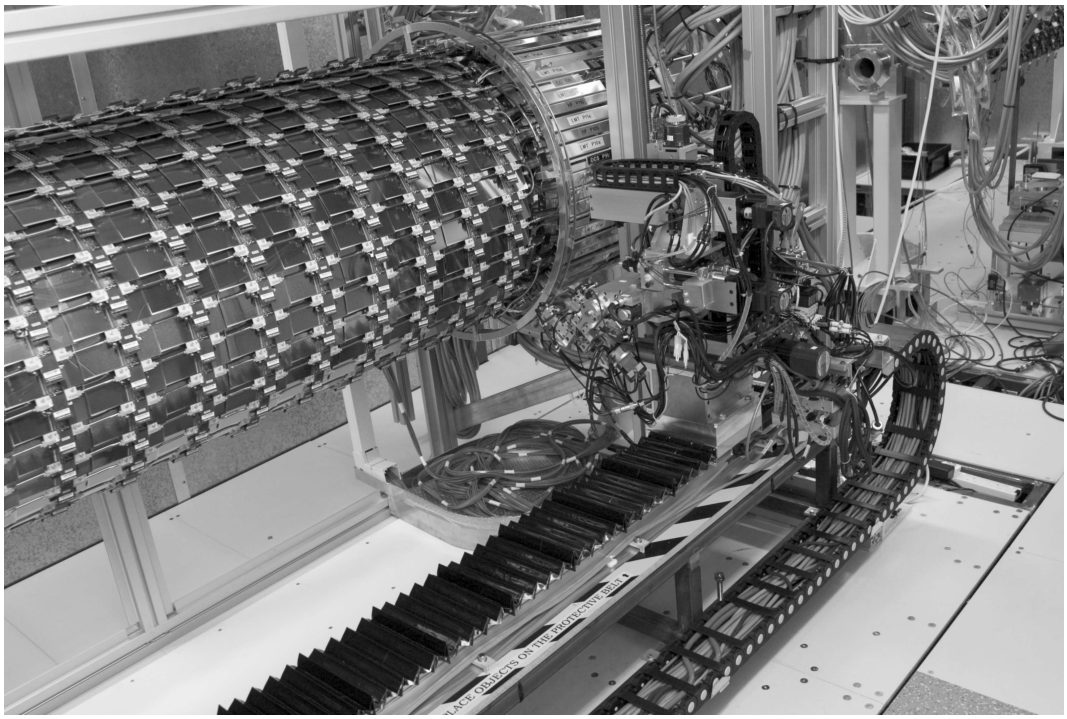

Figure 19. Robot in its assembly position in front of barrel 3.

In addition to the robotic procedures, additional assembly steps had to be performed by the operators using dedicated tooling: 1) the application of thermal grease,[19] on the cooling block before the insertion of the module, and 2) the application of two clips to clamp the cooling block to the module baseboard after the mounting. During the removal of a module, this grease joint had to be split by hand using a wedge tool. The robotic assembly of the barrel SCT was highly successful. Including replacements, over 2180 modules were mounted on the barrels. 40 modules had to be removed and replaced for various reasons, most of which were not associated with the assembly process. Only four modules were damaged during assembly. The precision requirement for the robot was moderate, as the location of the modules on the barrels was entirely determined by the precision holes on the mounting brackets and module facings. As long as the module was positioned with sub-millimetre precision, the shape of the bushes pulled the module into its correct location. However, an estimate of the precision could be made from the survey data of the mounting holes on the barrel. The r.m.s. of the distribution of measured versus expected separation between adjacent module mounting holes was 62 μm — this also includes the build tolerance of the barrel structures. All modules on all cylinders were tested after mounting at a coolant temperature of about 17°C ("warm operation"). These tests comprised small groups of modules (typically about 24) and were interleaved with the mounting. After the module mounting was completed, the full barrel was tested at different operation temperatures as described in section 5. During the mounting and testing, the barrels were protected in an aluminium frame, which was also used as the innermost layer in a double-walled container used for the shipment of the barrels to the module assembly site and from there to their final destination at CERN.

[19] Dow Corning DC340

2008 JINST 3 P10006

3.7 Transport of the barrels

3.7.1 Requirements

The cylinders underwent three major stages of transportation. At the first assembly site brackets were attached to cylinders and metrology performed. They were then shipped to the second assembly site where cooling, power and FSI were attached. From the second assembly site they were moved to the third where modules were attached and the barrels tested. The final transport was to CERN, the latter being a long journey with fully assembled detector barrels.

The barrels, when mounted in the assembly frames, weighed between 600 kg and 700 kg and were of dimensions 3.1 m (l) by 1.6 m (h) by 0.9 m (w) for the smallest and 3.2 m by 1.7 m by 1.1 m for the largest. Once equipped with services and modules, the delicacy of the components meant that it was crucial that the barrels were transported with extreme caution during the last two transportation steps.

Transportation took place in an air-sprung, temperature-controlled, humidity-controlled lorry. The acceleration experienced by the shipping container was required to be minimised to avoid damage to the silicon modules and shaking loose connectors. The temperature was required to be $20\pm3^{\circ}$C to avoid thermal stresses and the humidity kept at around 40%.

3.7.2 Designs of the transportation containers

At the last two assembly sites, the assembly frame was built up into a protective box using aluminium profiles and panels. This “inner shipping container” was then mounted on springs inside a second box, which was steel framed with plywood panels. The completed transport box was 3.6 m (l) by 2.1 m (w) by 2.1 m (h), and weighed 2.4 tonnes. The arrangement is shown in figure 20.

The springs were wire rope isolators, which were selected to provide both vibration isolation and high damping, which is essential to prevent oscillations.

Both the inner shipping container and the outer transport box were instrumented with accelerometers to record acceleration in all three directions, as well as temperature.

3.7.3 Transport

Prior to shipping barrels, a dummy load with the same mass as the inner shipping containers was instrumented and mounted in the outer transport box. This was loaded into a lorry using exactly the same process as was planned for the real shipments. Short test runs were undertaken and the results from the accelerometers indicated that the procedure would be safe. A final transport test was performed prior to the transport of barrel 3 by sending a detector test sector, equipped with functional barrel modules, to CERN. This concluding test with shipping containers exercised the pre-defined transport, loading and unloading procedures and was followed by retests of modules on the test sector after arrival at CERN.

For the transportation of the barrels, the wheels of the transportation frames were raised and the boxes were held in position by load-lock bars fixed to the sides of the lorry. The barrels were shipped one at a time, the route was along main roads, including the Channel tunnel, and was scheduled for minimum traffic congestion.

The journeys were carried out at safe speeds, taking around two days. On arrival at CERN, the accelerometers were checked, the barrels unloaded and then they were subjected to extensive

2008 JINST 3 P10006

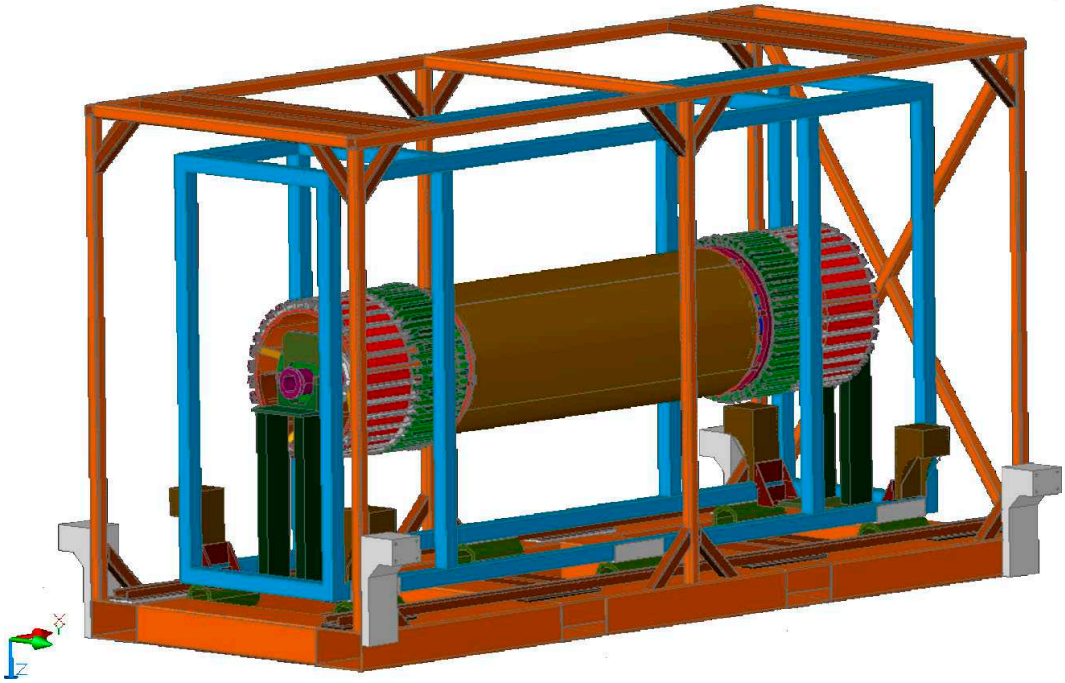

Figure 20. The inner shipping container and the outer transport box with the panels removed. The inverted "L" brackets on the outside of the containers mount wheels.

visual inspection. During the journeys, no damage was sustained, however a small fraction (<10%) of the cooling pipe clips moved position and were repositioned.

Once the lorry was sealed up, the temperature of the barrels remained between 18°C and 22°C and the humidity between 36% and 56%. Figure 21 shows the accelerometer record for the shipping of barrel 6. It shows the maximum acceleration in the vertical and horizontal directions recorded in each half hour period of the journey. High g forces (tens of g) are commonplace in standard transportation and do not necessarily represent a significant concern. The duration of the acceleration, any subsequent compensating accelerations, and the design of the object being accelerated are also crucial in determining the impact of a shock event. The energy delivered to a component compared with its mass is crucial, which is why vibration damping is vital to remove any resonant build up of energy absorption in suspended components.

Figure 21 shows two successive half hour periods at around 21 hours into the journey where events exceeding 1.2 g were recorded. In the vertical direction these were close to 13 g, but were of shorter duration than the resolution of the accelerometer (10 s) and of unknown origin.

3.8 Barrel thermal enclosure and grounding

3.8.1 Overview and requirements

The SCT barrel is contained in the thermal enclosure (TE). This consists of two outer thermal enclosure (OTE) half-shells and two side panels and end panels which are concentrically mounted to an inner thermal enclosure (ITE) cylinder. A photograph of the pre-assembled, empty thermal enclosure at the manufacturer's is shown in figure 22.

2008 JINST 3 P10006

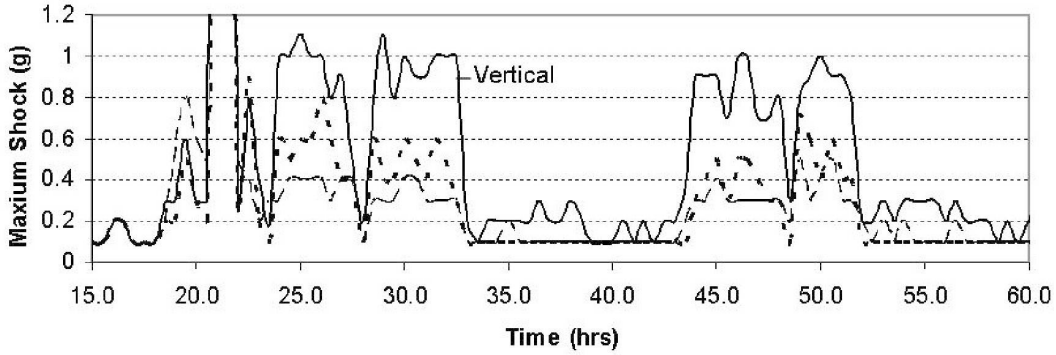

Figure 21. Maximum accelerations in each half hour interval in the three directions experienced by barrel 6 during transportation from Oxford to CERN. (rms values are much smaller)

The TE was manufactured by Lola Cars International.[20] It has the following functions:

- It provides mechanical protection for the SCT assembly.
- It provides thermal insulation between the SCT and TRT, which operate at different temperatures of $-7°C$ and $+25°C$, respectively.
- It contains a dry-nitrogen atmosphere to avoid condensation at a nominal overpressure of 4 mbar and separates the SCT and TRT gas volumes (the volume between SCT and TRT is flushed with CO_2, which is required for TRT operation).
- It acts as an electrical shield for the SCT barrel and provides a low-impedance path between the patch panels at opposite ends of the SCT.

The above functions must be realised while satisfying the constraints of minimum mass and tight envelope requirement — these made the design challenging. Heat transfer through the thermal enclosure walls is estimated to be less than 200 W total and is dominated by conduction through the OTE, both due to its large area and because it is adjacent to the warm TRT.

3.8.2 Outer thermal enclosure

The outer radius of the thermal enclosure is constrained by the radial envelope of the SCT barrel of 549 mm and is allowed to have a maximum thickness of 5 mm to clear the SCT modules on barrel 6. Along the horizontal axis, the OTE has to clear the SCT support rails inside the inner TRT cylinder. This requirement and its assembly led to a design which consists of two identical half-shells with flat side panels mounted on the horizontal axis (see figure 22). Using flat side panels along the horizontal axis allows to reduce the radial envelope of the thermal enclosure locally where more clearance between SCT and TRT is needed to accommodate the SCT support rails and support mechanics between SCT and TRT barrel. The disadvantage of side-panels is that the number and overall length of seams increases.

[20] Lola Cars International Ltd., Glebe Road, St. Peter's Road, Huntingdon, PE29 7DS, UK.

2008 JINST 3 P10006

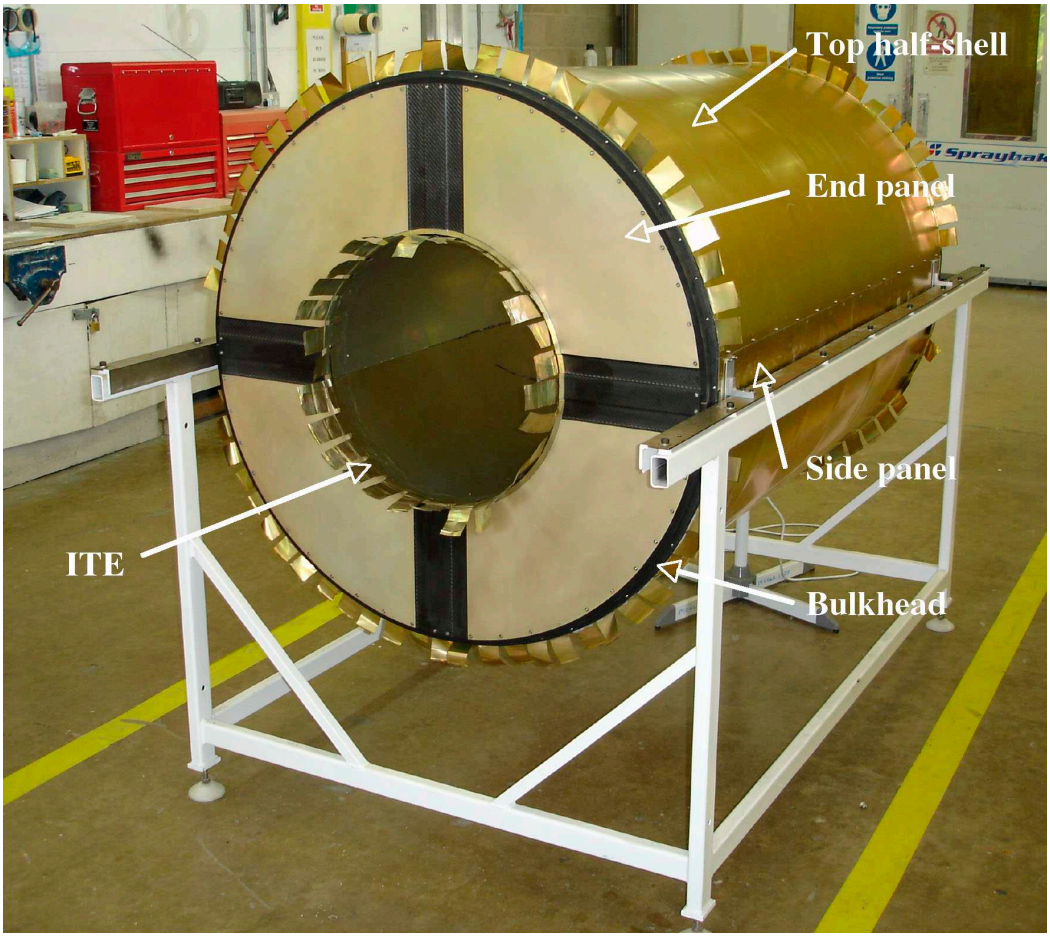

Figure 22. The thermal enclosure as pre-assembled at the manufacturer's.

The OTE is built as a sandwich structure of 0.6 mm thick CFRP, a foam core providing thermal insulation and stiffness, and an outer 0.5 mm thick aluminium sheet.

The CFRP is based on the CYCOM 919 prepreg by Cytek,[21] an epoxy resin system with a T300 fibre, frequently used in the racing-car industry. (Other parameters are 45% resin content, 2×2 twill woven cloth, 0.2 mm cured ply thickness; the elastic modulus is 57 GPa at 0° and 48 GPa at 90°.) Aluminium rather than CFRP was chosen for the outer layer to reduce costs by avoiding the construction of an additional precision mold tool. The use of dissimilar materials does not cause significant stresses due to thermal contraction, since during operating conditions, the aluminium skin is at room temperature (TRT temperature) and the thermal expansion of the CFRP (at -7°C) is small.

For thermal insulation, the cavity is filled with Pyrogel AR5401,[22] an aerogel with a thermal conductivity of 0.012 W/mK. The Pyrogel was wrapped in aluminised polyimide foil to minimise heat transfer by radiation. The Pyrogel panels are separated by strips of Airex foam as shown in figure 23 to provide dimensional rigidity to the sandwich. The overall thickness of the assembly is 5 mm.

[21] Cytek Engineered Materials, Anaheim, CA, USA.

[22] Aspen Aerogels, Inc., 30 Forbes Road, Building B, Northborough, MA 01532, USA.

2008 JINST 3 P10006

Figure 23. OTE half-shell with Pyrogel insulation and Airex stiffeners during manufacture (left) and ITE cylinder (right).

The OTE CFRP inner skins were cured on a carbon-fibre rather than a steel mould tool to negate any differential expansion problems during curing. The foam spacers and Pyrogel insulation panels were laid on, then the aluminium outer skin was bonded in place using Araldite 2011 epoxy adhesive under vacuum. This approach was followed also for the end and side panels and worked well. The inner surface of the OTE half-shells was laminated with 25 μm thick aluminised polyimide foil, again to minimise radiative heat transfer.

The OTE half-shells are not true half cylinders, but cover an angular spread of around 165° to allow for the mounting of the side panels. The CFRP inner skin of the half-shells incorporates a moulded end flange for mounting the services bulkhead.

The material represented by the OTE corresponds to 1.1% of a radiation length for particles at normal incidence.

3.8.3 Side panels

The side panels join the upper and lower half-shells to make up the OTE and allow the barrel mountings and their penetrations to be decoupled from the main TE assembly, which was an essential schedule requirement. The joint between these parts needed to be quite strong structurally, provide a seal to maintain the positive-pressure dry-nitrogen atmosphere within the thermal enclosure and ensure the electrical continuity of the outer skin be maintained around the circumference.

In terms of manufacture, the side panels are very similar to the OTE half-shells, but slightly less challenging due to their smaller size and flat profile. The inner skin was again a CFRP moulding and includes end flanges. The end flanges, which provide mounting points for the services bulkheads, were machined from aluminium and bonded to the inner skin.

3.8.4 Inner thermal enclosure cylinder

The inner thermal enclosure (ITE) has a diameter of 0.6 m. Unlike the OTE, it is made of a single wall of CFRP. This is possible since the SCT and the pixel detector both operate in a nitrogen atmosphere and their temperatures differ by only 7°C. The wall thickness of 0.5 mm is a compromise between optimum mechanical properties (pressure and mechanical envelope) and the requirement of minimum mass. A 100 μm thick aluminium skin on the inside of the ITE serves as the electrical screen. The ITE has rigid CFRP and aluminium end rings that provide rigidity, a mechanical seal

2008 JINST 3 P10006

face and a continuous electrical connection to the bulkhead. A photograph of the ITE is shown in figure 23.

A CFRP mould tool was used for the ITE production and the aluminium skin of the ITE was co-cured with the CFRP outer skin. This entailed taping the aluminium to the mould before laying the prepreg. A large enough single sheet of aluminium was not available, so three pieces were used, joined with conductive epoxy EP79.[23]

Tight envelope limits dictated challenging manufacturing tolerances. For most general features, an acceptable tolerance of ± 0.25 mm in the completely assembled form was achieved by the manufacturer. Because the ITE has little natural stiffness and could not support its own weight before the rigid end rings were applied, the mould tool was accurately surveyed before curing. A geometric parallelism tolerance of 0.4 mm was maintained over the end-ring faces and hole positions were located within a positional tolerance of 0.2 mm.

The material represented by the ITE corresponds to 0.4 % of a radiation length for particles at normal incidence.

3.8.5 Bulkhead

An aluminium bulkhead is bolted between the end panel and outer cylinder to feed through the LMT's, cooling pipes, optical fibres and DCS cables. A picture of the bulkhead is shown in figure 24.

The bulkhead is a three-layer assembly that allows sequential insertion of the SCT barrel services passing through to their respective patch panels. The services are sealed in using a combination of Techsil[24] silicone rubber elastomer and Loctite 5145.[25] With the exception of the cooling exhausts, the services do not have a connector break at this point to save space and reduce detector mass. The services bulkhead was CNC machined, while the many different types of PEEK cable feed-throughs were machined on a conventional mill.

3.8.6 End panels and heaters

Annular end panels incorporate channels on their outer face that increase rigidity and accommodate heater cables from the ATLAS pixel detectors. The build-up and thickness of the end panels is again similar to that of the OTE and side panels.

Due to limited space throughout the inner detector, the thermal insulation was chosen to be partly active. The outer surface of the TE is thus kept at a constant temperature (typically TRT temperature) above the prevailing dew point to avoid condensation. This is done using large laminated copper-polyimide heaters, the surfaces of which are etched, before gluing to the TRT inner surface with Araldite 2011. Similar heaters are fitted to the end panels.

The heater copper tracks are typically several metres long to create sufficient resistance for heating. The copper-polyimide heater panels surrounding the SCT barrel thermal enclosure are glued onto the curved inner surface of the TRT enclosure and to the end plates of the barrel. The former include 5 micrometers thick copper and are 6.4 mm wide. The latter are 8 micrometers

[23] EP79 from Master Bond Inc., 154 Hobart Street, Hackensack, New Jersey, USA.

[24] Techsil Ltd., 30 Bidavon Ind. Estate, Waterloo Road, Bidford on Avon, B50 4JN, UK.

[25] Henkel Loctite Adhesives Ltd., Technologies House, Wood Lane End, Hemel Hempstead, HP2 4RQ, UK.

2008 JINST 3 P10006

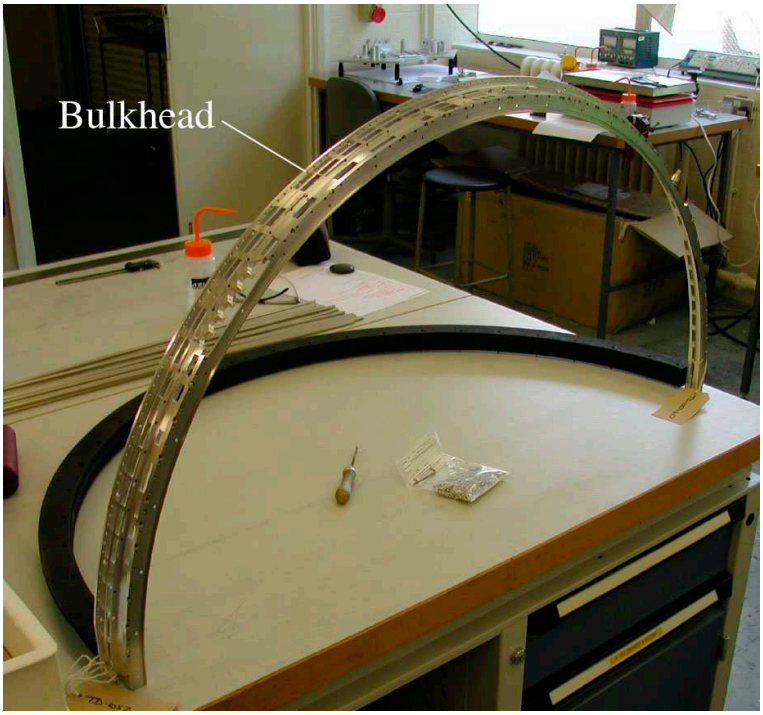

Figure 24. A photograph of the bulkhead for service feedthrough. Only the upper half is shown.

thick and have a track width of 0.75 mm. Total pad thicknesses (including polyimide) are about 0.5 mm. Each heater has two independent and parallel heating tracks for redundancy and two negative thermal coefficient (NTC) thermistors for monitoring the temperature.

All low voltage heater pads are supplied by 48 volt DC power supplies, located in the ATLAS US15 and USA15 service caverns, that uses pulse-width-modulation to provide the time-averaged power necessary to maintain the desired temperature. Typical heater currents are 1 A.

3.8.7 Grounding and shielding

The thermal enclosure is essential to achieve good electrical performance of the SCT barrel detector. It must act as a shield (Faraday cage) to suppress external electromagnetic radiation and provide a low-impedance path between the cable patch panels at each end of the SCT barrel. This required implementing high-quality corrosion-proof electrical joints that will not deteriorate throughout the lifetime of the SCT. The electrical shield has to be as continuous as possible; gaps and seams have to be minimised.

The electrical design of the thermal enclosure and its implementation were not straightforward. This was in part due to the difficulty of joining aluminium. Other difficulties arose when sheets or foils could not be bought or handled in the desired sizes and several pieces had to be joined. To prevent corrosion and increased resistance across aluminium joints, all aluminium parts were treated with Alochrome 1200 to resist oxidation, thereby providing a more reliable, long-term electrical connection. A novel spot-welding technique was developed at RAL to provide efficient electrical coupling in as many places as possible. This was used to weld aluminium tags to the OTE aluminium skin (see figure 22). During assembly, the tags were folded over the rim of the OTE and

2008 JINST 3 P10006

were bolted to the bulkhead. A similar technique was used for the ITE aluminium foil, where the tags are part of the foil.

A silver-coated nickel epoxy, EP79, was used for some electrically conductive joints. Many joints included commercial tin-plated Be-Cu radio-frequency gaskets.[26]

The DC resistance of the important electrical joints was monitored repeatedly during assembly and four-barrel integration, and showed no deterioration with time. The resistance across the lap joint of the OTE aluminium skin is $\sim$0.16 mΩ; the resistance between the adjacent aluminium foils lining the ITE ranges from 1 to 3 mΩ; the resistance between the OTE top and bottom shells across the side panel is $\sim$0.5 mΩ; the resistance of the ITE to the bulkhead is $\sim$10 mΩ.

3.8.8 Production techniques and experience

The TE is a technically complex project which was started relatively late and went through several design iterations due to changing requirements. The very limited envelope of 5 mm thickness allocated to the TE was a significant constraint. Given a more generous space allocation for the thermal enclosure envelope, the design of the TE could have been significantly simplified, possibly allowing for a fully cylindrical shape, relaxed tolerances and choosing a CFRP/insulator/CFRP sandwich for the OTE.

Sealing the thermal enclosure was cumbersome. The sealing of the long seams would have been simplified by giving the joint adequate stiffness.

Grounding and shielding specifications were considered late in the design and required a number of inventive solutions. Using copper rather than aluminium at the larger radii would have simplified the design greatly. Once the design was finalised, production of the thermal enclosure proceeded smoothly. Manufacturing of large precision CFRP objects and the various laminating steps did not pose a particular challenge to the manufacturer.

4. Assembly of the four barrels and integration to TRT

After the single barrels were assembled they were transported to CERN to complete the integration of the SCT barrel detector. Tests (described in detail in section 5) were carried out on the single barrels to assure their proper functioning before all four barrels were mechanically assembled together and inserted into the thermal enclosure.

4.1 Four-barrel assembly

4.1.1 Description of barrel assembly

The four barrels were individually assembled at RAL and Oxford University, before being shipped to CERN for their integration with each other and into the TRT. This phase took place in the CERN-SR1 building, where the room temperature was controlled to $\pm 2^{\circ}$C and the relative humidity to about $40\pm10\%$. The goal of this work was to install the four nested barrels inside the thermal enclosure. The thermal enclosure comprises two half-cylinders (half-shells) and two side panels, forming the Outer Thermal Enclosure (OTE), the Inner Thermal Enclosure (ITE) and two end panels. Details of this structure are contained in section 3.8. The heater pads that define the exterior

[26] Laird Technologies, http://www.lairdtech.com, part number 0C98-0550-17.

2008 JINST 3 P10006

operating temperature of the SCT barrel are mounted on the inside of the TRT barrel and on the TE end panels. The interface temperature between the SCT barrel and pixel barrel is controlled by heater pads on the pixel support tube (PST).

4.1.2 ESD precautions

Problems with electrostatic discharge (ESD) causing damage to components had been observed during earlier assembly stages at both Oxford and RAL. However, by the time the barrels arrived at CERN for the four-barrel assembly, these problems were well understood. A room was built inside the CERN-SR1 cleanroom which was used for the assembly of the barrels. Strict controls were put in place to diminish the risk of ESD damage to the barrel components. Access was controlled and all fixtures and personnel were electrically connected to a central ground point via 1 MΩ resistance. Personnel wore ESD-safe coats, overshoes and ankle or wrist grounding straps when working on the barrel. The walls of the room were of metal construction and were coated with an ESD-dissipative paint. The floor was also dissipative and the resistance measured to the underlying copper-mesh ground plane was around 10^{i} Ω. The surface resistivity was checked monthly and was always found to be approximately 10^{10} Ω/square.

4.1.3 Integration with the thermal enclosure and sealing

The ITE, OTE and TE side panels were delivered to CERN after a trial assembly and sign-off at the manufacturer's site. The OTE half-shells were attached to the upper and lower supports of the four-barrel assembly cradle ("SCT cradle"). They were moved vertically outwards to give the maximum clearance for the insertion of barrel 6 (see figure 25). The next stage of the OTE assembly involved the fitting of the side panels to barrel 6 (see figure 26). The clearance between the modules and the inner surface of the OTE was of the order of 2 mm, and to check that this was maintained at all ϕ locations, the barrel was rotated before insertion and the concentricity of the barrel module connectors and the spindle adjusted. Each half-shell of the OTE was lined with aluminium foil which would be electrically bonded to the outer aluminium skin of the OTE side panels. Although this would ensure that the SCT grounding was complete and also ensure that all metallic surfaces were referenced, it did present a potential hazard to the high-voltage supply of the silicon modules. To overcome this problem, 12 bands of 25 μm polyimide foil were glued around the inside of each half-shell at the correct z positions to ensure insulation from the module connectors carrying the HV connection.

4.1.4 Description of the procedure

The barrel 6 inner transport-container was dismantled, leaving the barrel, service cages and spindle supported on the pedestals and baseplate. The baseplate was lowered onto the rolling platform of the four-barrel assembly tooling and roughly aligned with the axis of the tooling. Extension supports were fitted to the ends of the spindles and these were attached to the assembly tooling. The spindle was disconnected from the pedestals and the baseplate lowered, thus transferring the weight of the barrel and services cages to the assembly tooling. After removing the baseplate and pedestals, the barrel was carefully aligned to the tooling axes. The weight of the barrel was transferred to the main cradle by attachment to the inserts that pass through the OTE side panels. The upper and lower half-shells of the OTE were lowered into position and attached to the side

2008 JINST 3 P10006

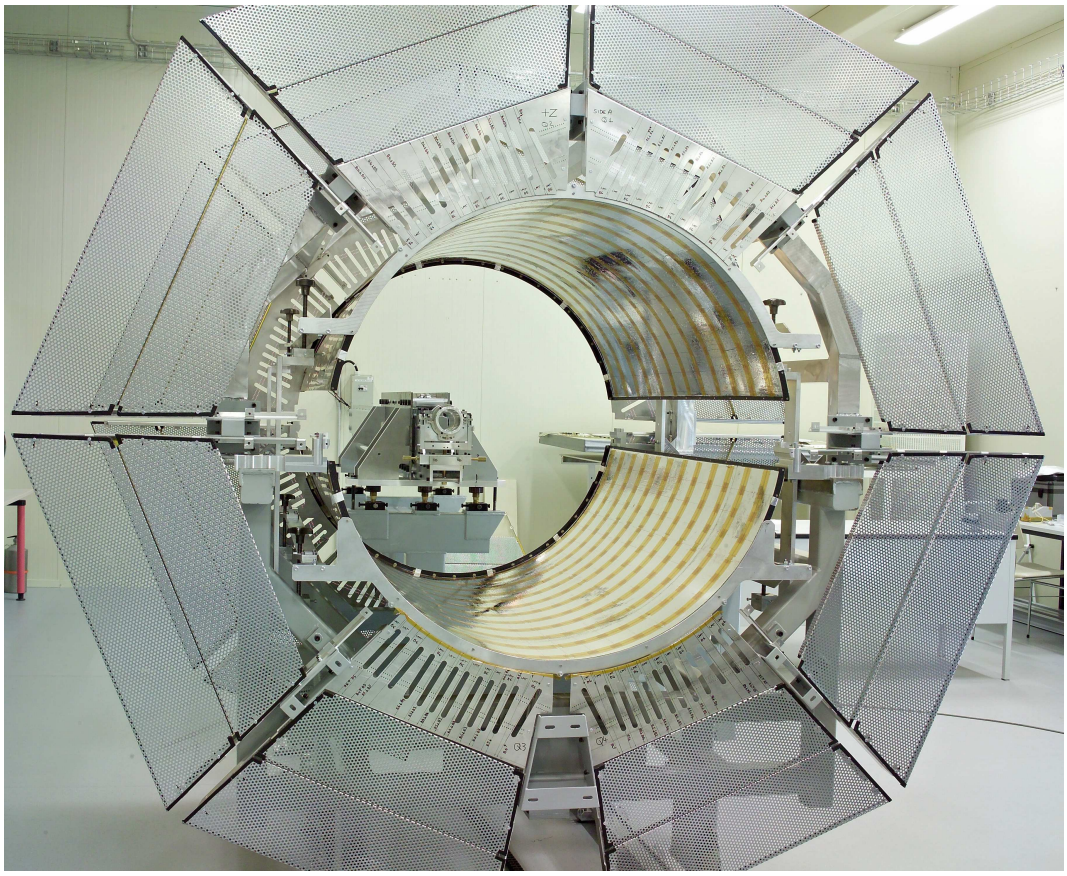

Figure 25. View of the Outer Thermal Enclosure (OTE) on its tooling with the Radial Services Support (RSS) in place.

panels of the OTE, thereby completing the cylindrical part of the gas-tight Faraday cage of the OTE. The side-panel joints were bolted and sealed. At this stage, it was necessary to unfold all the services from the barrel service cage and mount them on the radial support structure (RSS). The rear TE bulkhead was bolted in place, the rear feedthroughs were added and the LMT services were folded out, their outer ends being supported in a separate frame. Each LMT was aligned with the correct slot position in the inner bulkhead of the thermal enclosure. For most LMTs, the temporary patch panel (TPP) was removed and the PPB1 final patch panel was protected with ESD-safe foam packaging. For those LMTs that were to be used in the cosmic-ray test with the TRT, the TPPs were left untouched.

Readout fibres were wrapped in soft, anti-static foam over the MT connector and at each end of the spliced section and they were fixed to the RSS in the gaps in between the LMTs. The FSI fibre spools were mounted on specially constructed stands, which screwed onto the RSS. One FSI fibre was damaged during this operation and was repaired using a fusion splicer. Detector control system (DCS) sensor wires were grouped according to their final feedthrough allocation and their lengths were adjusted to fit with the final patch panels inside the ATLAS solenoid magnet. The Cu-Ni capillaries (with pre-installed sleeves) were fitted to the individual SCT barrels before their integration into the four-barrel assembly. The capillaries were leak tested on the barrels with an

2008 JINST 3 P10006

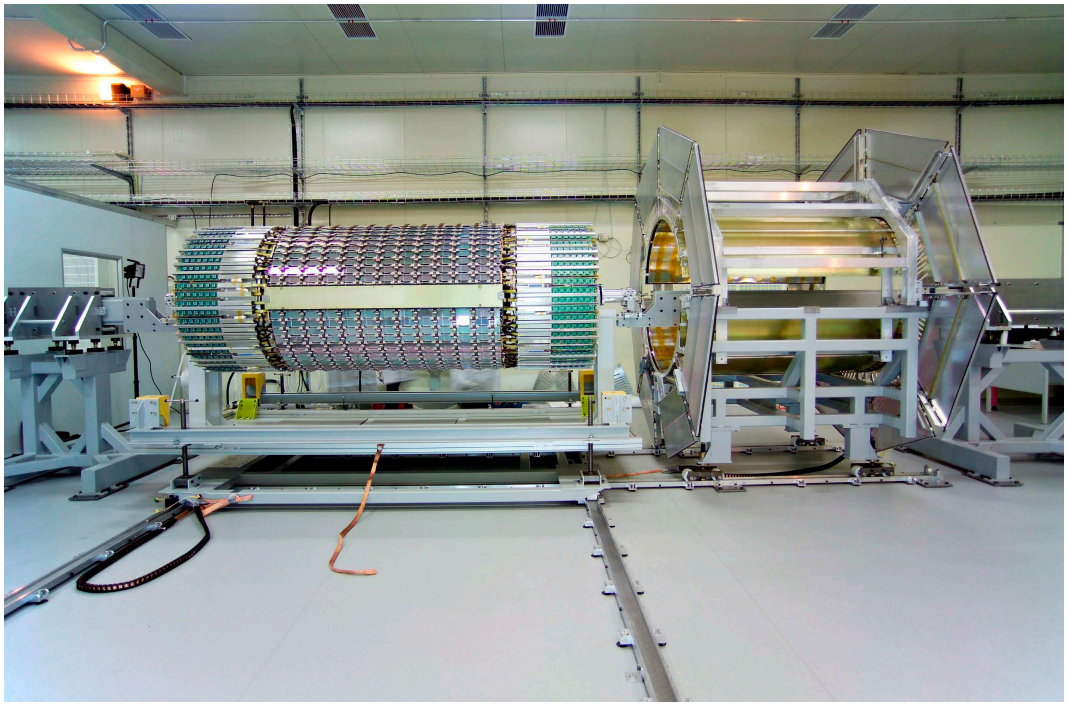

Figure 26. Barrel 6, with thermal enclosure side panels ready for insertion into the OTE.

acceptance criterion of 4×10^{-9} mbar·l/s. The Cu-Ni capillary connectors were sealed using 0.6 mm diameter indium-wire seals. The wire was degreased in acetone for five minutes, then washed in de-ionised water, followed by another five minutes in 10% hydrochloric acid. They were washed again in de-ionised water and allowed to dry. A matched pair of capillaries was chosen for each cooling loop to ensure identical mass-flow rates in each half of a loop. The ϕ location of each capillary (each has a unique serial number) was noted. During the installation of barrel 5, one of the barrel 6 capillaries was damaged. It was successfully replaced with a spare with a very similar mass flow at the standard pressure of 13 bar(a).

Once all the services had been removed from a barrel, the service cage was removed and the spindle withdrawn ready for the insertion of the next barrel. The unfolding process was repeated for all barrels, with services from subsequent barrels being placed on top of the earlier ones. Extra shelves running the length of the cradle were installed for the top and bottom test sectors in order to support the extra weight of the TPPs. Each barrel was supported from the one outside it by temporary interlinks. These were extended as each barrel was added. Eventually, these were replaced with the final CFRP interlinks.

With all services for the four barrels mounted on the RSS, the sealing of services into bulkheads could take place. The front covers of the feedthroughs were then fitted and sealed with either Techsil[27] or Loctite 5145 (Tempflex) and left to cure. Service drums consisting of mesh cylinders of the same radius as barrel 3 were mounted at each end of the four-barrel structure. The readout fibres, FSI fibres and DCS wires and patch panels were removed from the RSS and secured to the

[27] A two-part adhesive to which talcum power was added as a viscosity modifier. Techsil Ltd., 30 Bidavon Ind. Estate, Waterloo Road, Bidford on Avon, B50 4JN, UK.

2008 JINST 3 P10006

drums. PEEK grommets were fitted into slots on the inner bulkhead and glued into place using Techsil. Services were sealed into the bulkheads, again using Techsil. It was found that although Techsil forms a very good seal around fixed objects, it does not work so well if the services are likely to be manipulated at later stages of the installation. This was a particular problem for the LMTs, where a gap could open at the back of the grommet when the tapes were folded forwards. Refilling the gaps with Techsil was found not to be viable, so a thin bead of Loctite 5145 was applied to the back of the tapes in an attempt to improve the sealing. Once a grommet was filled with its 6 or 12 LMTs, the grommet lid was secured with two M1$\times$4 stainless-steel screws.

The final interlinks between the barrels were installed at this stage. A few grommets were also secured with Loctite 5145, as the weight of the LMT bundle was found to cause the grommet to be pulled away from the bulkhead. There were also two cases at each end where the castellations between grommets in the inner bulkhead had to be removed to allow a special double grommet to be inserted to correct an error in the bulkhead services routing. Before the adhesive had cured, pressure plates were fitted under each lid. These were clamped into place by a nylon screw threaded through the cover plate. After the glue had set, the portion of screw exposed above the lid was removed. The middle bulkhead was then installed. This ensured the correct location of the capillaries and "soft" services. The capillary sleeves were fitted into their grommets in the middle bulkhead and glued into place using Araldite 2011. The remaining length of the capillary was coiled and stored on the support drums. DCS wires and opto-fibres were sealed into grommets using similar methods as for the LMTs. The fibre grommets were sealed first with un-filled Techsil (without talcum filler). The low viscosity of this mix allowed the glue to flow around the individual fibres. Once this had set, Techsil was then injected into the grommet to fill up any larger gaps. The two halves of the outer bulkhead were screwed to the middle bulkhead, using Techsil as a sealant.

At this stage, the pipes ("spiders"; see section 3.4.3) that would connect the ends of the cooling loops to the bulkhead connectors were installed. The copper spiders were annealed and in this state, fine adjustments could be made to ensure they fitted without applying significant force on the exhaust connection or other services. Indium wire of 0.8 mm diameter was used for the seal. The other end of the spider was then clamped into the TE bulkhead and then leak tested by pressurising the loop with helium, with both capillaries closed, and searching for leaks greater than $\sim 2\times10^{-9}$ mbar·l/s. Figure 27 shows one barrel end with all services routed through the bulkhead and the spiders installed.

The cooling reference disk (CRD) was cut to shape using a template. The Litz wires from the cooling loops were pulled through holes in the CRD and were soldered to the disk. The CRD was grounded by trapping strips from its outer edge between the middle and outer bulkheads. The ITE was then inserted using an adaption of the four-barrel assembly tool. The TE end panels were bolted in place, making sure to connect all foil connections, while the continuity between the side panels and the OTE was made using screws and Alochromed aluminium foil bonded with conductive epoxy EP79. Once the end panels were in place, the foils from the ITE were folded out, trimmed to length and sandwiched in between the end panel and the retaining ring. The final task was to install the manifolds and connections of the environmental nitrogen pipes.

4.1.5 Barrel interlinks

The Interlinks are precisely machined radial CFRP spokes which link the four SCT barrels together.

2008 JINST 3 P10006

Figure 27. Barrel end with all services routed through the bulkhead.

There are eight equispaced spokes at each barrel end. The two horizontal ones on each barrel end are linked to the SCT barrel support on their outer end and provide support points for the pixel detector on their inside end.

The assembly method chosen dictated the use of temporary interlinks for all the phases of the four barrel assembly. These temporary interlinks were heavier and made of successive short aluminium alloy parts, allowing each barrel to be fastened into its external neighbouring barrel without obstructing the way for the next barrel to be installed.

When all the four barrels were assembled and precisely attached together, the temporary interlinks were removed sequentially one by one and replaced by the final CFRP parts which are dowel-pinned and bolted to the cylinders. A photograph showing one of the final interlinks in the installed 4 barrel assembly is shown in figure 28.

2008 JINST 3 P10006

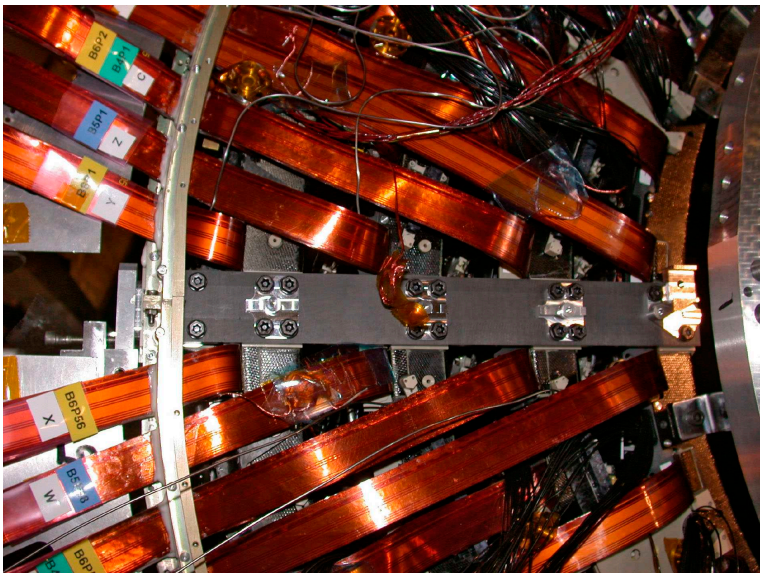

Figure 28. Photograph showing one of the 8 interlinks at one end, after the four barrel assembly.

Figure 29. The SCT barrel and support cradle being set up for its transfer on the cantilever tool.

4.1.6 The Intermediate Service Support Structure (ISSS)

The ISSS, shown in figure 29 on both ends of the SCT barrel and in figure 30 from one end of the SCT barrel before the SCT was inserted into the TRT, consisted of two lightweight, aluminium structures mounted at each end of the SCT barrel. These structures were supported on steel frames that were fixed to either the barrel cradle or to the ID rails in either the ID trolley or inside the ATLAS solenoid respectively. The ISSS was designed to contain all of the SCT services in eight segments at each end of the barrel. The ISSS was designed to provide the safe storage of all services during the SCT insertion into the TRT and the subsequent connection of services inside

2008 JINST 3 P10006

the cryostat. For all services, the respective minimum bend radii were observed. After securing all cables, fibres and pipes inside the ISSS, it was decided not to fit the sector lids during insertion into the TRT as this would have violated the envelope — they were fitted immediately after insertion. On completion of the final envelope checks, the SCT barrel assembly was declared ready to move onto its cantilever stand, prior to insertion into the TRT.

4.1.7 Tests done during four-barrel assembly

Prior to the four-barrel assembly, all cooling loops had been tested and no leaks had been found. During the four-barrel assembly, each cooling loop was evacuated from the exhaust connector, with the two capillaries blanked off. A helium leak-detector with a sensitivity of around 5×10^{-10} mbar·l/s. was connected to the loop while helium gas was directed at the visible joints. During these tests, three of the exhaust flanges were found to have developed leaks (of the order of 10^{-4} mbar·l/s). The leaks were on barrel 3 (2 leaks) and barrel 6 (1 leaks). In each case, the leak was located at a solder joint near the outside of the exhaust manifold. All three exhaust connectors were from an early production and the problem was traced to the Ni/Cu/Au plating on the manifold. It seemed that the copper was delaminating from the underlying nickel layer. To overcome this problem, PEEK inserts were machined and glued into 42 of the 44 manifolds using Hysol 9396[28] and secured with a bead of Araldite 2011 along the visible edge. In two manifolds, it was not possible to fit these inserts so the inner surface was sealed with Araldite 2011. On all manifolds, TorrSeal[29] was applied externally around the solder joint to provide a second seal. An analysis was carried out to estimate the maximum force that could be transmitted to these exhaust manifolds by thermal expansion and contraction of the spiders — see section 3.4.3 for further details. The effect was found to be most pronounced for the long (barrel 3 and barrel 6) exhausts. The hinged support was implemented by loosening the pipe from its rigid bulkhead mounting to give it an 80 μm float, and then the couplings were sealed from the inside using Loctite 5145.

The barrel assembly involved the removal of most of the TPPs. For those to which access could be arranged, the integrity of the LMTs was checked by measuring the loop impedances of the lines and by checking the hybrid thermistor values. The few breaks that were discovered were either repaired or overcome by modification to the final patch panel.

To leak test the thermal enclosure, a dry-air supply was mixed with argon and connected to a digital flow meter (0-40 l/min). The input was split to feed the four internal nitrogen pipes. A 0-to-4 mbar pressure switch, set to operate at 0.9 mbar, was connected to the middle bulkhead. A gas bubbler, set to 0.6 mbar, was attached to the exhaust line to create a back pressure. Initially, many leaks were found and the leak rate was so large that an overpressure of 0.15 mbar could only be achieved with a flow rate of 2500 l/hour. The most significant leaks were at the exit of the DCS wires, around one capillary and several fibre grommets, behind most LMTs, some exhaust spiders and the joints between the TE side panels and the OTE half-shells. After sealing these, a 0.6 mbar overpressure was achieved using 2.5 times the nominal flow rate (approximately 2.5 m^3/hour). At nominal flow, there was an overpressure of 0.2 mbar. This will lead to larger than expected[30] losses

[28] Henkel Corporation Aerospace Group, 2850 Willow Pass Road, P.O. Box 312, Bay Point, CA 94565, USA.

[29] Varian, Inc. Corporate Headquarters, 3120 Hansen Way, Palo Alto, CA 94304-1030, USA.

[30] N_2 losses to the ID volume were expected to be $\lesssim$100 l/hr for the full SCT

2008 JINST 3 P10006

of nitrogen to the Inner Detector environmental gas (CO_2). The consequences of this leakage are currently being studied.

4.1.8 Photogrammetry survey

Three consecutive photogrammetry surveys were performed on the SCT barrels shortly after four barrel assembly:

- Survey 1 [27]: This is the most detailed survey of the three. It recorded the relative position of the eight radial interlinks that support the four cylinders at either end of the barrel, as well as the FSI targets and pixel supports (with a horizontal and vertical $x-y$ precision of 20μm.). Four external reference targets were surveyed.

- Survey 2 [28]: This survey recorded a change of the external reference targets, with a precision of 100μm, before the SCT was inserted into the TRT.

- Survey 3 [29]: This was recorded just after the SCT had been inserted into the TRT, with an estimated precision of 150μm to the concentricity of the detectors.

The first set of the three photogrammetry measurements was used to investigate barrel deformations. An analysis of the data at each end of the barrel, in comparison with circle hypothesis revealed radial deviations of the order of 100μm. The data could be well fitted by ellipses. There was a rotation of about 0.5 radians in the directions of the major axes of the ellipses found at the two ends of the barrel. These features can be explained by a finite-element analysis (FEA) model assuming a three point mount scenario. An interpolation of the measured targets to the module positions was performed. Details on survey 3 and its comparison to track based alignment measurements from cosmic ray data are given in section 4.2.3.

4.2 Integration into the TRT

This section describes the final integration of the completed SCT barrel inside the TRT barrel.

4.2.1 Support requirements of the SCT inside the TRT

In accordance with the general support scheme of the inner detector [26], the SCT is supported from rails integrated into the TRT inner shell. The rails are made of CFRP except for the bearing areas, which are made of aluminium alloy. These aluminium parts also offer features to be connected to the tooling for blocking things safely during transport. The four SCT supports are rigidly attached to the outermost barrel and to the interlink system linking the four barrels together and they penetrate through the thermal enclosure. They have a short vertical adjustment capability and can be locked for transport.

4.2.2 Integration procedure

The tools used for the integration of the SCT into the TRT are:

- The ID barrel trolley, designed to support the ID barrel for tests, transport and installation into the pit.

2008 JINST 3 P10006

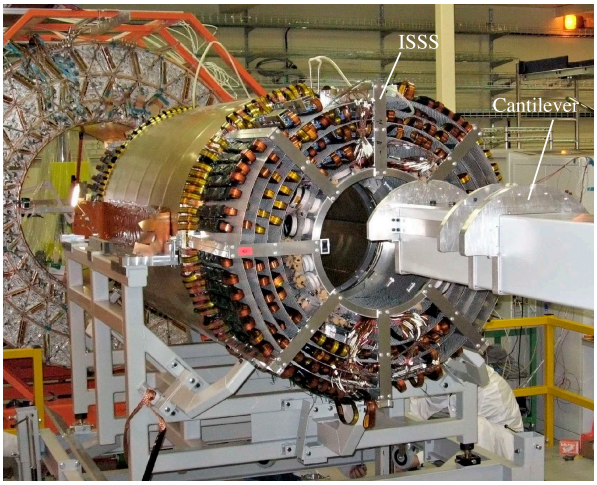

Figure 30. Transfer of the barrel onto the cantilever tool.

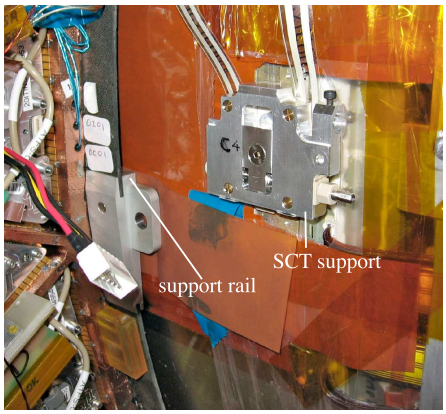

Figure 31. SCT support installed on the barrel. The end of the support rail inside the TRT barrel can be seen to its left.

- The SCT cradle, designed to support the SCT barrel during its assembly and tests. The cradle is also used to transport the SCT barrel inside CERN-SR1 up to the insertion area.
- The ISSS, attached at both ends of the SCT barrel to support the service extensions during insertion into the TRT, transport and installation.
- The SCT barrel cantilever tool, designed to support the SCT barrel from one end during the insertion operation.

As described in section 4.1, at the end of the four-barrel assembly, the SCT barrel detector was supported in the SCT cradle using temporary non-adjustable supports fastened to the four final support positions. All temporary aluminium interlinks were replaced one-by-one by the final CFRP ones; these were bolted and pinned in place with dowels. These interlinks also provide precise survey-target locations, which were used to do a photogrammetric survey before closing the thermal enclosure and arranging the services on the ISSS's.

After completion of the four-barrel assembly, the cradle and SCT barrel were transferred from the barrel assembly area to the insertion area and raised by hydraulic jacks on a rail system to allow for its introduction onto the SCT barrel cantilever tool. Figure 29 shows the SCT barrel on the cradle being set up for its transfer on the cantilever tool. The barrel was raised until its axis was above the axis of the cantilever tool. The SCT barrel was moved over the fixed cantilever stand with the cradle being guided by the floor rail system (figure 30). Then, by lowering the cradle, the SCT was simply docked to the saddle system attached to the cantilever arm passing through the bore of the SCT barrel. The cradle was removed and the cantilever/SCT barrel adjusted with respect to the rail system on which the TRT barrel trolley rolled during the insertion manoeuvre. A geometry check was performed by moving a template along the rails.

The TRT barrel was transferred from its assembly cradle into the ID barrel trolley. The four TRT supports were adjusted vertically in such a way as to have the same compression load on the pressure-sensitive foils integrated in its feet. The ID trolley was then transferred from its wheels to the insertion rail system and its axis adjusted to be properly positioned and parallel with the axis

2008 JINST 3 P10006

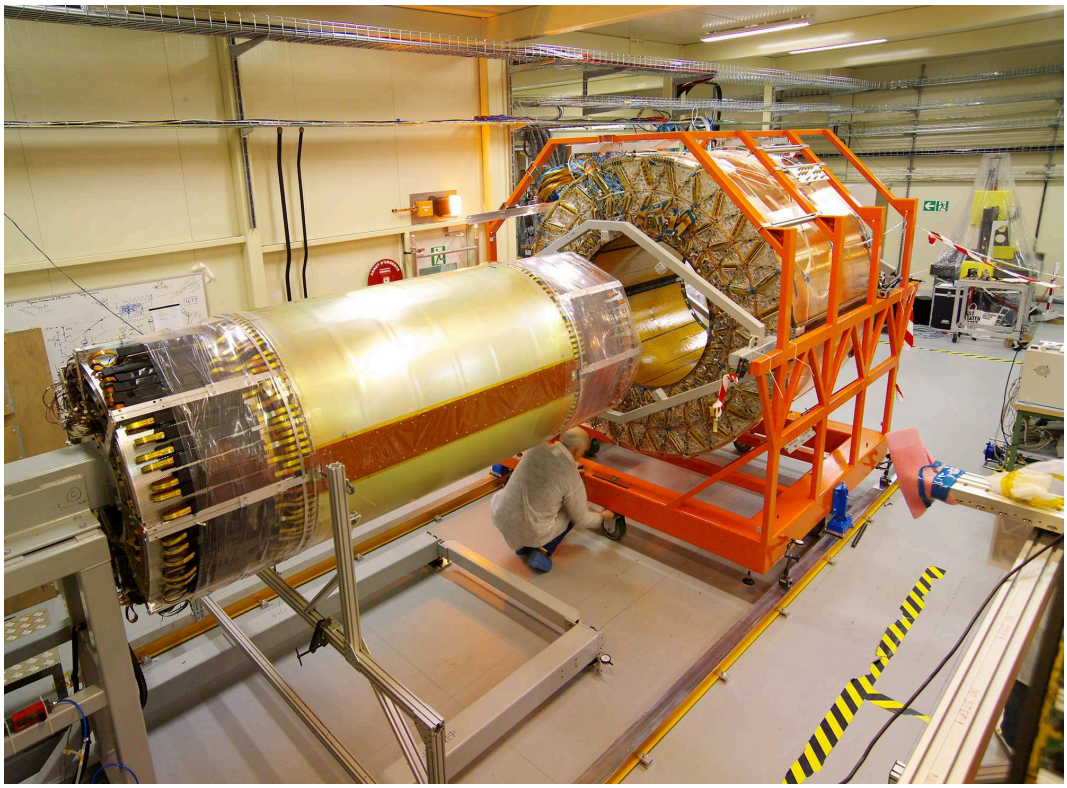

Figure 32. Translation of the TRT barrel inside the trolley over the SCT barrel.

of the rail system. Fine tuning of the relative adjustment of the TRT and SCT was done and the insertion was achieved by translating the ID trolley on the rails around the SCT, which was only supported from its far end on its cantilever tool (figure 32). Since the clearances in the region of the SCT supports (figure 31) were too small, the SCT supports were removed. Consequently the insertion was stopped approximately 100 mm before the SCT was in its final position, and the final SCT supports were fastened to the near end of the SCT barrel — see figure 31. Then the insertion continued up to a point where the SCT protruded from the TRT on the far end to allow for the mounting of the two remaining SCT supports. The trolley was then moved backwards to reach the final relative position in z of the two subsystems. Some final adjustments were made and the SCT feet were lowered to make contact with the rails of the TRT. A front strut was installed to block the cantilever beam in a way so as to avoid spring-back problems. Then the cantilever support was lowered to transfer the weight of the SCT from it to the TRT.

4.2.3 Relative alignment between SCT and TRT

After the successful insertion of the SCT barrel into the TRT and the transfer of the SCT weight onto the support rails mounted inside the TRT inner cylinder, a theodolite survey [29] was carried out to measure the position of the SCT barrel with respect to the TRT barrel. Table 3 summarises the observed misalignments of the SCT with respect to the TRT central axis. The detectors are positioned at their nominal relative z positions to better than the survey measurement precision along the z-axis of 0.2mm.

2008 JINST 3 P10006

Table 3. Relative translation and rotation between the SCT barrel and the TRT barrel at the origin, extracted from the survey measurements.

Δx [mm]	Δy [mm]	$\Delta rotX$ [mrad]	$\Delta rotY$ [mrad]
-0.42	$+0.33$	$+0.154$	$+0.165$

The relative alignment of the SCT and TRT barrels was verified by using the reconstruction of cosmic-ray tracks in the SCT and TRT during combined tests in CERN-SR1 (see section 6.3.2). A special procedure was implemented to determine the relative SCT-TRT displacement:

- TRT and SCT tracks were fitted separately and the SCT tracks were extrapolated to the first TRT straw layer.
- A 2D residual was formed from the difference in the track coordinates in the plane perpendicular to the straw-layer surface (the TRT has no sensitivity along the wire direction).
- The track χ^2 was calculated and minimised by shifting the location of the SCT and TRT in the detector geometry description used for track reconstruction. Because of the setup used during these tests (tracks almost vertical and no TRT sensitivity along z), only the displacement along x (Δx) and the rotations ($\Delta \mathrm{rot}Y$ and $\Delta \mathrm{rot}Z$) around the y- and z-axes, respectively, could be determined.

This alignment procedure was applied on tracks collected from two different runs: one at the beginning and one at the end of a stable period of data taking. Further details on track reconstruction and the alignment methods used are given in reference [23]. The two resulting estimates of the SCT-TRT misalignment were consistent within their estimated uncertainties. The track-based measurements were found to be consistent with the survey measurements summarised in table 3.

5. Tests of single barrels

The performance of SCT barrel modules was monitored through the assembly and integration to check for damage of components or deterioration of their performance (e.g. noise performance of modules). Detailed tests were carried out on every module before mounting to barrels, followed by a retest of each module after it was mounted to its barrel. Once a barrel was completed, the function of all modules was tested in simultaneous operation and performance characterisation, the so-called "single-barrel tests". Single-barrel tests were carried out in Oxford before transport, and at CERN-SR1 after transport for barrel 3, the first barrel to be shipped to CERN. This showed no sign of deterioration. Single-barrel tests on barrels 4 and 6 were carried out before transport only; and on barrel 5, after transport only. Visual inspection and a minimal set of functional checks (e.g. continuity tests of LMT's, verification of DCS sensors) were carried out on all barrels after transport.

5.1 Test setup for single barrels

For the operation and tests of the SCT barrels during macro-assembly, the first implementation of the final SCT off-detector system was used. The test systems in Oxford and CERN-SR1 used the

2008 JINST 3 P10006

same off-detector supply and readout as well as test procedures, with the exception of the detector cooling plants, which were specifically built for each site. The test system required for the operation and readout of the SCT barrels has the following main components:

- Power supply and environment sensor system, which are controlled by the detector control system (DCS). The SCT interlock system provides temperature-based safety interlocks to the power supply system.
- The readout system of SCT modules based on the final SCT readout driver module (ROD) system.
- Detector cooling is provided by an evaporative cooling system based on C_3F_8 (CERN-SR1 and Oxford) and C_4F_{10} coolants (Oxford only).

These tests used the final DAQ [21] and DCS [20] supply hardware. In addition to enabling the modules to be re-characterised electrically [21], the tests provided the opportunity to monitor the longer-term stability and uniformity of other operation-related parameters such as cooling, module temperatures and the optical communication.

The visual inspection after transport focused on abnormalities on or near modules (displacement of module/cooling block clips or shunt-shield connections, displacement of services at barrel ends, damage to wire bonds). High-resolution photographs of the full barrel surface and ends were recorded for future reference. The visual inspection was followed by electrical continuity tests of all low-mass tapes to detect any broken tracks. Figure 33 shows barrel 5 during the visual inspection.

5.1.1 Detector control system

The SCT DCS system is divided into two main parts: the power supply (PS) [10] control and the environmental monitoring. The PS system controls and monitors the powering of the SCT detector modules. Each module is powered by two independent, floating power supplies. The high voltage (HV) card provides the bias voltage to the silicon sensor and the low voltage (LV) card powers the analogue and digital voltage needed for the readout chips and the opto components on the harness. The LV card also reads out thermistors located on the hybrid (1 NTC sensor per module side). The cards are connected to a crate controller board (based upon the ELMB[31]), which is then read out through a CAN[32] bus and the data are sent to a PVSS[33] project.

The environmental project monitors the temperature and humidity inside the detector volume. Several temperature sensors are placed in critical locations: at the exhaust of the cooling pipes, next to the FSI nodes to measure gas temperature, and attached to the CFRP mechanical structure. In addition, radiation-hard humidity sensors are placed on each barrel. Their measurements, coupled with temperature readings, are used to calculate the dew point, which is continuously monitored and compared to ambient temperatures to avoid condensation. The environmental parameters are read out using ELMB's connected to the DCS project with a CAN bus, similar to the PS system. The temperature sensors on the cooling pipe are also used in the interlock system. This fully hardware-implemented system turns off the power to the modules in about one second if the temperature goes

[31] ATLAS Embedded Local Monitor Board.

[32] CAN in Automation(CiA), http://www.can-cia.de.

[33] PVSS-II, ETM, Austria,http://www.pvss.com/.

2008 JINST 3 P10006

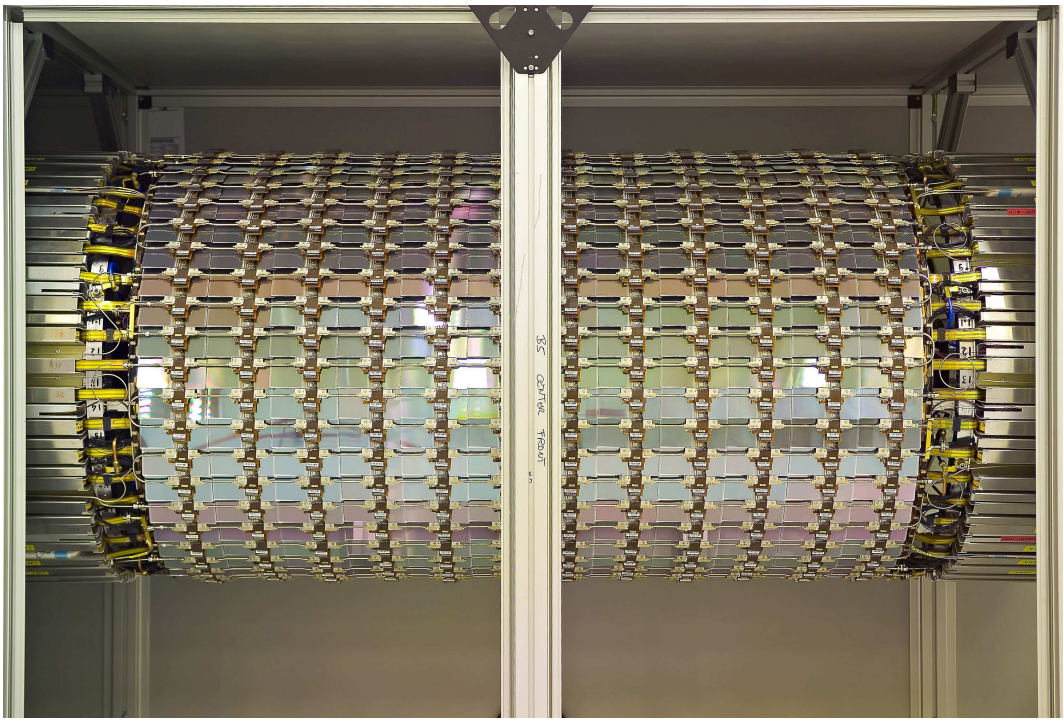

Figure 33. Complete barrel 5, with all services and modules installed, during visual inspection on arrival at CERN.

above a predefined threshold, hence protecting the modules from overheating if the cooling stops. The interlock acts on all modules of one cooling loop.

5.1.2 Detector readout system

Control, readout and online calibration of the SCT were performed using the SctRodDaq [21]. The SctRodDaq was developed within the ATLAS TDAQ software framework [22], whereby multiple C++ and Java applications can communicate across multiple processors using CORBA.[34] The version of SctRodDaq used for tests in Oxford and CERN-SR1 comprised several PC's, a 6U VME crate for trigger timing control (TTC) specific modules, and a 9U VME64x crate housing up to 14 readout driver modules (ROD's), 14 back of crate cards (BOC's) and a timing interface module (TIM). The ROD's are used for the main control and data handling, whereas the BOC's provide the ROD interface to the front-end modules and to the rest of the ATLAS DAQ chain. The TIM provides the interface to the ATLAS TTC system. Each ROD/BOC pair is connected optically to up to 48 SCT modules. Details of this readout system, its hardware and software components are described in [21].

5.1.3 Test procedure

The SCT uses a binary readout architecture whereby a hit is registered if the pulse height from the strip exceeds a preset threshold. For calibration of the SCT modules, triggers are generated

[34]Common Object Request Broker Architecture defined by the Object Management Group.

2008 JINST 3 P10006

internally by the ROD's or by the TIM and sent to the modules. Known test-charges are injected by the front-end chips and the occupancy (the per-channel fraction of triggered events for which the pulse height exceeds the threshold) is determined as a function of threshold. Histogramming of the threshold scan is done by the ROD and analysed offline on a channel-by-channel basis. The test procedure is described in further detail in reference [25]. The following tests are carried out on each module.

In the setup phase of the module readout, each module is configured, a trigger is sent to it and the returned event of this module is checked to confirm that the communication works ("module probe"). A "hard reset" is issued by the LV power supply to the module which reverts back to its default "clock/2" state, whereby the input clock is divided by two in frequency and passed onto the output data-link, if the reset functions correctly. After the modules are configured, the opto-receiver threshold on the BOC is optimised for reliable readout by an "RX threshold scan". The correct communication is further verified with a so-called "NMask scan" in which a known test pattern of varying length is written to the ABCD3TA mask registers, read back and compared.

After module setup, the digital function of the module is verified with a test of the ABCD3TA pipeline cells and a check of the redundancy readout, which allows to by-pass a chip if it is faulty [8]. Following the successful completion of digital tests, the analogue performance is tested for each channel. In the "3-point-gain" test, three test charges (1.5 fC, 2.0 fC and 2.5 fC) are injected in each channel and its gain is measured by a threshold scan for each test charge. From the S-curve of the threshold-scan data, the gain is extracted as the threshold at 50% efficiency. A fit of a complementary error function to the threshold scan yields the output noise at 2.0 fC. This is used to extract the equivalent noise charge (ENC), defined as the output noise divided by the channel gain. With this test, it is possible to identify defective channels (noisy or dead) as well as bonding defects (noise too high or low).

The noise occupancy is defined as the single-channel noise occupancy per bunch-crossing. It is usually averaged over an ABCD3TA chip (128 channels) or a complete module (1536 channels). The noise occupancy is measured with a threshold scan without charge injection. The noise occupancy is given as the number of noise hits per channel and Level-1 (L1A) trigger, at a threshold of 1 fC (the operational threshold in the experiment). The special test, using two consecutive triggers of varying delay [25], was used to check for light-leaks in the opto readout system. This can cause additional noise when the 850 nm laser light leaks out of its enclosures and is absorbed in the active silicon sensors. Furthermore, this test is sensitive to electrical pick-up of the digital signals present during the readout cycle.

5.2 Results of electrical tests on single barrels

Results presented here were obtained during single-barrel tests after a cylinder was fully populated with modules. Module ENC noise (average ENC noise per chip derived from the 3-point-gain test) for the four barrels immediately after assembly is shown in figure 34. The measured ENC noise varies between the barrels due to their different operating temperatures. The barrels were operated at hybrid temperatures of 11.3°C, 12.4°C, 16.4°C and −0.4°C for barrels 3, 4, 5 and 6 respectively. ENC noise results for warm operation, with hybrid temperature typically ∼28°C, are given in [21] for single barrels and in section 6 for the completed SCT barrel inside the TRT.

2008 JINST 3 P10006

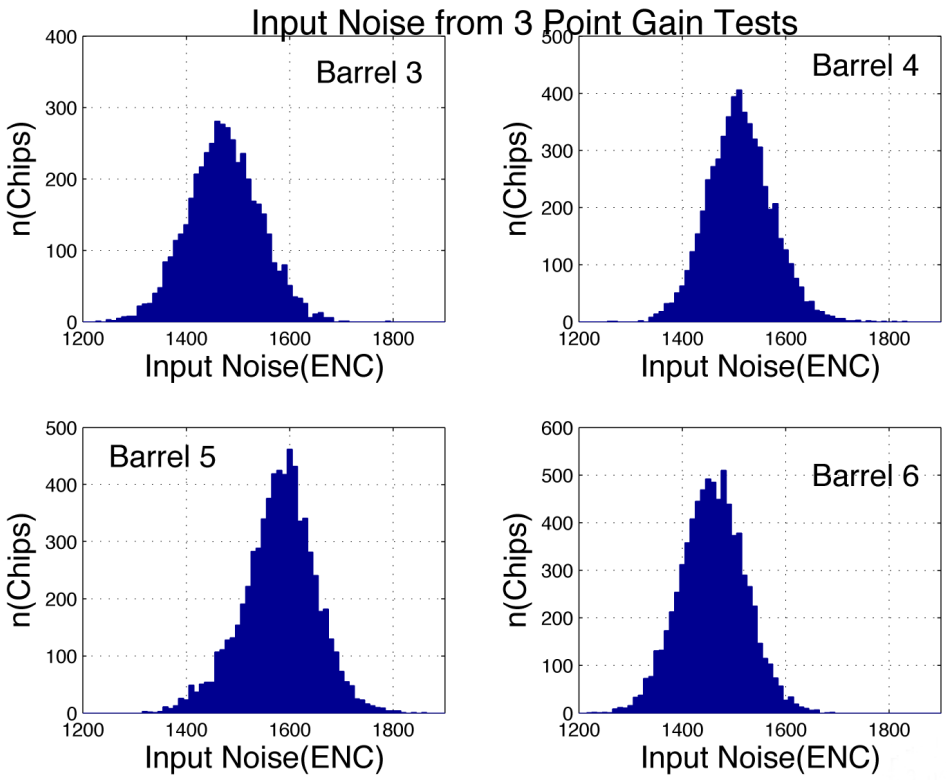

Figure 34. Average chip ENC noise for the four barrels as determined in a 3-point gain measurement during single-barrel tests. The barrels were operated at hybrid temperatures of 11.3°C, 12.4°C, 16.4°C and −0.4°C for barrels 3, 4, 5 and 6 respectively.

Table 4. Number of dead channels in SCT barrels.

Barrel 3	Barrel 4	Barrel 5	Barrel 6	Total
1190	483	1342	3667	6683
				0.206%

The characterisations of modules on the barrels were carried out at a range of temperatures. Figure 35 shows the dependence of ENC noise on the hybrid temperature. This shows a slope of 5.9 $e^-/°C$ and an ENC noise of 1480 e^- at 0°C.

The number of defective channels per module is shown in figure 36. The tail in the distribution, corresponding to modules with $\geq$10 defective channels, is due to the use of ASIC's with 1 faulty channel [4]. The specification for the number of defective channels is $<$1%, i.e. $<$15 channels per module. The total number of defective channels per barrel is summarised in table 4. The overall total number of defective channels is 0.2% of channels in the SCT barrel. No deterioration in ENC noise or numbers of defective channels was observed as a result of assembling the modules to the cylinders.

The channel noise occupancy at 1 fC threshold, averaged over the module, is shown in figure 37. The average channel noise occupancy of 4.45×10^{-5}, measured on the completed barrels, matches the noise occupancy measured during module production [4]. The specification for the SCT single-channel noise occupancy is 5×10^{-4}, hence all modules are well within specification.

2008 JINST 3 P10006

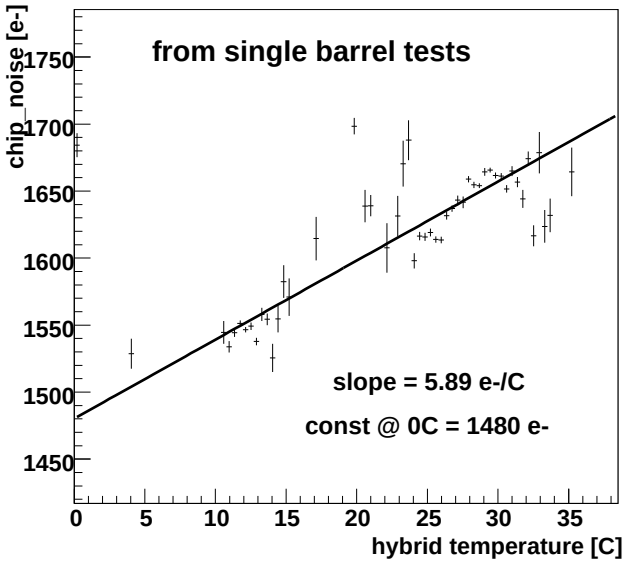

Figure 35. ENC noise versus hybrid temperature measured during single-barrel tests.

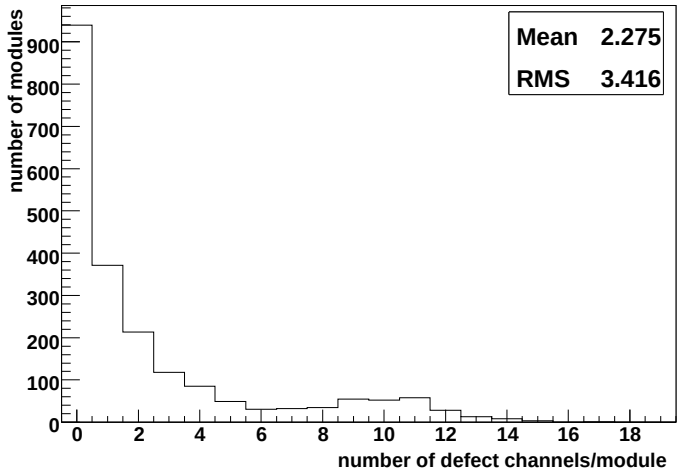

Figure 36. Number of defective channels per module as determined in a 3-point gain measurement after module assembly to the barrels.

5.3 Results of thermal tests on single barrels

A crucial aspect of the assembly of the SCT is the proper performance of the module cooling. Up to 10 W of power per module has to be removed at a temperature which safeguards against thermal runaway. To limit the effects of radiation damage, the temperature on the silicon sensors should be around -7°C. The design of the module and the cooling system achieves this goal at a coolant temperature in the pipe of around -25°C. Any serious degradation of the thermal impedance between the heat sources (ASIC's) and the coolant will compromise the long-term operability of the affected module in the high-rate environment of the LHC.

2008 JINST 3 P10006

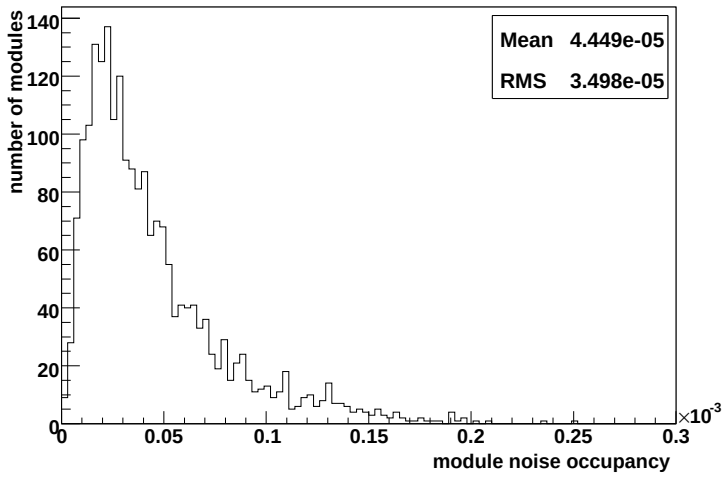

Figure 37. Average module noise occupancy measured on the completed barrels.

Of particular concern is the quality of the grease joint between the cooling block surrounding the cooling pipe and the module baseboard: firstly, because of the delicacy of the grease application and secondly, as the expected temperature gradient across this joint is already about 2°C.

In the evaporative cooling system, the coolant temperature in the evaporator can be adjusted by controlling the back-pressure (see section 3.2). In the ATLAS ID evaporative-cooling system, each cooling loop on the detector is connected to one cooling circuit with its own back-pressure regulation as shown in figure 14. During the assembly, the uniformity of module temperatures was studied in "warm" (coolant temperature about 17°C) and "cold" (about −7°C) operation. Cold operation was achieved by using C_3F_8 as a coolant at an evaporation pressure of about 3.3 bar(a), whereas warm operation was achieved either by operating the system with perfluorobutane (C_4F_{10}), for which the saturation curve is shifted towards higher temperatures (for tests at Oxford), or by evaporating the original coolant, C_3F_8, at higher pressure (6.5 bar(a), for tests at CERN). The choice of these temperatures was driven by the dew point achieved during the tests — this had to stay safely below the coolant temperature.

The temperature of the hybrids on the SCT modules is measured by two thermistors,[35] one on the top and one on the bottom side of the module [4]. The data from the thermistors are read out through the low voltage supply cards, from where they are transferred via CANbus to the PVSS-based DCS software projects. While this system monitors temperatures continuously, for the analysis discussed, the focus is on the spatial uniformity of the thermal behaviour and not the dynamic behaviour of the system. Therefore module temperatures discussed here are single values obtained in stable conditions.

For this analysis, the temperature of a given module was obtained as the mean of the two temperature sensors on the two hybrids. On average, modules were slightly hotter by 0.33°C on the side facing the CFRP barrel (bottom) than on the outside (top). The uncertainty on the temperature measurement of one module is 0.66°C. Before the temperature uniformity of the assembled barrels could be assessed, two systematic effects had to be removed:

[35] Semitec 103KT1608-1P.

2008 JINST 3 P10006

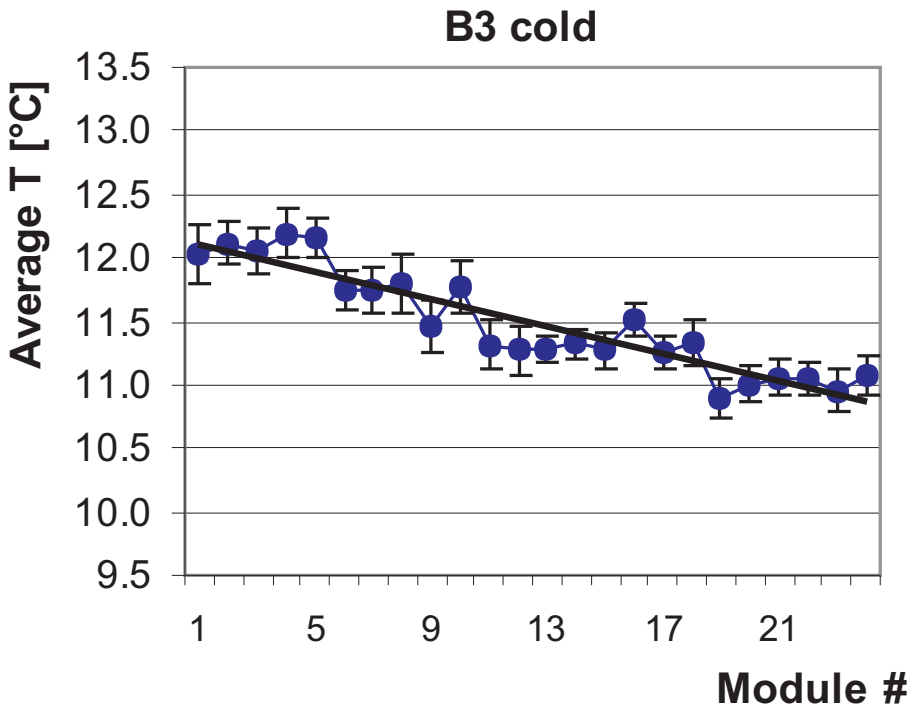

Figure 38. Average module hybrid temperature along a stave for barrel 3 during cold tests at Oxford. The coolant enters the pipe near Module 1 and leaves the pipe near Module 24.

1. Fluctuations between cooling loops, which were likely caused by small differences in the back-pressure regulators and/or gravitational effects.

2. Variations of the temperature along the loop due to the frictional and momentum pressure drop in the pipe (as an example, see figure 38).

After removal of the systematic effects, the r.m.s. of the distribution of the module temperatures for the complete barrels (for warm and cold test runs) was between 0.6 and 1.1°C, with the larger values typically obtained for the outer barrels. On barrels 3, 4, 5 and 6, the numbers of modules whose hybrid temperature exceeds a threshold 2.3°C above the average temperature were 0, 4, 5 and 14 modules respectively (0%, 0.8%, 0.9% and 2.1% of the total number of modules on each barrel). This threshold was taken as three times the measurement error plus variations expected from powering. These 23 modules (1.1 % of the complete barrel) with larger than the typical temperature variation fall into two categories:

- Modules where the temperature of one thermistor is significantly different from the temperature recorded in the other thermistor on the same module. Modules with this characteristic have only been used on the outer barrels, where radiation damage to the silicon strip detectors will be lower.

2008 JINST 3 P10006

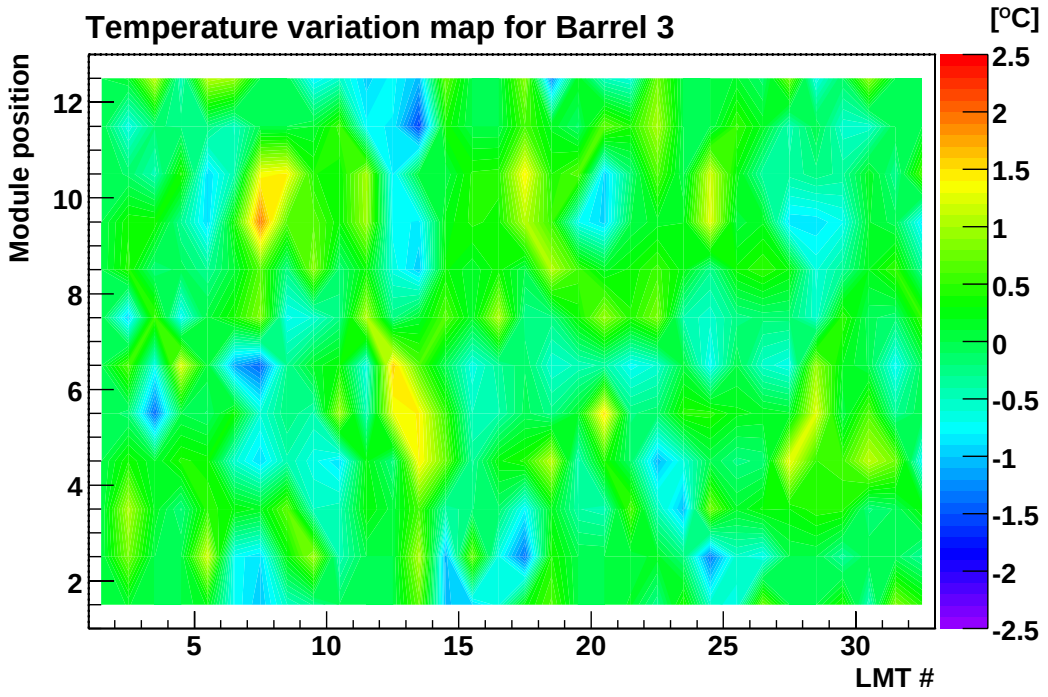

Figure 39. 2-dimensional distribution of the relative hybrid temperatures after corrections for systematic effects for the barrel 3 reception tests at CERN.

- Modules which are close to the input and output of the cooling pipe. The cooling pipe was clamped to the structure close to these modules and this additional constraint prevented the pipe from conforming well to the module baseboard surface. In a few cases, thermal performance could be recovered for this class of modules by loosening and re-tightening of the cooling-loop support bracket at the barrel end.

These studies show that a high degree of uniformity of the thermal impedance throughout the barrel SCT has been achieved. This is essential for the safe operation of the modules over the lifetime of the experiment (see figure 39).

6. Final combined tests before installation

The tests described in this section were carried out in the CERN-SR1 test area with the already assembled SCT and TRT barrels, following the insertion of SCT into TRT barrel. For the final test of the completed barrels, two opposite detector sections were connected to the supply and readout systems of the SCT and TRT. The schematics in figure 40 (right) illustrate the chosen test sectors for the TRT and SCT, as well as the scintillator arrangement. The photograph shows the barrel during the cabling of the top sector, before the bottom sector was cabled. Further details on this test setup and combined tests between SCT and TRT are given in references [23, 24]. The goals of the final tests were to gain operational experience with the combined barrels, to measure the noise performance in the final arrangement prior to installation in the ATLAS cavern and to collect

2008 JINST 3 P10006

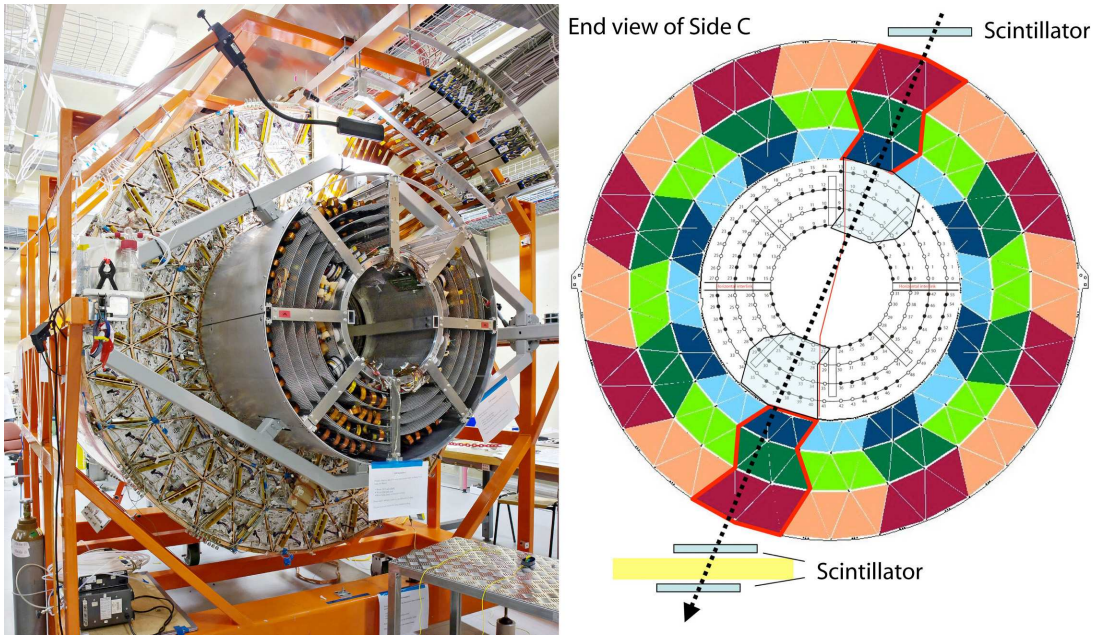

Figure 40. ID barrel setup for the cosmic-ray test (left) and the configuration of module groups chosen for this test (right).

a cosmic-ray data set. This was subsequently used to test the tracking performance of the SCT and the SCT combined with the TRT [23].

6.1 Operation of the SCT inside the TRT

Two SCT sectors, comprising a total of 468 barrel modules on barrels 3, 4, 5 and 6, were connected to the power supply, cooling and readout systems. The power supply, interlock, environmental monitoring and readout systems were identical to those described for the CERN-SR1 system in section 5.1.1, with the addition of the SCT timing and trigger control (TTC) system for synchronisation to the TRT and cosmic-ray trigger. The detector services were arranged in a configuration as close as possible to the final configuration for ATLAS. Two sections of the inner and outer heat spreader plate (HSP) were mounted around the SCT services. (The HSP is required for electromagnetic shielding and for cooling of services. Once the SCT is installed together with the TRT in the cryostat, the heat spreader plate encloses the SCT barrel services along their routing above the TRT barrel electronics.) The HSP ground was connected to the thermal enclosure bulkhead and to the SCT detector ground. The SCT was electrically isolated from the TRT, tooling and support structure (except for special tests) to match the final ground installation of ATLAS and it was connected to a single grounding star-point. The SCT barrel volume was flushed with dry air at a rate of 36 l/min to maintain a dew point of -40°C during the tests. Additional dry-air flushing was provided in the service volume between the TRT electronics and the SCT HSP to prevent condensation on services or the bulkhead.

During the final tests, a total of 12 barrel cooling loops were operated with the CERN-SR1 C_3F_8 evaporative cooling system at a typical back-pressure setting of 5.6 to 5.8 bar. For this setting, with modules powered, configured and read out, a cooling-pipe temperature of $14\pm1^{\circ}$C

2008 JINST 3 P10006

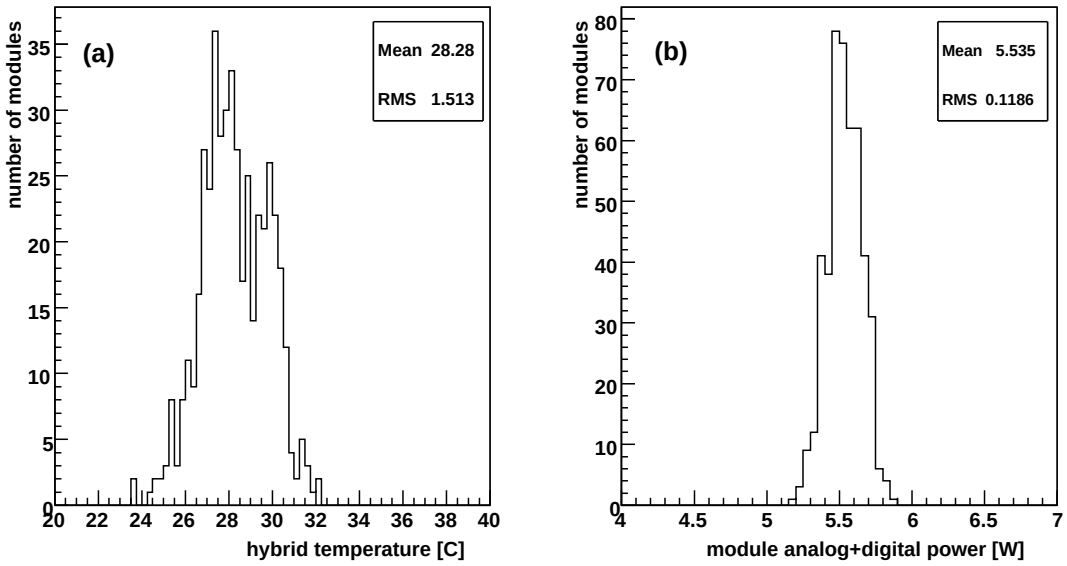

Figure 41. (a) Hybrid temperature for warm operation and (b) module power consumption at the start of a typical noise occupancy scan.

was measured. Figure 41a shows the distribution of hybrid temperatures measured at the start of a noise-occupancy calibration scan. For this back-pressure setting, the mean was 28.3°C and the r.m.s spread was 1.5°C. No correction for loop-to-loop variation or variation along the cooling loop was carried out for this study. The recorded temperatures indicate that the thermal performance of barrels was maintained during four-barrel assembly and integration to the TRT. The module power, as the sum of analogue and digital power consumption of the ASIC's, is shown in figure 41b for the same run.

6.2 Results of barrel calibration tests inside the TRT

The calibration tests after integration with the TRT were aimed at determining the number of defective channels in the tested sectors and the analogue performance (noise, gain) in comparison to the tests on single barrels. While this was not a complete test of the detector, the results can be considered as representative for the SCT barrel performance after integration with the TRT. The following tests have been carried out (see section 5.1.3 and [25] for reference):

- Check of module supply: Vdd and Vcc supply currents and voltages, detector bias voltage and current, temperature readout of hybrid thermistor.
- Digital tests: opto scan (RX threshold), NMask, bypass tests [21].
- Analogue tests: three-point gain, response curve, noise occupancy, double-trigger noise, synchronous-trigger noise-occupancy.
- Sensor leakage current for all modules.

2008 JINST 3 P10006

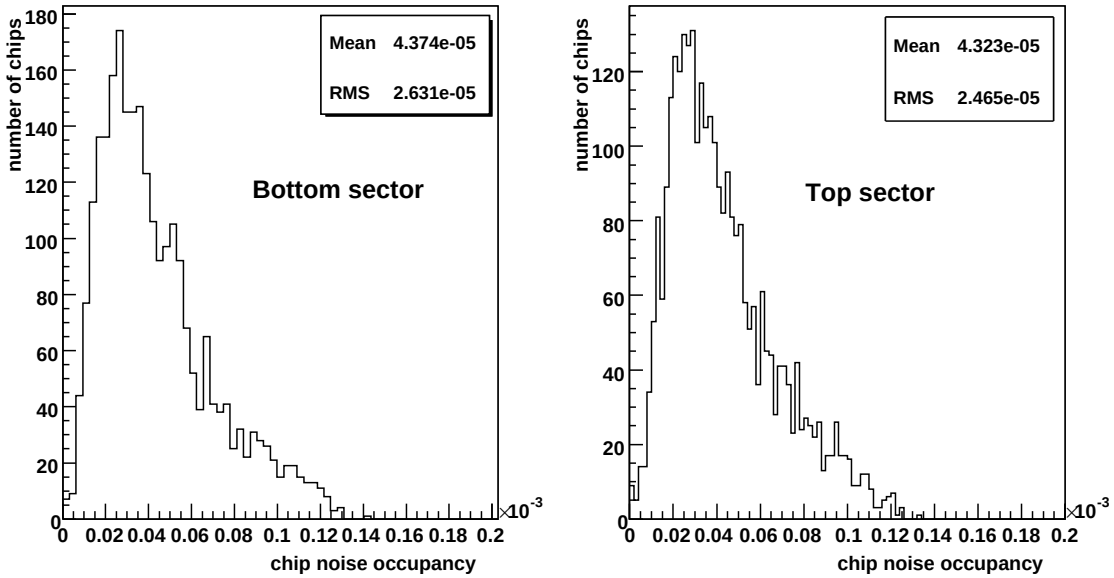

Figure 42. Noise occupancy for front-end chips in bottom and top test sectors after the SCT integration with the TRT.

- Detector timing: check of hit coincidences between module sides during a scan of the level-1 trigger accept (L1A) delay with respect to cosmic-ray trigger.

Checks of the module supply and digital tests were carried out during the setup phase of the detector in order to achieve a reliable readout of all modules.

During the setup phase for these calibration tests, the total number of defective links was determined. For the total barrel, not only for the sections used in the final test, six and four data and TTC links respectively were found to be dead after the final integration of the four single barrels. These are thought to be due to fibre breakages at the services thermal feedthroughs. It should be noted that the data for defective data links are not lost but can still be accessed through the readout redundancy [11].

The initial tests were followed by the commissioning of the top sector and the bottom sector with analogue calibration tests. Figure 42 shows the noise occupancy for all chips on the top and the bottom sector. The average noise occupancy was 4.4×10^{-5} — this matches the noise occupancy found in the single-barrel tests. The ENC noise, as measured in a three-point gain measurement, is shown for the four barrels individually in figure 43. For a hybrid operation temperature of 28°C, the mean ENC noise was 1681 e^-, consistent for the four barrels.

To allow a direct comparison of ENC noise between (a) tests after the four-barrel assembly and integration with the TRT with (b) tests carried out on single barrels, it was important to correct for the known dependence of noise on the operating temperature (as shown in figure 35 with 6 e^-/°C). Figure 44 shows the difference between the ENC noise as measured on the SCT inside the TRT and the temperature-corrected ENC noise measured on single barrels. A slight increase in noise of 32 e^- (2%) is observed after the four-barrel assembly and integration with the TRT. The gain, as

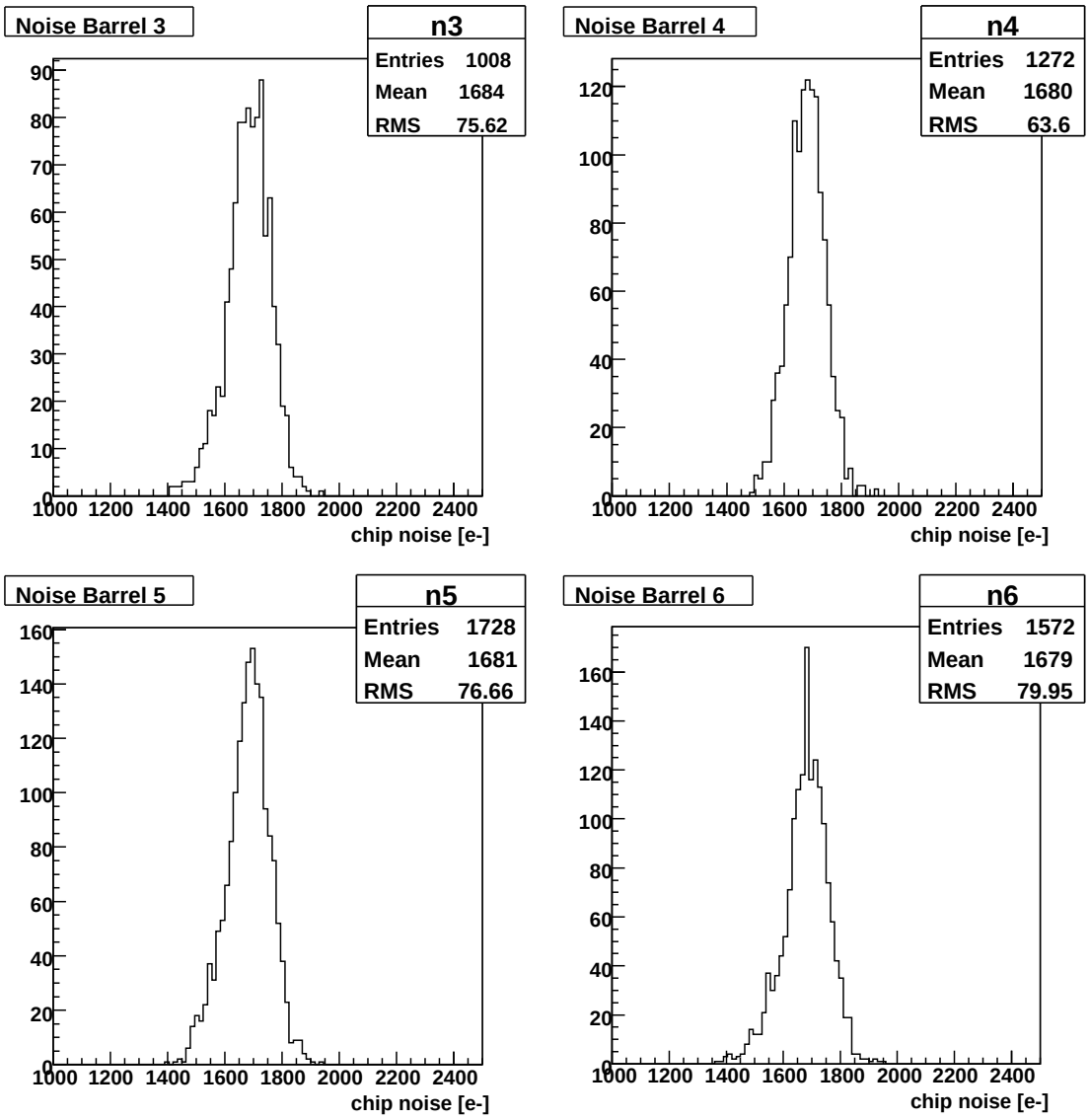

Figure 43. Chip ENC noise for individual barrels after the SCT integration with the TRT.

measured after integration, is shown in figure 44 and shows no change.

As preparation for cosmic-ray data taking, the SCT L1A trigger was timed in with respect to the scintillator trigger. This was done using the ROD histogramming of hit coincidence between the two sides of modules while the offset between SCT L1A and the cosmic-ray trigger was varied [30]. A coincidence is defined as a hit on each sensor side of a module, with the additional requirement that the physical location of the hits overlap within the readout width of a chip (approximately 1 cm). With the typical noise occupancy, the rate of accidental noise coincidences is minimal. Figure 45 shows the number of coincidences as a function of the L1A delay in units of bunch-crossings. The plot shows the enhancement of coincidences when the correct trigger delay (set to 0 in this measurement) was set. Since the cosmic-ray trigger is uniformly distributed over the 25 ns wide clock-cycle, coincidences are registered in two adjacent time-bins.

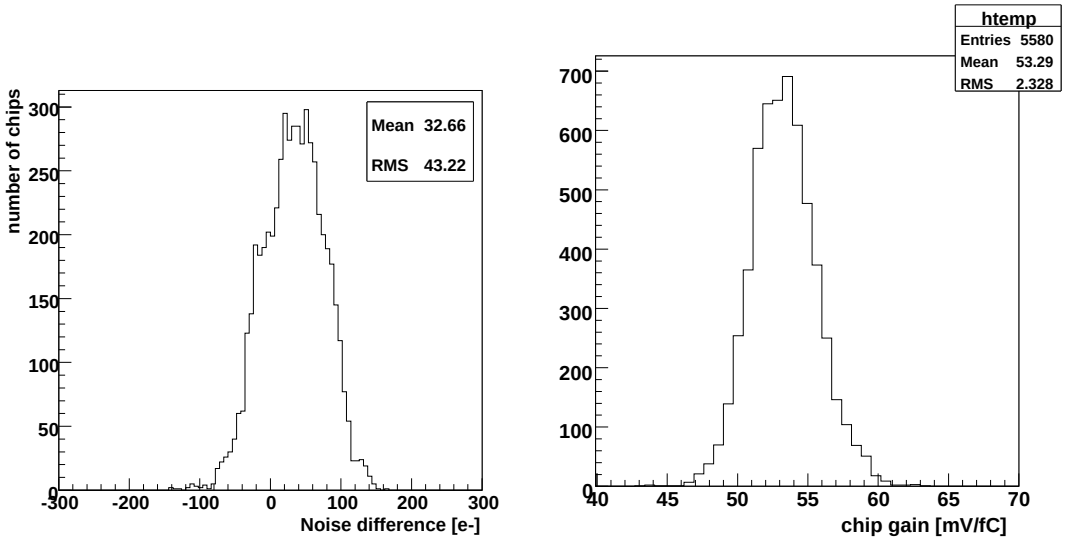

Figure 44. Difference in ENC noise between measurements with the SCT in the TRT and the single-barrel noise measurements (left), and the mean analogue gain of front-end chips as measured after the SCT with the TRT integration (right).

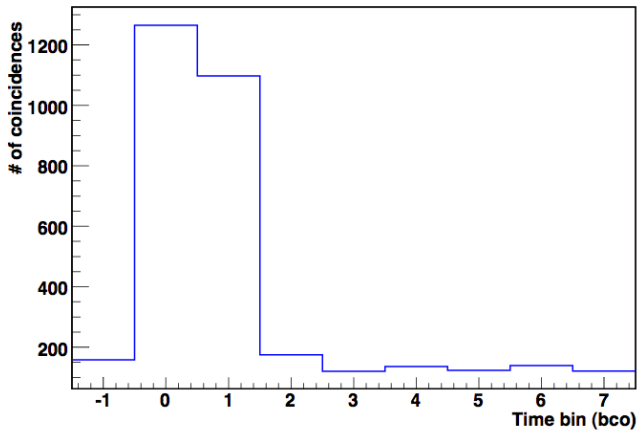

Figure 45. Number coincidences between hits in both sides of a module as function of the delay between L1A and the cosmic-ray trigger. This information was collected during SCT timing-in for cosmic-ray runs.

6.3 Noise and cosmic-ray tests with the TRT

In addition to the calibration tests, the SCT was run in a physics mode, analogous to the final ATLAS configuration. Data were passed through the ATLAS ATHENA [31] framework. This converts the raw-hit information in the SCT into space-points and tracks for further analysis. This output was then used to examine the noise occupancy, efficiency and tracking performance of the detector, as well as providing a basis for detailed studies of detector alignment. A brief summary of the tests performed in CERN-SR1 is given here; full details may be obtained from [23].

2008 JINST 3 P10006

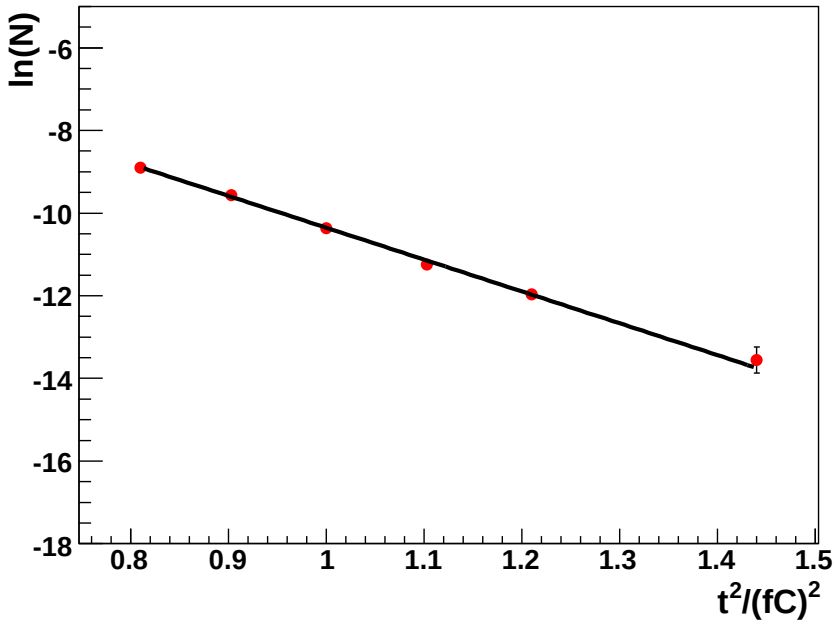

Figure 46. A plot of $\ln N$ vs t^2 for one side of a barrel SCT module. A straight line has been fitted, indicating that the distribution follows the expected shape.

6.3.1 Noise tests

Several noise tests were performed with random triggers during the CERN-SR1 commissioning period in an attempt to characterise thoroughly the behaviour of the detector in the presence of the TRT. Data were taken at trigger rates of 500 Hz, 5 kHz and 50 kHz, from which it was concluded that there is no significant variation of the SCT barrel noise occupancy with trigger rate. Data were collected with different module-threshold settings in order to obtain a curve of $\ln(N)$ vs t^2, where N is the single-strip noise occupancy per bunch-crossing and t is the threshold. Figure 46 shows the results of the threshold scan as $\ln(N)$ versus threshold squared. The straight line fit to the data confirms the expected gaussian noise distribution. The results revealed that all modules were performing comfortably within specification. Grounding issues were investigated by running the barrel under two different grounding schemes, without effect on the noise occupancy.

One significant test with regards to the SCT/TRT integration involved the examination of cross-talk between the two subsystems. Runs were taken in which the trigger offset between the SCT and TRT was slowly varied around the correct value, thus providing a probe of possible pickup induced in the SCT by the TRT readout cycle. Runs were taken with TRT off and on. No evidence for cross-talk was found in any of the tests, and the final noise occupancy values for the SCT running in conjunction with the TRT indicate a noise performance within the design specification.

6.3.2 Cosmic-ray tests

Observation of cosmic muons passing through the SCT barrel provides valuable input into tracking and alignment studies. In addition, the large samples of tracks collected during the CERN-SR1

2008 JINST 3 P10006

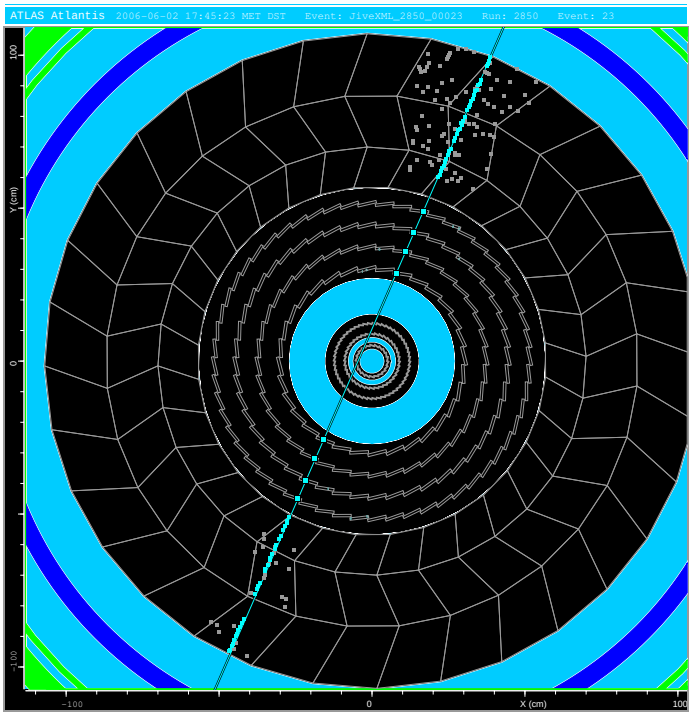

Figure 47. A reconstructed cosmic-ray track with SCT and TRT hits.

commissioning period allowed a first preliminary efficiency measurement to be made of the SCT modules in the final detector configuration.

Figure 47 shows a reconstructed cosmic-ray track with both SCT and TRT hits. From this, it can be deduced that both that the TRT and SCT are well timed-in and that the pattern recognition and tracking algorithms are performing well. The selection of high-quality tracks (obtained by cutting on such quantities as the number of hits in the SCT, the track χ^2 and the incident angle of the track on a module) permits detailed studies of module efficiency and alignment. Figure 48 shows the hit efficiency per layer, with nominal module locations and after alignment. After alignment, the unbiased hit efficiency in all barrel layers is measured to be within specifications, i.e. greater than 99%. Furthermore, since the cosmic-ray trigger was not synchronised with the readout clock, the collected data could also be used to study the dependence of the SCT efficiency on the arrival time of the particle. The hit efficiency was found to remain high for a range of 4 ns around the nominal trigger time.

With respect to the tracking performance, the SCT detector resolution can be extracted from the r.m.s. of the residual distribution for the SCT hits after allowing for track extrapolation errors and correcting for any misalignments. This procedure is most reliable for high-momentum tracks for which an r.m.s of around 28 μm is obtained. With a track extrapolation uncertainty of around 16 μm, this corresponds to a detector resolution of 23 μm, in agreement with expectations. Due to the absence of a magnetic field, it was not possible to determine the particle momentum. Therefore, the influence of low-momentum tracks on the measured residual distribution had to be minimised by cutting on the track χ^2, as described in [23].

2008 JINST 3 P10006

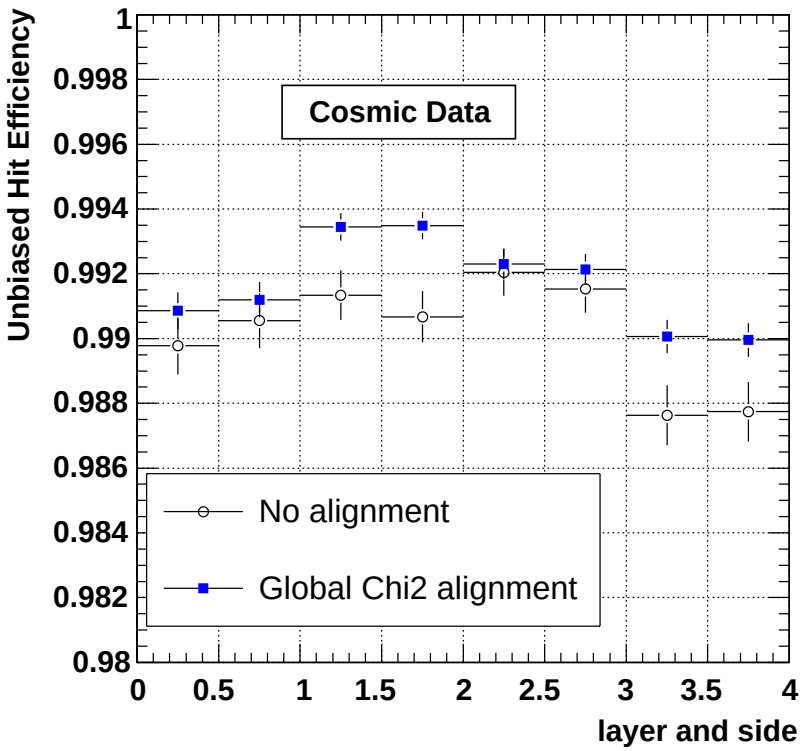

Figure 48. Hit efficiency measured for the different barrel layers from cosmic-ray data. The efficiencies are shown separately for each side within a layer. Use has been made of the different available alignment corrections obtained by the SCT alignment methods described in reference [23].

7. Summary

This paper describes the engineering design philosophy, fabrication, construction and integration of a low-mass charged-particle tracking system that has been installed in the ATLAS detector. The tracker is required to operate inside a 2 T solenoidal magnetic field, to provide hermetic coverage up to $|\eta|$ =2.5 and to generate up to four space-points for each charged track. This performance must be delivered without placing excessive material in front of the calorimeters. Therefore, the design has been driven by the need to select materials with the longest radiation lengths and optimal strength-to-weight ratios. The complete SCT barrel supports 2112 double-sided silicon modules and their associated services. Early results from the cosmic-ray runs in the CERN-SR1 assembly building indicate that the modules are positioned with the required accuracy. For high momentum-tracks, an r.m.s of around 28μm is obtained for the hit residuals. Allowing for the track extrapolation errors of around 16 μm, this is compatible with the expected detector resolution of 23 μm.

For the complete SCT barrel, the average channel noise occupancy per bunch-crossing is 4.4×10^{-5} — this matches the noise occupancy found in the single barrel tests. For a hybrid operation temperature of 28°C, the mean ENC noise is 1681 e^-, consistent for the four single barrels. Furthermore, the unbiased hit efficiency in all barrel layers was measured to be within specifications, i.e. greater than 99%.

Clearly, some compromises have been made to achieve these goals and the resultant decision to

2008 JINST 3 P10006

reduce the number of connectors within the solenoid volume resulted in many variants of services assemblies and increased the lengths of services that needed to be stored and manipulated during the integration process. As a corollary to this, it is hoped to achieve benefits in the long-term reliability of the tracker.

The engineering challenges offered by the construction of the SCT barrel have brought together a large, multi-national team of technicians, engineers and scientists who have worked in true collaboration to meet the deadlines and targets of the project. Not all scheduled dates were achieved but perhaps this was to be anticipated, given the complexity and technical demands imposed on the team by the innovative design.

Acknowledgments

We are greatly indebted to all the technical staff who worked on the barrel engineering and integration project from the ATLAS SCT Institutes. We acknowledge the support of the funding authorities of the collaborating institutes including the Spanish National Programme for Particle Physics; the Research Council of Norway; the Science and Technology Facilities Council of the United Kingdom; the Polish Ministry of Higher Education and Science; the German Ministry of Science; the Swiss National Science Foundation; the State Secretariat for Education and Research and the Canton of Geneva; the Slovenian Research Agency and the Ministry of Higher Education, Science and Technology of the Republic of Slovenia; the Ministry of Education, Culture, Sports, Science and Technology of Japan; the Japan Society for the Promotion of Science; the Office of High Energy Physics of the United States Department of Energy; the United States National Science Foundation; the Australian Research Council (ARC) and Department of Education, Science and Training (DEST); the Dutch Foundation for Fundamental Research on Matter (FOM); the Ministry of Education, Youth and Sports of the Czech Republic, Ministry of Industry and Trade of the Czech Republic, and Committee for Collaboration of the Czech Republic with CERN; the National Science Council, Taiwan; the Swedish Research Council.

A. Acronyms

CF	Carbon Fibre
CFRP	Carbon Fibre Reinforced Plastic
CTE	Coefficient of Thermal Expansion
CRD	Cooling Reference Disk
DCS	Detector Control System
ENC	Equivalent Noise Charge
ESD	Electrostatic discharge
FEA	Finite Element Analysis
FSI	Frequency Scanning Interferomtry
HEX	Heat Exhanger
HSP	Heat Spreader Plate
ISSS	Intermediate Service Support Structure
L1A	Level 1 Accept trigger

2008 JINST 3 P10006

LMT	Low Mass Tape
PPB n	Patch Panel Barrel n
ROD	Readout Driver Module
RSS	Radial Service Support
TDAQ	ATLAS data DAQ framework
TE	Thermal Enclosure
TIM	Timing Interface Module
TPP	Temporary Patch Panel

References

[1] ATLAS collaboration, *ATLAS : technical proposal for a general-purpose pp experiment at the Large Hadron Collider at CERN*, CERN-LHCC-94-43.

[2] ATLAS collaboration, G. Aad et al., *The ATLAS Experiment at the CERN Large Hadron Collider*, 2008 *JINST* **3** S08003.

[3] ATLAS collaboration, *ATLAS Inner Detector Technical Design Report*, CERN, April 1997.

[4] A. Abdesselam et al., *The barrel modules of the ATLAS semiconductor tracker*, *Nucl. Instrum. Meth.* **A 568** (2006) 642.

[5] A. Abdesselam et al., *The ATLAS semiconductor tracker end-cap module*, *Nucl. Instrum. Meth.* **A 575** (2007) 353.

[6] A. Ahmad et al., *The silicon microstrip sensors of the ATLAS semiconductor tracker*, *Nucl. Instrum. Meth.* **A 578** (2007) 98.

[7] R. J. Apsimon et al., *Application of advanced thermal management technologies to the ATLAS SCT barrel module baseboards*, *Nucl. Instrum. Meth.* **A 565** (2006) 561.

[8] F. Campabadal et al., *Design and performance of the ABCD3TA ASIC for readout of silicon strip detectors in the ATLAS semiconductor tracker*, *Nucl. Instrum. Meth.* **A 552** (2005) 292.

[9] Y. Unno et al., *Application of Cu-polyimide flex circuit and Al-on-glass pitch adapter for the ATLAS SCT barrel hybrid*, *Nucl. Instrum. Meth.* **A 541** (2005) 286.

[10] P.W. Phillips, *The ATLAS SCT Power SupplySystem*, Proceedings of Topical Workshop on Electronics for Particle Physics (TWEPP 2007), Prague, Czech Republic, 3-7 September 2007.

[11] A. Abdesselam, *The optical links of the ATLAS Semiconductor Tracker*, 2007 *JINST* **2** P09003.

[12] V. Vacek, G. Hallewell, S. Lindsay and S. Illie, *Perfluorocarbons and their use in cooling systems for semiconductor particle detectors*, *Fluid Phase Equlibria* **174** (2000) 191.

[13] V. Vacek, G. Hallewell and S. Lindsay, *Velocity of sound measurements in gaseous per fluorocarbons and their mixtures*, *Fluid Phase Equilibria* **185** (2001) 305.

[14] M. Olcese et al., *Evaporative Cooling System for the ATLAS Inner Detector*, 2008 *JINST* **3** P07003.

[15] P. Bonneau, *Evaporative cooling system for Pixel/SCT*, ATC-TL-EP-0001, EDMS Id 391168 (2006).

[16] P.A. Coe, D.F. Howell and R.B. Nickerson, *Frequency scanning interferometry in ATLAS: remote, multiple, simultaneous and precise distance measurements in a hostile environment*, *Meas. Sci. Technol.* **15** (2004) 2175.

2008 JINST 3 P10006

[17] S.M. Gibson, P.A. Coe, A. Mitra, D.F. Howell and R.B. Nickerson, *Coordinate Measurement in 2-D and 3-D Geometries Using Frequency Scanning Interferometry*, *Opt. Laser Eng.* **43** (2005) 815.

[18] S.M. Gibson, *The ATLAS SCT alignment system and a comparative study of misalignment at CDF and ATLAS*, D.Phil. Thesis, Oxford UK (2004).

[19] R.B. Nickerson et al., *Robotic mounting of ATLAS barrel SCT modules*, *Nucl. Instrum. Meth.* **A 568** (2006) 686.

[20] A. Abdesselam et al., *The Detector Control System of the ATLAS SemiConductor Tracker during Macro-Assembly and Integration*, 2008 *JINST* **3** P02007.

[21] A.J. Barr et al., *The Data Acquisition and Calibration System for the ATLAS Semiconductor Tracker*, 2008 *JINST* **3** P01003.

[22] ATLAS collaboration, *ATLAS high-level trigger, data-acquisition and controls : Technical Design Report*, CERN-LHCC-2003-022, ATLAS-TDR-016.

[23] E. Abat et al., *Combined performance tests before installation of the ATLAS Semiconductor and Transition Radiation Tracking Detectors*, 2008 *JINST* **3** P08003.

[24] H. Pernegger, *Integration and test of the ATLAS Semiconductor Tracker*, *Nucl. Instrum. Meth.* **A 572** (2007) 108.

[25] P.W. Phillips, *Functional testing of the ATLAS SCT barrels*, *Nucl. Instrum. Meth.* **A 570** (2007) 230.

[26] M. Olcese et al., *Engineering Overview of the ATLAS Inner Detector*, in preparation.

[27] D. Mergelkuhl and A. Wiart, *ATLAS - SCT Barrel Detector Photogrammetric Measurement of SCT Barrel, FSI and Pixel JIG Measurement Week 46 of 2005 (14.11.2005)*, ATL-IS-UR-0004, EDMS Id 681215.

[28] A. Behrens, V. Correia Pieres Carmona and J.-N. Joux, *ATLAS - SCT Barrel Detector External Reference Points Transfer*, ATL-IS-UR-0007, EDMS Id 705191.

[29] V.Correia Pires Carmona et al., *Measurement of SCT and TRT Barrels*, ATL-IS-UR-0003, EDMS Id 708009.

[30] B. Demirkoz, *Cosmic tests and performance of the ATLAS SemiConductor Tracker Barrels*, *Nucl. Instrum. Meth.* **A 572** (2007) 43.

[31] ATLAS collaboration, *ATLAS computing : Technical Design Report*, ATLAS-TDR-017, CERN-LHCC-2005-022.

2008 JINST 3 P10006